MSc. Thesis

Recycling Space Debris as a Stepping Stone Towards a Permanent Lunar Presence

Yannick Heumassej

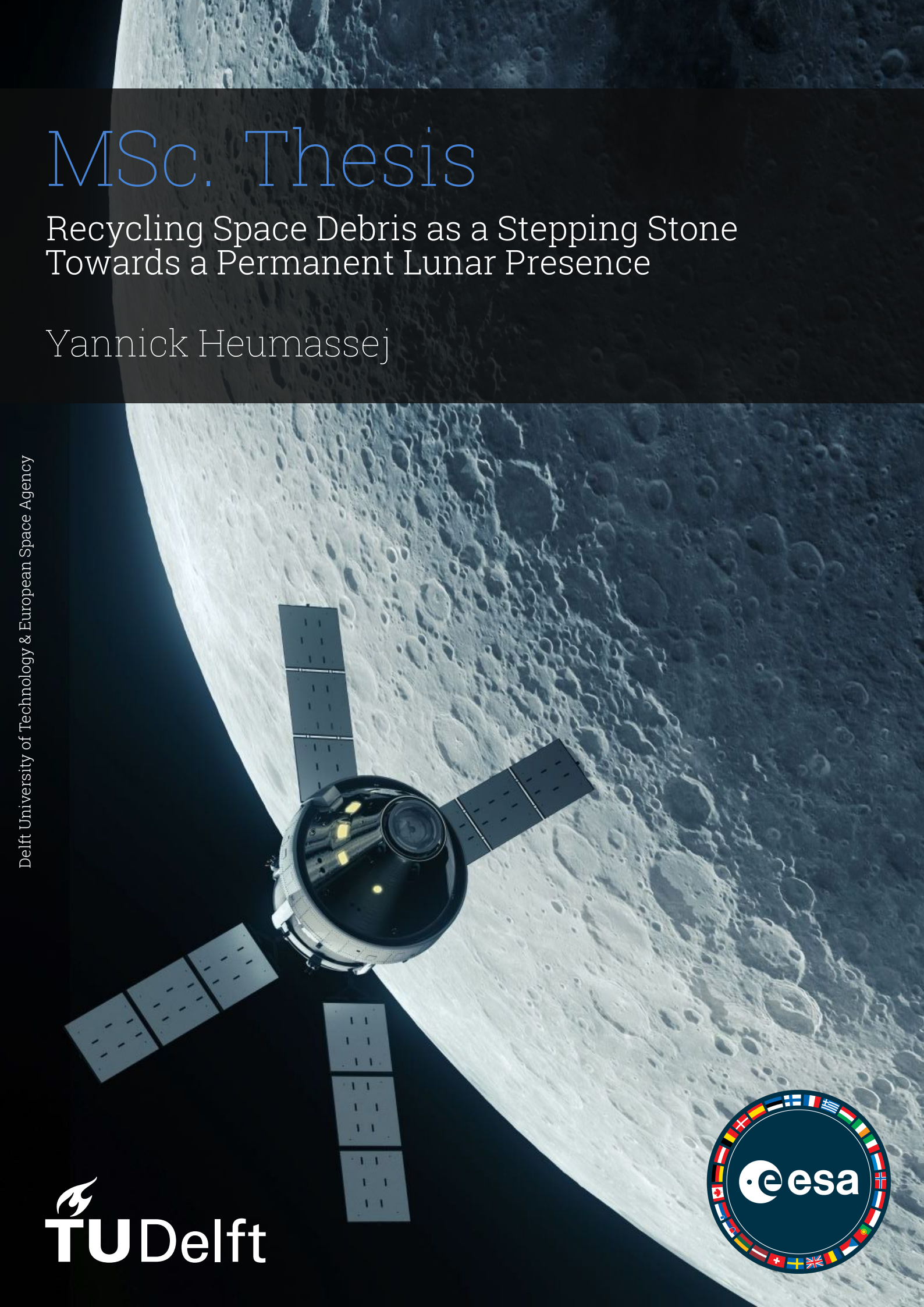

Delft University of Technology & European Space Agency

TU Delft

esa

MSc. Thesis

Recycling Space Debris as a Stepping Stone Towards a Permanent Lunar Presence

by

Yannick Heumassej

to obtain the degree of Master of Science
at the Delft University of Technology,
to be defended publicly on Friday May 31st, 2024 at 14:00.

Student number:	4667107	
Project duration:	April 3rd, 2023 – May 31st, 2024	
Thesis committee:	Dr. E. Mooij	TU Delft, Chair
	Dr. A. Cervone	TU Delft, Supervisor
	Dr. S. Vincent-Bonnieu	European Space Agency, Supervisor
	Dr. J. Guo	TU Delft

Cover: Orion for Artemis II, by Lockheed Martin [1]

An electronic version of this thesis is available at http://repository.tudelft.nl/.

TU Delft

Preface

The work presented in this report is the culmination of a thesis research carried out as the final part of a Master of Science in Aerospace Engineering at the Delft University of Technology, specifically within the specialization of Space Systems Engineering.

The exploration of space beyond Earth has always been my greatest fascination and now that humanity has set its sights back on the Moon, we may finally be at the dawn of a permanent human presence on the Lunar surface. Yet simultaneously, my studies have made me increasingly aware of our responsibility to explore space in a sustainable manner. The ever growing space debris problem has spiraled to a point where we can no longer turn a blind eye. When it came to writing my thesis, I always wanted to address a practical problem within the context of space exploration, while maintaining a broad mission overview rather than diving into minute details. The innovative topic of space debris recycling has given me that chance to utilize my broad education and to think outside of the box in order to propose feasible mission concepts. Despite being challenging and sometimes deeply confusing, it has been an incredibly rewarding experience.

I would like to thank my two supervisors, Dr. Angelo Cervone (TU Delft) and Dr. Sebastien Vincent-Bonnieu (ESA) for their continuous guidance, patience and expertise. I truly appreciated the freedom and encouragement to tackle this complex problem from various angles. Additionally, I would like to thank the European Space Agency for the incredible opportunity to work on-site at the European Space Research and Technology Centre (ESTEC) for 9 months, which has been the defining experience of my student career. My thanks therefore also go out to the numerous ESA staff members with whom I've had the pleasure of collaborating. I would also like to thank my friends and family, which despite being across the country never ceased to support my efforts to finish this academic journey. In particular, I want to thank my mother, whose unwavering support and unyielding resolve have been the light in many dark days throughout not just this thesis, but my life in general. Without her I would have never gotten this far.

Yannick Heumassej
Delft, May 2024

"Our planet is a lonely speck in the great enveloping cosmic dark. In our obscurity, in all this vastness, there is no hint that help will come from elsewhere, to save us... from ourselves."

- Dr. Carl Sagan (1994) [2]

Abstract

This study proposes the novel concept of recycling space debris as a means of supplying material resources for the establishment of a permanent Lunar presence while simultaneously cleaning up Earth's orbital environment. This expands the scope of traditional debris mitigation efforts, which focus only on removing debris. As a first step, the study presents the creation of a space debris database. A novel classification is made to characterize space debris in terms of material resources and reserves usable for recycling. It is concluded that plentiful defunct upper stages currently drift in Geostationary Transfer Orbits (GTO), presenting substantial risk to other space assets. Their high relative metal content and elliptical orbits make these stages prime candidates for an efficient transfer to the Moon using an Orbital Transfer Vehicle. But as various perturbations have shifted the orbits of upper stages in GTO over the years, the orbital transfer alignment is found to be a critical complexity for a recycling mission. Several mission scenarios are analysed from debris capture to processing on the Lunar surface. The total energy expenditure across the entire mission is used as a novel tool to characterize and compare these scenarios to one another and to the alternative: a direct material delivery mission featuring ESA's Argonaut lander. By harnessing the unique advantages of electric propulsion, this study shows that the concept of recycling defunct rocket stages is both feasible and viable. A direct, single-target recycling mission shows potential to require 30% lower energy investment per kg of raw material delivered compared to a standard lander mission. A novel thrust-arcing trajectory solves the alignment problem through flexible steering of the apogee to facilitate a Lunar encounter at minimal performance cost. Factoring in the potential to spread launch energy expenditure through a secondary client in a rideshare configuration results in an increase to over 60% less energy investment per kg. A preliminary analysis shows that even greater efficiencies could potentially be achieved through a continuous mission that returns multiple upper stage.

Ultimately, the novel concept of coupling space debris mitigation to advancing long-term Lunar exploration presented in this study shows significant potential and warrants further study. Moreover, a comprehensive analysis of the energy cycle highlights the potential for improved energy efficiency over conventional lander missions. Finally, the use of global energy expenditure as a tool for relative analysis shows potential as an adequate means of analysing space missions featuring distinct segments.

Executive Summary

For the first time since the end of the Apollo program in 1972, mankind has set its sights back onto the Moon. This time with the intent to stay. Spearheaded by the Artemis programme, the establishment of a permanent human presence on the Moon is a crucial milestone for the advancement of human space exploration. Yet despite this renewed vision and the enormous technological advancements in recent decades, the continued exploitation of space has also created a significant danger. The massive growth of the space industry in recent history has caused an exponential increase in the total number of satellites launched each year, which has turned space debris from an afterthought to one of the space industry's most critical problems. Despite continued efforts to reduce the impact of space debris and safeguard Earth's orbital environment, long-term sustainable debris mitigation strategies remain an essential need for the future. But while the majority of currently established efforts focus strictly on the removal of debris, space debris could potentially be leveraged as an invaluable source of raw material resources. Resources that could be an invaluable supplement for the establishment and continued growth of a permanent Lunar presence, as launching the required raw materials to the Lunar surface would be an incredibly costly and energy-intensive endeavour, even when considering the recent advancements in the launch industry. The recycling of space debris could alleviate these downsides while being more readily achievable than proposed in-situ resource utilization efforts, making it an attractive stepping stone.

The recycling of space debris is a novel concept that remains relatively unexplored within the context of Lunar exploration activities. As such, the aim of this study is to gain a gain an understanding of the energy cycle of a space debris recycling mission specifically for Lunar applications and to lay out the framework for such a mission, by designing and optimizing an energy-efficient space debris recycling mission concept, analyzing several different mission scenarios. The study is governed by the primary research question: How can space debris be recycled to create an energetically viable means of supplying raw material resources for the establishment and growth of a permanent human presence on the Moon? Considering viability depends on feasibility, the analyses performed throughout this study also focus on the underlying question regarding whether a space debris recycling mission is a feasible endeavor. Through the definition of embodied energy cost as a defining metric, a consistent analysis can be maintained across the various mission phases. This, combined with traditional metrics used for the assessment of space missions, such as mass and power constraints, results in a holistic overview of the space debris recycling mission concept, balancing both feasibility and viability.

A comprehensive literature review forms the basis of the study, which began with the generation of a detailed database of all space debris currently in orbit around Earth. The DISCOS database, published and maintained by ESA, was used as the primary resource for the generation of this dataset, with supplementary resources being leveraged to ensure a comprehensive view of all space debris sources. Analysis of the constructed database revealed that a total debris mass of approximately 6887.4 tons currently orbits Earth. Defunct rocket bodies make up the majority of the debris at a mass fraction of 58.1%, with inactive satellites and other miscellaneous debris objects making up the remaining 39.5% and 2.4%, respectively. Through the gathering and analysis of orbital tracking data, it was found hat the majority of debris mass is clustered around three main orbital regions, these being Low Earth Orbit (LEO), Geostationary Transfer Orbit (GTO) and Geosynchronous Equatorial Orbit (GEO). While the established 25-year rule for the mitigation of debris in LEO has been a great step in the right direction, over 65% of the total debris mass drifts in higher altitude orbits with significantly longer lifetimes. The concept of resources and reserves, commonly used in terrestrial geology, was translated to space-based resources and applied to the space debris dataset to highlight potential targets and identify the principle constraints, which revealed that a substantial part of the identified space debris resources can be considered reserves within the context of a European mission. Old European rocket bodies and inactive commercial GEO satellites are the two main space debris target classes that define the recoverable reserves, representing a total recoverable mass of 1629.8 tons.

A comprehensive trade-off process was performed to determine the most optimal space debris target class within these two proposed space debris target. Active collaboration with senior ESA and TU Delft staff was undertaken to determine criteria weighting through an Analytic Hierarchy Process (AHP). Based on the assessment of debris risk, availability, transfer energy cost, raw material return potential and over-

all mission complexity, it is concluded that defunct Ariane 4 and 5 upper stages drifting in GTO represent the ideal targets for a space debris recycling mission. This is based primarily on the fact that these upper stages threaten both the highly populated LEO region at their apogee as well as the critically important Geostationary ring combined with their significantly greater raw material return potential due to a high recoverable material fraction of up to 60%. Tumbling rates remain a potentially problematic aspect for any kind of space debris recovery mission. However, through analyzing the evolution of rotational periods based on light curve measurements, it was found that effectively all defunct upper stages in GTO are slowing down exponentially as a result of the perturbing forces acting upon them. This opens up the potential feasible target pool for feasible capture over time. Inactive GEO satellites alternatively present a less complex and more stable target in terms of capture and orbital transfer, though this advantage does not make up for the lack of incentive for their active removal and their low raw material return potential.

Alongside the proposed recycling of space debris, using a conventional Lunar lander presents a more direct and readily accessible alternative when considering the supply of raw materials to the Lunar surface. As such, ESA's Argonaut lander was defined as the principle alternative for direct comparison regarding the performance and viability of the proposed space debris recycling mission concepts while maintaining the vision of European autonomy. The space debris recovery and recycling mission was broken up into three distinct mission phases: the Earth phase, Space phase and Lunar phase. The Earth phase is primarily defined by the launch. Utilizing Ariane 6 as Europe's principle heavy lift launch vehicle, launch dominates the global mission energy analysis with an estimated total energy expenditure of 5.893 TJ in its Ariane 64 configuration making up as much as 99% of the total mission-wide energy cost in some scenarios. The Lunar phase is defined by material processing and utilization. Reducing complexity is key in this regard, as operations must ideally be as approachable and reliable as the recycling infrastructure is operated at least semi-autonomously. In this light, the Moon presents the ideal location for the establishment and operation of a recycling infrastructure due to the presence of gravity and the wealth of space available, both of which allow for the translation and implementation of well-understood technologies from the recycling industry on Earth. Solar-electric induction furnaces are proposed as an efficient material re-melting method that could readily be translated to the vacuum conditions of the Lunar surface. Finally, the debris is cast either in existing molds or in the Lunar regolith itself to form feedstock material which can readily be stored on the Lunar surface and can be utilized for a large variety of subsequent manufacturing processes whenever required. This creates an inherent degree of flexibility and scalability which allows the recycling infrastructure to evolve with a growing human presence on the Moon. While the alternative, direct material delivery mission using the Argonaut lander does not require these recycling operations, the manufacturing of the associated raw material that makes up its payload is also analyzed.

The transfer from Earth orbit to cis-Lunar space is facilitated by a proposed Space Debris Servicing Vehicle (SDSV), an Orbital Transfer Vehicle (OTV) capable of capturing and transporting defunct upper stages in GTO. The use of robotic arms or nozzle probing is highlighted as ways of securing debris targets, with the latter being the most likely candidate technology to ensure a robust and strong connection between the SDSV and the debris target in order to form a combined system stack. Several orbital transfer scenarios, propulsion architectures and upper stage debris targets were explored and analyzed to identify and assess the performance and constraints for an efficient and feasible transfer. Single-target missions are the ideal starting point for a debris recycling mission concept given the innovative nature of the mission. A zero-patched conics approach was used for the assessment of the orbital mechanics and the determination of the required ΔV for the relevant manoeuvres. Within the identified target pool of Ariane upper stages in GTO, the Ariane 4/5 H10 (1764 kg) and Ariane 5 ESC-A (5000 kg) make up a total of 90 potential targets for recovery and recycling. Given that these objects are already in orbit, the larger mass of the ESC-A has little impact on the SDSV launch mass, which combined with a greater frequency of 63 objects in orbit makes it the ideal target for a space debris recycling mission. But as various perturbations have shifted the orbits of upper stages in GTO over the years, conventional assumptions for Lunar transfers must be reconsidered and assessing the orbital alignment, transfer cadence and individual target priority are nontrivial. So much so that the problem of orbital transfer alignment was found to be one of the key complexities involved for a space debris recycling mission.

Two feasible orbital transfer architectures were found through the applied analysis. Through the solving of the alignment problem and specific debris target selection, these transfer architectures allow for flexible and reliable mission cadence for any initial orbital conditions. The first of these is based on a conventional, direct Lunar transfer utilizing a completely chemical propulsion system, which was studied as a baseline option. Such a transfer presents the potential to leverage the high perigee velocity of the GTO debris orbit

for an efficient transfer. It was found that given any initial conditions for the Argument of Periapsis (AoP) and Right Ascension of the Ascending Node (RAAN) of a piece of debris and the standing of the Moon, two unique points exist which can be reached by using the natural J2 drift in order to facilitate the orbital transfer alignment with little to no performance cost other than an increased mission time of at most 380 days. The introduction of intermediate circular ”staging” orbits was explored as additional mission scenarios in order to reduce the large potential waiting times in the Van Allen belts. However, neither circularizing into LEO at perigee or into GEO at apogee was found to be feasible due to the excessive propellant requirements for the staging orbit injection manoeuvres. The second feasible orbital transfer architecture revolves around the implementation of low-thrust, Solar electric propulsion for the main orbit-raising manoeuvre in a hybrid propulsion architecture. This low-thrust manoeuvre was designed and analyzed using the FreeFlyer orbital simulation suite. The high specific impulse inherent of electric propulsion systems yields a substantial decrease a in propellant mass though comes at the cost of a significantly longer flight time depending on the thruster layout used. In order to facilitate the orbital alignment for a Lunar encounter, a thrust-arcing strategy is utilized which can shift the apogee passage point can be shifted within the orbital plane even in the worst case where a complete 180° shift is required. For both of these feasible mission scenarios, the combined stack of the SDSV and the captured ESC-A upper stage debris target are crashed onto the Lunar surface following a controlled retro-propulsive termination burn to slow down its velocity to 1200 m/s before impact, disintegrating it into scrap fragments to be recycled.

By compiling the analyses of all mission phases into a global mission energy analysis, the highlighted space debris recycling scenarios were directly compared to eachother as well as the alternative Argonaut mission scenario in order to assess the complete mission viability. Through this analysis, it is shown that space debris recycling missions are significantly more efficient. When comparing the total embodied energy cost per kg of raw material, the direct, chemical transfer mission scenario and the low-thrust hybrid transfer mission scenario yield values of 1.980 GJ/kg and 1.973 GJ/kg, respectively compared to the 3.047 GJ/kg associated with the Argonaut. Though while the Argonaut requires a dedicated launch of Ariane 64, this is not the case for the debris recycling mission concepts. Capturing payload mass in orbit circumvents the strict launch mass restrictions as a constraining factor for conventional Moon missions and yields a substantial margin of leftover launch vehicle payload mass capacity. This allows for the introduction of a secondary client in a rideshare configuration, distributing launch energy and significantly reducing the influence of the launch as the dominant energy sink. This reduces the total embodied energy cost per kg of raw material to 1.52 GJ/kg and 1.20 GJ/kg for the direct, chemical transfer mission scenario and the low-thrust hybrid transfer mission scenario, respectively. Compared to the Argonaut, this is a reduction of 50% and 61%, respectively. Beyond assessing single-target missions, a preliminary analysis was performed for multi-target missions. Spreading the transfer functionality over a dedicated debris transfer landing vehicle alongside the debris transfer vehicle is proposed to account for the additional required performance for the return journey from cis-Lunar space back to Earth. While such a continuous mission is subject to numerous substantial assumptions, it highlights the potential for even greater efficiency gains as it only requires a single launch to capture several targets.

Ultimately, this study has addressed the innovative mission concept of recycling space debris. By assessing the complete process chain, establishing a general mission framework and analyzing several different mission scenarios, a better understanding of the global mission energy expenditure was achieved. Ultimately, though no single definitive conclusion covers the complexity and novelty of the problem, this study has proven that strong potential exists for a space debris recycling mission to be both feasible and viable as a means of supplying raw material resources to the Lunar surface with substantially increased energy efficiency compared to a conventional Lunar lander mission. The findings presented in this study, both in terms of mission feasibility and viability, show that the concept of space debris recycling warrants further study. Furthermore, the concept of recycling space debris allows for the creation of value which traditional space debris mitigation measures have critically lacked. Fundamental mission constraints such as the existing legal framework are mitigated at least in part by targeting old Ariane upper stages, which makes the vision of European autonomy not only possible but potentially desirable. The work presented in this study establishes a baseline of fundamental knowledge for future studies to build off of and foster a more sustainable, safe way of dealing with our precious orbital environment, ensuring the potential for space exploration for generations to come.

Contents

List of Figures

List of Tables

Nomenclature

Abbreviations

Abbreviation	Definition
AA	Aluminium Alloy
ADN	Ammonium Dinitramide
AEPS	Advanced electric Propulsion system
AHP	Analytical Hierarchy Process
AoP	Argument of Periapsis
API	Application Programming Interface
ATV	Automated Transfer Vehicle
BHT	Busek Hall Thruster
CDF	Concurrent Design Facility
CNES	Centre National d'Études Spatiales
CONOPS	Concept of Operations
CR	Consistency Ratio
DISCOS	Database and Information System Characterising Objects in Space
EAC	European Astronaut Centre
ECA	Evolution Cryotechnique type A
EL3	European Large Logistics Lander
EoL	End-of-Life
EPS	Étage à Propergols Stockables
ESA	European Space Agency
ESC-A	Etage Supérieur Cryotechnique de type A
ESM	European Service Module
ESOC	European Space Operations Centre
ESTEC	European Space Research and Technology Centre
GEO	Geosynchronous Earth Orbit
GTO	Geostationary Transfer Orbit
HAN	Hydroxyl-Ammonium Nitrate
HTPB	Hydroxyl-Terminated Polybutadiene
IADC	Inter-Agency Space Debris Coordination Committee
IBS	Ion Beam Shepherds
ISRO	Indian Space Research Organization
ISRU	In-Situ Resource Utilization
ITT	Invitation To Tender
JANAF	Join Army-Navy-Air Force
LCA	Life Cycle Assessment
LEO	Low-Earth Orbit
LEOP	Launch and Early Operations
LH2	Liquid Hydrogen
LLPM	Lower Liquid Propulsion Module
LOX	Liquid Oxygen
LRO	Lunar Reconnaissance Orbiter
LTO	Lunar Transfer Orbit
MEV	Mission Extension Vehicle
MMH	Monomethyl Hydrazine
MMT	MiniMegaTORTORA
MON-3	Mixed Oxides of Nitrogen (3% Nitric Oxide)
MORO	Moon Orbiting Observatory
NASA	National Aeronautics and Space Administration

NIST	National Institute of Standards of Technology
NORAD	North American Aerospace Defense Command
NTO	Nitrogen Tetroxide
OF	Oxidizer to Fuel Ratio
OHRC	Orbiter High Resolution Camera
OTV	Orbital Transfer Vehicle
PPE	Power and Propulsion Element
PSR	Permanently Shadowed Regions
RAAN	Right Ascension of the Ascending Node
SDSV	Space Debris Servicing Vehicle
SLS	Space Launch System
SMAD	Space Mission Analysis and Design
SMART	Small Mission for Advanced Research in Technology
SSA	Space Situational Awareness
TLE	Two-Line Element
TLI	Trans-Lunar Injection
UCS	Union of Concerned Scientists
ULPM	Upper Liquid Propulsion Module
US	United States
USA	United States of America
VNB	Velocity, Normal & Binormal

Symbols

Symbol	Definition	Unit
a	Semi-major axis	[km]
C_p	Specific heat coefficient	[J/kg-K]
e	Eccentricity	[-]
E	Energy	[J]
g_0	Earth surface gravitational acceleration	[m/s^2]
h	Altitude	[km]
H	Enthalpy	[J]
i	Inclination	[deg]
I_{sp}	Specific impulse	[s]
J	Legendre polynomial coefficient	[-]
M	Mass	[kg]
n	Mean motion	[rad/s]
p	Semi-latus rectum	[km]
P	Power	[W]
Q	Heat	[J]
r	Orbital radius	[km]
R	Planetary radius	[km]
t	Time	[s]
T	Orbital period	[s]
ΔV	Velocity increment	[km/s]
δ	Sensitivity analysis performance modifier	[-]
ϵ	Specific orbital energy	[km^2/s^2]
η	Efficiency	[-]
μ	Gravitational parameter	[km^3/s^2]
ω	Argument of periapsis	[deg]
$\bar{\omega}$	Longitude of periapsis	[deg]
Ω	Right Ascension of the Ascending Node	[deg]

1 Introduction

Ever since the dawn of the space age in the early 1950's, humanity has set its sights on the sky. However, in the efforts to both explore and commercialize the space environment, it has gotten polluted. Old rocket stages and defunct satellites now litter the space around Earth. The implications of such debris were only identified in 1978, when Kessler and Cour-Palais [3] highlighted that an increasing number of objects in orbit would create the threat of a chain reaction of collisions that could jeopardize access and utilization of space for generations: the Kessler syndrome [4]. More recently, the concept of space debris removal missions has gained significant traction in both the institutional as well as the commercial world [5], as estimations indicate more than 128 000 000 objects larger than 1 mm to be in orbit at present [6]. With the exponential growth of the space industry as a whole, long-term sustainable debris mitigation strategies are an essential need for the future. Though while the vast majority of the currently established debris mitigation efforts focus strictly on the removal of debris, the notion that space debris could be leveraged as a material resource is relatively unexplored. Indeed, space debris could prove to be an invaluable material resource for further space exploration activities.

Simultaneously, the human exploration of the Moon is receiving increasing amounts of interest spearheaded by NASA's Artemis programme [7]. Establishing a permanent human presence on the Moon is a crucial milestone for the advancement of human space exploration. However, the building of a Lunar base is an enormous effort that would likely require a large amount of materials. Launching such materials to the Moon is incredibly costly, even when considering the recent advancements in the launch industry. The utilization of space debris could be a potential source of highly refined, space-grade materials [8, 9]. In this way, the space debris problem as well as the Lunar resource problem could be tackled simultaneously. However, the recycling of space debris especially for Lunar applications is a novel concept that would require advanced capturing, transferring and processing techniques. This thesis research will focus on gaining a better understanding of the energy cycles involved in the space debris recycling process specifically regarding Lunar applications, while laying the foundation for future studies in this novel field. Additionally, the intent is to assess also the overall viability of such a mission as well as to give a series of recommendations for the European Space Agency (ESA) to advance its efforts into establishing a sustainable space ecosystem.

The study presented in this report will begin with an elaboration of the study definition, a general background of the research problem and an explanation of the research question and study objectives in Chapter 2. This chapter will also include a brief summary of the literature review study performed prior to the study presented in this report. Chapter 3 will detail the determination of the optimal space debris target for a recycling mission through a comprehensive trade-off. With the target defined, a number of mission-critical input variables are known, which allows for the definition of a mission architecture in Chapter 4. Subsequently, Chapter 5 and 6 will detail the main mission design and perform energy analyses for each of the main mission segments through the exploration of several different mission scenarios. The results of these analyses will be compiled in a global mission energy analysis in Chapter 7. Finally, all of the acquired knowledge is condensed to answer the main research questions and form a conclusion in Chapter 8, which will include a number of recommendations for further study.

2

Study Definition, Background & Objectives

Before diving into any mission design and analysis efforts regarding the concept of recycling space debris for Lunar applications, this chapter serves to establish the definition, background and general objectives of the study. The objectives of the study will be highlighted by introducing the two main research problems, after which a research objective and associated research question are formulated. Finally, a brief summary of the literature review work preceding this thesis research will be given.

2.1. Background & Problem Definition

The study detailed in this report presents a complete Master Thesis written as the final part of the Space Systems Engineering Master within the Aerospace Engineering Master programme at the Delft University of Technology. The thesis was co-supervised by the European Space Agency (ESA), which offered the opportunity of working on-site at the European Space Research and Technology Centre (ESTEC) in Noordwijk for 9 months through an internship. The goal of this study was to investigate the concept of space debris recycling, tackles two main research areas that have seen a large growth in interest within the space industry in recent years. A brief background on these two areas is detailed below in order to highlight the motivation and significance of this study.

2.1.1. The Space Debris Problem

Space debris is defined by the Inter-Agency Space Debris Coordination Committee (IADC) as ”all human made objects including fragments and elements thereof, in Earth orbit or re-entering the atmosphere, that are non-functional” [10]. By this definition, space debris is anthropogenic in nature. The presence of space debris can be traced back to the very beginning of the Space Age in the early 1950’s. During these early days of the space industry, what happened to satellites after they reached the end of their operational lifetime was generally found to be of little concern. Only in 1978 were the implications and especially the dangers of long-term debris buildup identified by Kessler and Cour-Palais [3]. In their now famous manuscript, they highlighted the threat of what was later dubbed the Kessler Syndrome [4]: a chain reaction of collisions that could jeopardize humanity’s access to space entirely. The massive growth of the commercial space industry in recent history has seen to an exponential increase in the total number of satellite launches each year, which has turned space debris from an afterthought to one of the space industry’s most critical problems. At the moment of writing this report, it is estimated that over 34 000 objects larger than 10 cm are currently in orbit, and over 900 000 objects larger than 1 cm [6].

One of the most successful partial solutions to the space debris problem that has been implemented in recent history is the 25-year guideline mandated by the IADC. This guideline requires satellites to be de-orbited within 25 years after the end of their operational lifetime. For Low-Earth Orbit (LEO), defined by the IADC as any orbit with an altitude below 2000 km [10], this is done through atmospheric re-entry often facilitated by a final propulsive manoeuvre at End-of-Life (EoL). For higher orbits however, the notion of ”de-orbiting” entails merely the removal of the satellite from its operational orbit. The principle case in which this applies is the Geosynchronous Earth Orbit (GEO), which is an equatorial orbit at 35 786 km altitude featuring an orbital period of exactly 24 hours. For this vital region of space, atmospheric re-entry is generally not possible due to the propellant cost involved. Instead, the IADC mandates that satellites must

raise their orbit by at least 235 km into a so-called graveyard orbit in order to ensure they do not re-enter the GEO ring for at least 100 years [10]. However, this is ultimately not a long-term sustainable solution as objects with an altitude over 1000 km generally have orbital lifetimes of over 1000 years [11]. New solutions are a necessity for the containment of the space debris problem. ESA is one of the leading organizations exploring such solutions through its Zero Debris debris approach. As of November 2023, ESA's updated policy and requirements on the mitigation of space debris have gone into effect [12, 13]. One of the principle mandates in this policy is the fact that the previously established 25-year rule for spacecraft disposal has been reduced to a maximum of 5 years [13].

Active debris removal is one of those proposed solutions in which, as the name implies, space debris is actively removed from orbit. The European Space Agency is one of the acting space agencies in this field with the first active debris removal mission, ClearSpace-1, set to launch in 2026 [14]. However, such space debris removal missions generally target debris in LEO and focus only on the removal of debris from orbit through atmospheric re-entry. One of the defining problems of such space debris mitigation missions has therefore always been a lack of inherent monetary value to the space industry and its operators. After all, satellites are effectively worthless at the end of their operational lifetime, so investing strictly in their removal is something that is only pursued by space agencies. The concept of recycling space debris however presents a route to this desired value for space debris mitigation missions. Though instead of monetary value, the value is presented in the form of material resources.

2.1.2. Lunar Exploration & Permanent Settlement

After the end of the Apollo program 1972, interest in the Moon had dwindled significantly due to the lack of funding after the incentive of the Space Race died down. For several decades there were hardly any missions to the Moon, until in the early 90's multiple nations set their sights back on the Moon [15]. China and Japan saw successful missions to the Moon, with ESA following suit in 2003. India followed in 2008 with Chandrayaan-1. However, the prospect of a Lunar lander wouldn't be attempted until 2013, when China successfully landed Chang'e-3 along with its Yutu rover. Ever since the early 2000's there has been a steady stream of new missions seeking to explore the Moon in many different ways. A particularly interesting development has been the Israeli Beresheet lander, which was largely privately funded, indicating that the commercial industry has began to actualize its interest in the Moon [15].

The single most impactful development that really has rekindled the desire for Lunar exploration is the Artemis program. This program is led by NASA with the intention of returning humans to the Moon for the first time since the end of the Apollo program. The Lunar Gateway is an integral part of the Artemis Program. The Gateway is a planned space station around the Moon that will operate as a staging ground for human activities on the Lunar surface [16]. One of the long-term goals of the Artemis program is the establishment of a permanent Lunar base, both for scientific endeavors and as an eventual forward outputs for for human missions to Mars [16]. The establishment and operation of such a permanent Lunar settlement will be the single most ambitious project in the history of human space flight. Even with the collaboration of many of the world's space agencies, it will likely take numerous years and dozens of intermittent missions to set up even a temporary human settlement [7]. While the ultimate goal is to create a self-sustainable human presence on the Moon, the initial stages will inevitably be highly dependent on resources sent from Earth. All of this will require a vast amount of material resources, much of which will be in the form of raw material resources in order to allow flexible expansion and in-situ construction. The south pole (specifically the Shackleton crater) has been identified as the primary location for a permanent Lunar base because of the presence of water in the form of ice in Permanently Shadowed Regions (PSR) [16]. The return to the Moon is an integral part of the European Space Agency's (ESA) vision. Alongside various European national space agencies, ESA is committed to several Moon exploration missions, including the exploration of local resources. Ultimately, Lunar exploration has seen a resurgence in interest both from the institutional as well as the commercial world, with as common goal the establishing of a permanent human presence on the Moon.

2.2. Research Questions & Objectives

The recycling of space debris within the context of Lunar exploration applications presents a novel and innovative concept which remains a rather unexplored topic. Given the broad scope of the identified research areas, a clear definition of the problem sample to be studied is important to ensure the study is focused and that analyses can achieve the appropriate depth without getting lost in the various branches of the problem. The goal is not to dive into only a single aspect of the mission, but rather to study the premise of

recycling space debris on a higher level in order to establish a fundamental understanding of the entire mission concept. In order to convey this scope of the study, the research objective statement was formulated as follows:

> *To gain an understanding of the energy cycle of a space debris recycling mission specifically for Lunar applications and to lay out the framework for such a mission, by designing and optimizing an energy-efficient space debris recycling mission concept, analyzing several different mission scenarios.*

As seen from the objective statement above, energy was chosen as a defining metric by which to assess the various processes within a space debris recycling mission. Energy is a fundamental physical characteristic that can be traced to practically every physical process. This makes it an attractive metric to study for a mission that has various different segments that otherwise are difficult to connect together. Energy, particularly embodied energy, is a metric often used for the study and comparison of manufacturing processes [17]. A space debris recycling mission can in many ways be seen from the perspective of a manufacturing process rather than a traditional space mission. Hence, translating such an approach to assess recycling space debris from a global mission perspective has potential to be a promising tool for the assessment of multiple mission scenarios. The potential for recycling space debris to find traction depends entirely on the existence of incentive. A gain in energy efficiency compared to alternative concepts to deliver raw materials to the Moon could, if achievable, be an important first step to highlighting such potential. Through the definition of a global mission energy expenditure as a defining metric, a consistent analysis can be achieved in which several mission scenarios can be compared by a single variable. This leads directly to the main research question, which was defined as follows.

> ***Research question:***
>
> *How can space debris be recycled to create an energetically viable means of supplying raw material resources for the establishment and growth of a permanent human presence on the Moon?*

This research question reflects the more high-level research objective as well as the use of energy as a connecting variable between the various mission scenarios and the different mission phases within those scenarios. The definition of viability is drawn from an energy point of view. Viability in the context of recycling space debris highlights the need for a specific reference mission scenario to be compared against. It was therefore chosen to define an alternative mission scenario, with viability being primarily judged on a basis of energy investment required for a given mass of raw material returned. Additionally, feasibility is a prerequisite matter that should be analyzed before viability. For if a mission cannot be performed altogether, a hypothetical viability loses much of its meaning as the mission cannot be considered. As such, the analyses performed throughout this study will also focus on the underlying question regarding whether a space debris recycling mission is a feasible endeavor. More traditional metrics used for the assessment of space missions, such as mass and power constraints, will also be used here. While viability depends on feasibility, these two concepts can also contradict one another, as the most energy-efficient mission scenario is not necessarily the most favourable one. Striving for ever increased energy efficiency can lead to unrealistic mission requirements or reliance on unreasonable assumptions. As such, the mission design process will contain a balancing act between viability and feasibility. By looking at both perspectives, a holistic view of the space debris recycling mission concept can be achieved. In order to structure the research and formulate comprehensive conclusions, a number of sub-questions were established, which are defined as follows.

> ***Research sub-questions:***
>
> *1. What is the most suitable space debris target for a recycling mission?*
>
> *2. What is the the complete process chain for a space debris recycling mission?*
>
> *3. What are the major challenges and roadblocks to overcome for a space debris recycling mission?*
>
> *4. In what ways can a space debris recycling mission be optimized for increased energy efficiency?*
>
> *5. What aspects of a space debris recycling mission can justify an increased energy expense?*
>
> *6. How can a space debris recycling mission evolve to continuously suit a growing human presence on the Moon?*

The first three of these questions primarily serve to break down the main research question, targeting considerations regarding ideal target choice and detailing the complete process chain as well as the major fundamental challenges to overcome. Determine the ideal space debris target is an especially important matter as it defines most of the input parameters for the various subsequent steps in the process cycle. The latter three sub-questions serve primarily to provide additional meaningful depth. This includes expanding on the balance of viability and feasibility highlighted earlier.

2.3. Literature Study Outcomes

Prior to the main thesis research, a comprehensive literature review was performed. This document details the compilation and assessment of literature relevant to the specific thesis topic and effectively lays the groundwork for the main thesis work to be performed. This section summarizes the most important findings of the performed literature review and serves to provide a foundational baseline of knowledge to contextualize the work detailed in this study [18]. Additional information from the literature study beyond what is listed in this section will be referenced throughout this report whenever relevant.

As a first step in the literature research process, a detailed database was generated of space debris currently in orbit. The foundation of this database was the DISCOS database published and maintained by ESA's Space Debris Office, which presents an exhaustive reference that archives relevant information on all objects that have ever been launched [19]. A Python script was written to access, filter and compile relevant data through the Automated Programming Interface (API). Alongside the DISCOS database, several additional sources such as the CeleStrak database [20] were used as supplementary resources to account also for the inactive satellites that make up a distinct portion of the space debris population and thus create a comprehensive dataset. Through the generation of this dataset, it was found that a total debris mass of 6887.4 metric tons orbits Earth as of the writing of this report. A summary of the total space debris mass distribution is tabulated in Table 2.1. The "Miscellaneous" category was defined as a grouping term for a wide variety of objects that are typically of relatively low mass, including payload adapters, deployment rails, radiator covers, heat shields, de-spin weights etc.

Table 2.1: Summarized breakdown of the combined space debris dataset.

Space debris category	Mass [tons]	Mass fraction [%]
Inactive payloads	2719.5	39.5
Other debris	4167.9	60.5
• Rocket bodies	4002.5	58.1
• Miscellaneous	165.4	2.4
Total	6887.4	100

It can be seen that defunct rocket bodies make up the majority of the space debris mass at a mass fraction of nearly 60%. Within these rocket bodies, it was found that the Kosmos-3M upper stage, Ariane 5 ESC-A upper stage and Blok-DM-2 upper stage are the three largest contributors with total individual debris masses of 409.7, 380.1 and 227.8 tons, respectively. This means that many of these identical upper stages exist in orbit, exceeding tens or even hundreds of instances depending on the specific object. With regards to long-term applicability, such large individual object frequencies were considered a key advantage for the target selection as it would allow for the execution of the same mission over multiple targets with minimal modifications required. Following the generation of this space debris dataset, the objects were mapped in space by using orbital tracking data. Specifically, NORAD Two-Line Elements (TLE) sets were used to extract the main orbital elements for every object within the generated space debris dataset. Since this orbital tracking data is updated regularly, it is important to note that the data used for this study was collected and archived as of the 16th of May 2023. Figure 2.1 shows the results of this orbital mapping analysis [18].

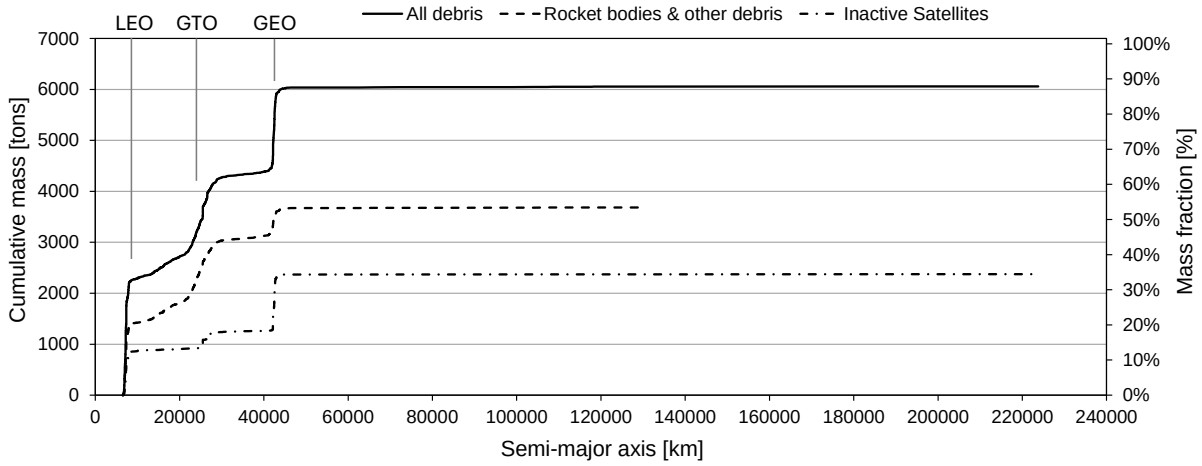

Figure 2.1: Cumulative mass distribution of the space debris dataset in terms of the semi-major axis of their orbits. [18]

From Figure 2.1, it can be seen space debris is clustered around three main orbital regions, which correspond to Low-Earth Orbit (LEO), Geostationary Transfer Orbit (GTO) and Geosynchronous Earth Orbit (GEO). Where debris in LEO and GEO includes a larger frequency of satellites, the GTO region inbetween is populated primarily by the defunct rocket upper stages that make up the majority of total debris mass. Debris in orbits higher than GEO is present, but represents such little mass that it cannot be seen at the scale of the graph presented in Figure 2.1. A total debris mass of approximately 21 tons orbits at semi-major axis values above 60 000 km, which includes objects such as the Vela satellites, two Titan IIIC transtages and the Explorer 47 satellite at the very end of the graph with a semi-major axis of over 223 000 km. Though despite being by far the most popular region for space flight, the amount of debris in LEO is not proportional to sheer volume of satellites primarily. This discrepancy is a result of the inherently lower lifetime of LEO satellites due to the larger atmospheric drag associated with such low orbital altitudes limiting the accumulation of space debris, as well as the 25-year rule mandated by the Inter-Agency Space Debris Coordination Committee (IADC) [10]. But while this established 25-year rule has been a substantial step in limiting the amount of new debris accumulating in LEO, it does not extend to higher orbits with much longer orbital lifetimes, which were found to contain over 65% of the total space debris mass. With debris piling up since the early 60's, even the geostationary graveyard orbit will not be a sustainable solution for much longer given that it was defined specifically to prevent re-entry into the geostationary ring for 100 years. The results shown in Figure 2.1 highlight the need for revised long-term debris mitigation strategies specifically for higher orbits, as the total debris mass is threatening to exceed even that in LEO.

The concept of resources and reserves was adopted from geology to assess considerations and constraints regarding the degree of recoverability of space debris targets and to highlight what part of the space debris population can realistically be targeted. The McKelvey diagram shown in Figure 2.2 summarizes the performed analyses and gives a complete overview of the resources and reserves within the context of a space debris recycling mission for Lunar applications [18]. Reserves are the subset of resources, in this case space debris, which are accessible and can be recovered. If this is not the case, that marks the specific space debris objects as nonviable resources. Additionally, resources can be demonstrated or inferred. For the space debris analysis, objects that are actively tracked and well understood were considered as demonstrated, whereas objects with uncertainty regarding their status, such as crashed satellites on the Moon, were labeled as inferred.

	Identified Resources			Undiscovered Resources	
	Demonstrated		Inferred	Probability Range	
	Measured	Indicated		Hypothetical	Speculative
Recoverable	Reserves - European rocket bodies - Inactive commercial GEO satellites 1629.8 tons		Inferred Reserves - Crashed satellites on the Moon - Defunct Lunar rovers & landers 188.8 tons*	- Launch failures - Lunar Gateway waste material - In-orbit energy collection systems (e.g. SOLARIS)	- In-orbit logistical infrastructure (e.g. propellant depots)
Nonviable	Nonviable Resources - Non-European objects - Military intelligence satellites - Scientific satellites - Objects in LEO - Objects not actively tracked 5257.6 tons		Inferred Nonviable Resources - Objects < 10 cm - Inactive Moon-orbiting satellites < 72.5 tons	- Objects < 10 cm - Future collision debris	- Military intelligence satellites

* includes non-European objects

Figure 2.2: McKelvey diagram of the space debris resources, in the context of a recycling mission for Lunar applications. [18]

Considering the study was performed in collaboration with ESA, the reserves were judged specifically from the viewpoint of European autonomy, which despite being the major bottleneck in terms of debris target choice still leaves an estimated 1629.8 tons of mass as potentially recoverable reserves. Another principle bottleneck was found to be the legal constraints regarding the recovery of space debris which are still determined by the Outer Space Treaty from 1967 [21]. A significantly updated legal framework for any sort of active space debris removal is therefore a necessity. For these reasons, any objects not belonging to European countries or being under European jurisdiction were considered nonviable resources. Military intelligence satellites were omitted for similar reasons [18]. Objects in LEO were excluded from the pool of prospective targets due to their substantially lower individual object masses and large distance from the Moon. Finally, a certain degree of target consistency is essential for long-term mission viability. Hence, scientific satellites were omitted given that they are mostly unique designs [18].

The scope of recycling space debris and its re-utilization can generally be classified into two categories. Directly re-using hardware such as antennas, batteries, solar arrays and propellant tanks, while attractive on the surface, is limited in applicability and presents numerous complexities. The high degree of standardization required and accessibility of hardware are simply not present within the space debris population. Rather, recycling raw materials from space debris is the more flexible and feasible application, as satellites and rocket stages contain significant masses of highly refined, space-grade aluminium that could serve a wealth of purposes especially in the early days of a Lunar settlement. In this way, recycling space debris provides a potentially easier way of accessing raw materials as compared to other proposed options such as In-Situ Resource Utilization (ISRU) efforts which are typically characterized by highly complex processes and excessive energy costs. Additionally, key alloying metals like zinc and copper are extremely scarce in the Lunar regolith, thus limiting the manufacturing of such high-performance alloys even if ISRU activities could reach an industrial scale. Particularly the casting of raw feedstock material was identified as a utilization strategy to provide long-term adaptability and scalability to a space debris recycling infrastructure. The presence of gravity in particular makes the Moon an ideal location for the establishment of such an infrastructure, avoiding many of the complexities involved for operating an orbital recycling station. Additionally, the vast space available on the Lunar surface presents great potential for creating a scalable infrastructure that could even be inspected and serviced continuously as it operates in tandem with a permanent human presence on the Moon.

3

Space Debris Target Selection

The choice of space debris target plays a critical role in the overall concept of a space debris recycling and utilization mission, as various characteristics of the space debris target serve as key input parameters for subsequent aspects of the mission. These characteristics include the mass of the debris, its orbital location, geometry, ownership and various other aspects, all of which either directly or indirectly influence key considerations to be taken into account in the mission design. In this chapter, the selection of the target space debris objects will be detailed through a collaborative trade-off process.

3.1. Trade-off Methodology

In order to determine the most suitable target for a space debris recycling mission, a trade-off was performed. In order to make the trade-off comprehensive but not excessively detailed and complicated at this first stage of the overall mission design, a more classical trade-off approach was chosen. In such a classical trade-off, concepts are assessed using relative scoring based on a set of predetermined, weighted trade-off criteria. The weights of these criteria were determined in a collaborative Analytical Hierarchy Process (AHP), which employs pairwise comparison between criteria to determine the global weights based on inputs from various participants. This approach will be explained further in subsection 3.1.3. Subsequently, the performance of the space debris targets was analysed and scored for each of the established criteria, resulting in a final cumulative score for every target.

3.1.1. Space Debris Target Class Options

The overall space debris resources and reserves currently in orbit around Earth were identified and analyzed in an extensive Literature Study performed prior to this thesis research [18]. This analysis highlighted two main 'classes' of objects as recoverable reserves for a space debris recycling mission within the imposed technical and legal constraints, these being European rocket bodies and inactive commercial GEO satellites. It was chosen to perform the trade-off based on these defined classes since the most critical parameters are all relatively the same between the various vehicles within each class, leaving additional freedom for the choice of a specific target within that class for the later mission design phases.

Considering the European rocket bodies currently drifting in space, the bulk of the mass is represented by old Ariane upper stages such as the Ariane 4 H10 and the Ariane 5 ESC-A. While some of these do drift in Low-Earth Orbit (LEO), the vast majority of these stages are in a Geostationary Transfer Orbit (GTO). It was highlighted already in the Literature Study that objects in high-energy orbits such as GTO and GEO would be ideal targets for recovery considering the majority of the energy required to launch for the Moon has already been delivered [18]. As such, it was chosen to omit any stages in LEO and focus on those present in GTO. Cumulatively, it was found that these European rocket stages in GTO make up a total mass of approximately 396.9 tons. Given their nature as rocket stages, these objects are quite heavy ranging from 1190 to 5000 kg per object depending on the particular stage and its respective configuration. This large mass is often coupled with a large volume, though in principle these objects are relatively simple in their geometry and material makeup. For the commercial GEO satellites, the range of options is inherently a lot wider considering the large variety of industry players involved. Numerous of these satellites however were observed to be based on the same general spacecraft bus architecture employed by key system integrators. Additionally, these commercial GEO satellites often belong to a larger fleet of similar satellites performing similar functions. It was found that over 670 inactive satellites currently drift in or around the

Geostationary ring, summing up to approximately 1104.1 tons. It should be noted however that not all of these satellites are commercial in nature, and therefore not all of them are potential targets, especially with the wealth of different operators involved. As such, targeting the larger commercial fleet operators would be the most realistic. Intelsat in particular was identified to be a suitable potential target fleet, with over 70 inactive satellites in Geostationary orbit and a previously proven willingness to participate in In-Orbit Servicing (IOS) missions through the successful MEV-1 and MEV-2 missions [18].

A brief summary of the main characteristics of the identified space debris target classes is given in Table 3.1. These characteristics will be expanded upon and explained more thoroughly during the analysis of the two space debris target classes. Note that for the GEO satellites, the Intelsat fleet was taken as a representative case with individual object masses depending heavily on the particular spacecraft bus. These are approximations of the average mass of these vehicles reported in the DISCOS database, with the Intelsat IV bus on the lower end (700 kg) and the newer Intelsat VII and VIII buses (up to 2200 kg) at the upper end.

Table 3.1: Summary of the two identified space debris target classes.

Characteristics	European GTO Rocket Stages	Commercial GEO Satellites
Total debris mass	396.6 tons	< 1104.1 tons
Single object mass	1190 - 5000 kg	700 - 2200 kg
Primary orbital region	GTO	GEO
Recycling material	Aluminium alloys	Aluminium alloys
Metal content	> 60% [9]	< 22%

3.1.2. Criteria Definition

In order to perform the trade-off, a number of trade-off criteria were defined based on which the space debris target classes would be assessed. When defining these criteria it was important to cover a relatively wide variety of characteristics in which the space debris target classes differed in a meaningful way. This ensured that any potential nuances, even at this preliminary level, were captured in the trade-off process. A set of five criteria were defined, which are explained below.

Risk posed by debris

Perhaps the most relevant characteristic of any piece of space debris is the inherent risk that it presents to other assets in space. This risk is relevant not only for actively used satellites, but also other pieces of debris, as potential collisions could create substantially more debris which could increase the overall threat of space debris exponentially if left unchecked. Within the context of any sort of space debris removal mission, clearing a piece of debris with a high associated risk is therefore a lot more beneficial. In this sense, this risk can directly be interpreted as the 'value' of removing a particular piece of space debris. Note therefore that a higher risk is considered 'better'. The overall risk a piece of space debris represents is influenced primarily by its orbit and the spatial density of other objects within this orbit, so a piece of debris in a 'congested' orbit presents a higher risk of collision than one in a relatively empty orbit.

Transfer energy cost

The energy expenditure of a space debris recycling mission is a critical aspect to consider when assessing the overall viability of such a mission. Transferring a piece of space debris from its orbit to the cis-lunar environment is one the principle energy sinks within the process cycle. The energy needed for this transfer is heavily dependent on the orbit of the debris, which was already defined previously. Even within the two defined space debris target classes, several general transfer strategies or 'paths' from the debris orbit to the Moon will be considered in order to assess efficiency and any potential operational implications.

Raw material return

The amount of recoverable raw material to be gained from a specific piece of debris can be interpreted as the value returned by the mission in a more tangible sense, on the Lunar surface. This criterion represents the total amount of potential raw material to be returned from a single object within the identified space debris target classes, as well as the quality of that material. As such, the raw material return is influenced by characteristics that are largely consistent between targets within a specific class, which include the mass fraction of recoverable material, the types of materials and the total recoverable mass per target object.

Mission complexity

This criterion represents the overall complexity of the mission, from capture to Lunar arrival. Complexity is a key driver in overall mission feasibility and viability, as an overly complex mission can prove especially difficult or even unrealistic to realize in the first place. Especially for an innovative mission such as space debris recycling particularly for Lunar applications, it was considered that the value of simplicity should be not be underrated. Complexity is an inherently broad term and is influenced by several aspects particularly relevant for this specific mission, such as the overall size and geometry of the debris, tumbling rates, potential infrastructure and mission integration. Note that this idea of complexity can also be interpreted as an inverse reliability, which may impact the viability of performing the mission multiple times over a longer period.

Debris availability

Finally, the availability of the debris was taken as the final trade-off criterion. The availability of debris was defined as an umbrella term for many practical aspects regarding the potential of acquiring a certain piece of debris in the first place, both on the short and long term. Considerations for this criterion include the total number of targets available, their dispersion and how frequently they are tracked, as well as any legal aspects such as the issue of ownership and potential difficulties with recovery. For this study, it was decided to assess all these aspects within the context of an official ESA mission in line with the established vision of European autonomy.

3.1.3. Analytic Hierarchy Process

With the trade-off criteria defined, their relative weighting was determined using a collaborative Analytic Hierarchy Process (AHP). The analytic hierarchy process is a multiple criteria decision-making tool based on a mathematical model commonly used in various engineering fields [22]. The process employs pairwise comparison inputs to create a 'decision' matrix and determines the dominant eigenvector of said matrix to assess the relative merit of predefined criteria and alternatives as well as the overall consistency [23]. The overall process provides a systematic approach while remaining clear and transparent. For this study, AHP was used to determine the weight factors of the trade-off criteria.

In order to limit personal bias inherent in the trade-off process, active collaboration was undertaken with senior engineers, researchers and scientists from both the TU Delft and various ESA sites including the European Space Research and Technology Centre (ESTEC), the European Space Operations Centre (ESOC) and the European Astronaut Centre (EAC). Leveraging their extensive expertise across various fields of research was considered a substantial increase to the overall validity of the results. The AHP was found to be an excellent choice for this collaboration since taking inputs from multiple sources is easily implemented. A total of 10 participants were selected from research fields including but not limited to space systems engineering, space debris analysis & mitigation, Lunar exploration, materials science and propulsion engineering. It was chosen to conduct the AHP independently between participants, specifically avoiding any centralized or interpersonal discussion in order to keep the amount of bias and influence between participants to a minimum. For this, the online AHP tool by Goepel [23] was used to efficiently conduct the process, allowing all participants to fill out the pairwise comparison on their own accords after being given a detailed explanation of the study and its objectives in an individual meeting. The resulting weights as outputted by the AHP are listed in Figure 3.1. The trade-off criteria priority obtained from the pairwise comparison responses for each of the AHP participants are shown in Appendix A.

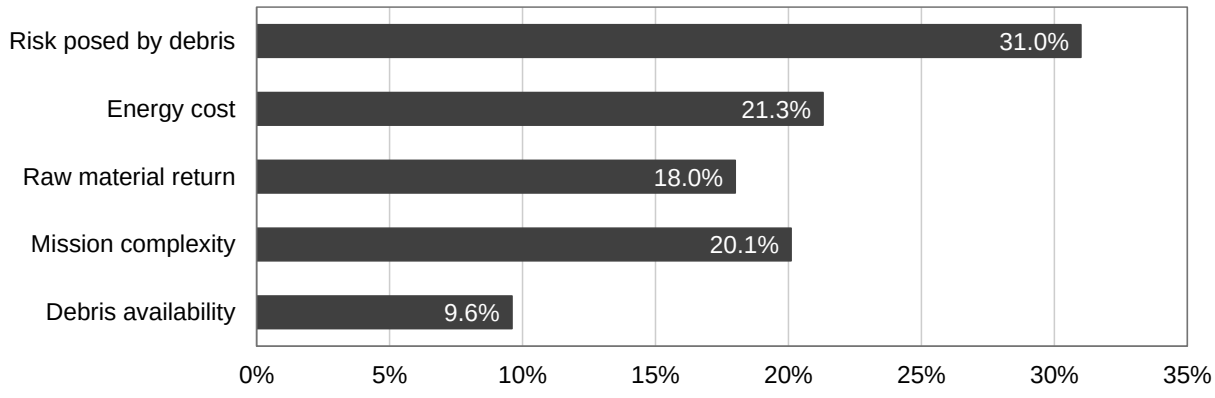

Figure 3.1: Criteria weighting results from the Analytic Hierarchy Process based on 10 participants.

A good Consistency Ratio (CR) of 1.1% was observed, though this was paired with a relatively moderate to low group consensus of 59.3%, indicating that sampling from a range of expertises yields also a range of priorities. Nevertheless, the risk posed by the debris was found to yield the highest criteria weight at 31.0%, with 7 out of 10 participants giving this criterion their top priority. Indeed, the incentive for debris recycling strongly hinges on the value of clearing debris, which explains this high weighting. Transfer energy cost, mission complexity and raw material return score relatively. These three criteria were also observed to have the most differences and thus the lowest consensus between the participants. Interestingly, debris availability was near universally valued the least important criterion. Further discussion revealed that given the criterion's reliance on policy that impacts much more than just a potential debris recycling mission, some of the participants believe potential roadblocks for debris availability will more easily be solved given the global precedent towards a more sustainable use of space. Hence they valued this criterion less than the others.

3.2. Criteria Performance Analysis & Trade-Off Results

In order to determine which of the two space debris target classes presents the most suitable target for a recycling mission, their relative performance was assessed based within the five established trade-off criteria. For the relative scoring, the method applied deviates from the traditional AHP, which employs pairwise comparison to judge translate performance into scores. However, considering there are only two alternatives for the space debris target class, the method as defined within the AHP causes rather stark shifts in scoring due to the integer steps in relative importance and eliminates the possibility of having scores closer together than 50%. Instead, it was chosen to apply a relative scoring for each of the criteria from 1 through 5, with a higher number indicating a greater performance within that specific criterion. This is in line with a simpler form of the classical trade-off methodology. In order to translate qualitative performance considerations to this quantitative score, the following justification was used:

1	Poor: unacceptable constraints
2	Insufficient: correctable deficiencies
3	Sufficient: meets requirements
4	Good: favorable characteristics
5	Excellent: exceeds requirements

It should be noted that the highest score of 5 was reserved for situations in which a debris target class truly exceeds requirements and expectations regarding a specific criterion which put it severely above the others. In turn, a score of 4 was assigned when a debris target class showed favorable characteristics in some regards, but may be affected by uncertainties or assumptions. A score of 3 then represented a nominal case with adequate performance and no key advantages or disadvantages. The score of 2 was assigned when a concept presented insufficient performance, but its main deficiencies showed potential to be corrected. Finally, a score of 1 represents a poor performance, with constraints which significantly hinder a debris recycling mission or prevent its execution outright.

Finally, each of the scores were multiplied with the respective criterion weight and summed over the five criteria to yield a total cumulative trade-off score. The performance of the two target classes was determined based on both quantitative and qualitative analysis. While scoring the alternatives based on criteria is inherently subject to a degree of subjectivity, the applied rationale is detailed below.

The risk posed by a specific piece of debris is a characteristic for which different modelling strategies are still being developed. Several established studies, such as the one presented by McKnight et al. [24], present a calculation of risk based on the multiplication of probability and consequence of collision, as shown in Equation 3.1.

$$\text{Risk} = \text{Probability} \cdot \text{Consequence} \tag{3.1}$$

These two respective metrics are then based on statistics such as annual collision rates, close encounters and spatial density of satellites within a particular cluster of space. It was found however that such statistical relationships were exclusively determined for Low-Earth Orbit (LEO). While LEO is indeed the most densely populated region in space, no such data was found for higher orbits such as GEO and especially for GTO, data was lacking. Nevertheless, the same general principles were used to determine a general sense of risk based on probability and consequence, though now qualitatively. In terms of collision, objects in GEO generally present a relatively low risk. After the end of their operational lifetime, GEO

spacecraft are transferred up to the Geostationary graveyard orbit of at least 235 km above their nominal operational altitude [10]. This ensures the spacecraft orbital altitude remains outside of the GEO protected zone for at least 100 years [10]. The GEO protected zone (visualized in Figure 3.2) is represented by a segment of a spherical shell defined by an altitude range of 200 km above and below the geostationary ring with an associated latitude range between −15° and +15° [10]. This means that defunct satellites in the graveyard orbit generally do not influence the active geostationary ring by design of the graveyard orbit. As such, the probability and consequence of potential collisions in GEO are limited. Note however that since the first GEO satellites were launched in the 60's, this 100 year intervention limitation is ultimately finite and already half passed. As such, risk will ultimately increase over time. It is for this reason that a performance score of 2 was assigned for the GEO satellites rather than 1. Rocket stages in GTO however carry a substantially higher collision risk. This is primarily due to the fact that these individually heavy objects cross both the LEO protected zone at perigee (approximately 250 km altitude) and the GEO protected zone at apogee (targeted at 35 786 km altitude). Given the larger range of utilized inclinations in LEO, the LEO protected zone is defined by a spherical region up to an altitude of 2000 km, as also shown in Figure 3.2. The excessive relative velocity between an object in LEO and a crossing object in GTO at its perigee combined with the high individual mass of rocket stages and the much larger spatial density of satellites in LEO make this crossing especially dangerous in terms of probability as well as consequence. Given this high level of risk, the highest score of 5 was assigned to the GTO rocket stages.

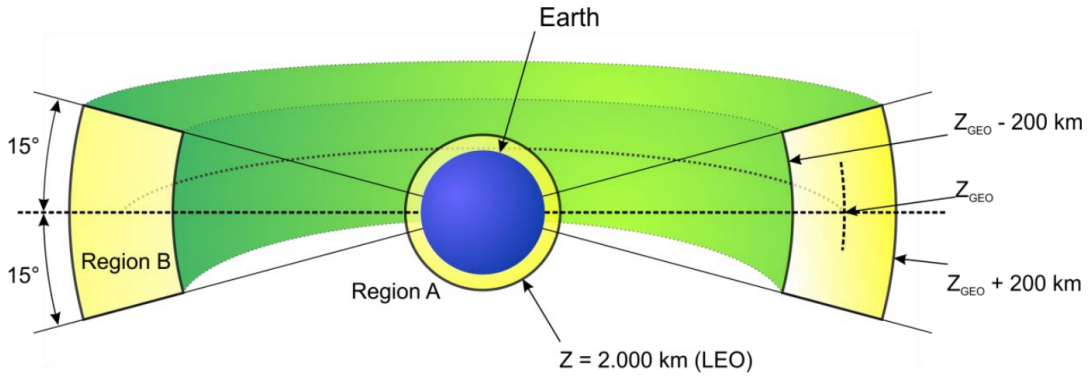

Figure 3.2: Visualization of the LEO protected zone (region A) and the GEO protected zone (region B) (not to scale). [10]

The assessment of the energy cost associated with the orbital transfer is a key part not just of this trade-off but the entire study presented within this report. Analyzing the transfer energy was a continuous process that required many iterations which influenced the values used to perform the performance assessment. As such, this analysis was continuously updated to reflect them most accurate performance. The transfer energy cost was translated to a trade-off performance score by determining the orbital transfer energy for the respective transfers from GTO and GEO to the Moon and comparing the relative energy cost to that of the alternative Argonaut mission scenario. Mapping this relative energy cost onto the defined scale of 1 through 5 yielded performance scores of 4 and 3 for GTO upper stages and GEO satellites, respectively. The complete process used to determine this orbital transfer energy cost is presented in detail later in this report, specifically in Chapter 6.

For the raw material that can potentially be extracted from a particular piece of debris, estimations were made based literature. Launch vehicle upper stages, by virtue of their structure primarily consisting of propellant tanks, generally have a higher structural mass fraction compared to satellites. Koch [9] presents raw material mass fractions for launch vehicle upper stages higher than 60% of the total upper stage dry mass available for recycling. Statistics in terms of specific material masses were not found to be publicly available. This is likely due to the fact that the space industry, especially the launch vehicle industry, is dominated by a small number of key players controlling a massive market capital. Protecting their designs is therefore vital for their bottom line. As such, the aforementioned raw material mass fraction of 60% was taken as a baseline value for the launcher upper stages. This exceptionally high metal fraction combined with their high individual object masses is the defining advantage of choosing launch vehicle upper stages as recycling targets. When considering the 5000 kg Ariane 5 ESC-A upper stage for example, a raw material mass of 3000 kg could potentially be recovered. However, since this 60% contains a degree of uncertainty due to a lack of validation, a performance score of 4 was assigned rather than 5. For GEO satellites, a representative raw material mass fraction was determined by first considering that the potentially harvestable raw material consists in principle of the satellite's structural components. The New SMAD [25] presents

statistical mass fractions for various classes of satellites, from which a structural mass fraction of 24% was found for the ”High Earth” class which was deemed representative for GEO satellites. This was multiplied with an additional factor of 90% to account for other, non-metallic structural elements [18]. While this is a relatively high factor, it was considered an adequate initial assumption. Furthermore, lowering this factor did not change the outcome of the space debris target selection. This in total yields an assumed raw material mass fraction of 21.6% for GEO satellites. The potential in terms of actual mass returned shifts even more in the favor of launcher upper stages considering they represent heavier individual target masses. This low raw material mass fraction combined with substantially lower individual object masses results in poor raw material yields even in the optimal scenario, where a 2000 kg dry mass satellite would yield only 432 kg of raw material. The GEO satellites were therefore assigned a score of 1.

Mission complexity was characterized qualitatively at this early stage in the mission design. Satellites in the geostationary graveyard orbit are in stable and predictable orbits. Their altitude changes only very slowly due to the lack of atmospheric density at such high altitudes, while their inclination shifts between 12° - 15° around their nominal inclination with a periodicity of 53 years primarily due to Luni-Solar perturbations [26]. This range of inclinations was also observed in the actual orbital elements of GEO satellites determined from the generated space debris database during the literature review prior to this study [18]. The GEO graveyard orbit is ultimately a very stable environment with a constant orbital velocity, slow-moving orbital perturbations and without interference of active satellites. This makes it a potentially ideal location for capture operations. Furthermore, the capture of GEO satellites has already been proven in the form of the MEV-1 and MEV-2 missions. As such, GEO satellites were assigned the highest possible performance score of 5 in regards to mission complexity. For launch vehicle upper stages in GTO however, a more dynamic situation is observed. Due to their elliptical nature and low perigee, these orbits are also subject to significant perturbations resulting from the Earth’s non-spherical gravitational field (i.e. the J2 effect). This effect, presented in detail later in this study, causes the orbits to rotate in space over time, primarily in their Right Ascension of the Ascending Node (RAAN) and argument of periapsis. This adds another layer of complexity to be considered for the launch trajectory and especially the alignment for the orbital transfer phase, which is shown later in this report to be one of the principle problems to be solved for a debris recycling mission. This, combined with the large variation in orbital velocity between perigee and apogee make recycling missions targeting GTO rocket stages substantially more complex. While these are deficiencies that impact the feasibility of the mission, they are potentially correctable through mission planning and careful target selection. As such, a performance score of 2 was assigned for the GTO rocket stages.

The final criterion, debris availability, also depends largely on qualitative reasoning. Launch vehicle upper stages in GTO are found to hold an advantage primarily due to their ownership. Legal constraints are perhaps the single largest currently existing roadblock preventing the execution of a debris recycling mission. Even after the end of its operational lifetime, ownership over any spacecraft remains with the launching parties, which in the case of GEO satellites often includes a commercial party as primary operator of the satellite. It is unlikely that such commercial parties and their industrial partners will willingly allow their satellites to be captured and used under the urge to protect their (intellectual) property, even after their operational life. This idea is substantiated by the fact that many GEO satellites are built on the same general bus platforms manufactured by a small group of key industry players. While not impossible, as seen by Intelsat willing to have their satellites captured and replaced by the MEV missions, it is unlikely that commercial satellite operators will agree with recycling without any additional incentive or global pressure. As such, a score of 2 was assigned to GEO satellites. A similarity can be drawn to the market capital of launch providers as discussed before. For rocket stages in GTO however these considerations are less impactful, especially within the context of European autonomy and the associated Ariane upper stages identified as potential space debris targets. ArianeGroup is a European corporation and key partner of ESA, which has strong ties that could make the establishment of a recycling contract a lot easier. Additionally, Ariane 5 has already been retired and is to be replaced by the superior Ariane 6. The restriction of specifically targeting Ariane upper stages in GTO is manageable as it still leaves a total of 112 potential targets to be captured. Finally, consistently capturing the same target was considered an advantage benefiting the case of GTO rocket stages compared to GEO satellites which display a greater variance in design, mass, grappling fixtures and other obstacles such as antennas. Given these favorable characteristics, launch vehicle upper stages in GTO were assigned a score of 4 according to the scoring rationale.

3.2.1. Trade-Off Results

Based on the information presented above, relative scoring between the two alternatives was performed, applying absolute scores from 1 through 5 as mentioned at the start of this section. These scores, along with the criteria weights determined through the AHP and the final subsequent score for each of the two space debris target class alternatives are presented in the trade-off matrix shown in Table 3.2. It should be noted that a higher score in risk posed by the debris is a positive trait for a debris recycling mission, as capturing a more dangerous piece of debris represents a higher value in terms of space debris removal. Similarly, a lower score in mission complexity represents a more complex mission, as complexity is a negative mission trait within the considered context.

Table 3.2: Trade-off matrix for the space debris recycling target class trade-off.

Trade-Off Matrix		**Space Debris Target Classes**	
Criterion	**Weight**	Ariane Upper Stages in GTO	GEO Satellites
Risk posed by debris	0.310	5	2
Transfer energy cost	0.213	4	3
Raw material return	0.180	4	1
Mission complexity	0.201	2	5
Debris availability	0.096	4	2
	Total score	**3.908**	**2.636**

It can be seen from these trade-off results that the launch vehicle upper stages in GTO are the optimal space debris target for a recycling mission to the Moon, performing better with respect to four of the five defined trade-off criteria. For the GEO satellites, the crucial downside is their lack of incentive in terms of debris removal considering the moderate risk they represent to operational space assets. This combined with their lack of substantial value return in terms of raw material makes them decidedly less attractive as a target for a potential recycling mission. The high observed cumulative trade-off score for the Ariane upper stages in GTO is predominantly a consequence of their substantially higher presented risk to existing space assets combined with a significantly greater raw material return potential. Their primary downside is a greater mission complexity due to the more dynamic nature in which (highly) elliptical GTO orbits move over time influenced by various perturbing forces. If those complexities and the associated design challenges can be overcome, these launch vehicle upper stages indeed present the ideal targets for a potential space debris recycling mission specifically for Lunar exploration applications.

3.2.2. Sensitivity Analysis

Because the criteria performance assessment was more susceptible to potential bias and subjectivity regarding the scoring of the two debris target classes for each of the defined criteria, a sensitivity analysis was performed. The goal of this analysis is to investigate how potential changes in the performance scoring influence the final outcome of the trade-off. In order to structure these changes, a performance modifier δ was defined. Considering there are just two debris target classes in the trade-off, the score of the winning class (GTO stages) was decreased by a factor δ and the score of the losing class (GEO satellites) was increased by a factor δ, for each of the trade-off criteria. This scoring modification rule is laid out in Equation 3.2 and 3.3.

$$\text{Score}_{\text{win, new}} = \text{Score}_{\text{win, old}} \cdot (1 - \delta) \tag{3.2}$$

$$\text{Score}_{\text{lose, new}} = \text{Score}_{\text{lose, old}} \cdot (1 + \delta) \tag{3.3}$$

Where the $\text{Score}_{\text{win, old}}$ and $\text{Score}_{\text{lose, old}}$ refer to the baseline trade-off scores as shown in Table 3.2. By applying the modification rules for various values of the performance modifier δ and monitoring how the total cumulative trade-off score changes, insights into the robustness of the analysis were achieved. The results of this sensitivity analysis are presented in Figure 3.3. It should be noted that it was chosen to prevent scores from going lower than 1 or higher than 5, in order to maintain consistency with the original scoring justification.

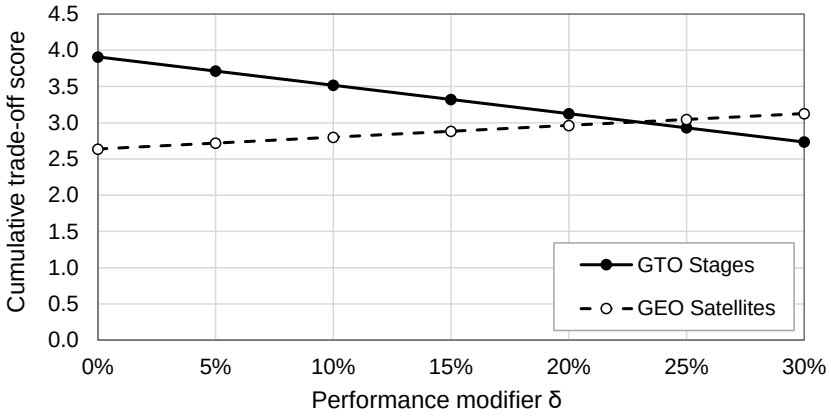

Figure 3.3: Results of the space debris target trade-off sensitivity analysis.

From this figure, it can be observed that there is significant margin for change in the performance assessment scoring for which the outcome of the space debris target trade-off as presented in Table 3.2 is maintained. This is especially true when considering that the performance modification goes both ways, as the winning concept had its scores reduced by a factor δ while simultaneously the losing concept had its scores increased by an equal factor. Even then, a value of δ over 20% will still result in GTO stages winning the trade-off. The break-even point at which the GEO satellites become the favorable debris target corresponds to a performance modifier value of 23%. Table 3.3 shows the trade-off matrix for this edge case scenario using δ = 23%. It can be seen that the total relative difference in criteria scores has departed significantly from the original scoring shown in Table 3.2. This large margin for potential change resulting from the sensitivity analysis highlights the robustness of the original trade-off outcome and substantiates the GTO launch vehicle upper stages as the ideal space debris targets for a space debris recycling mission.

Table 3.3: Trade-off matrix for the space debris recycling target class trade-off with a performance modifier δ = 23%.

Trade-Off Matrix		**Space Debris Target Classes**	
Criterion	**Weight**	Ariane Upper Stages in GTO	GEO Satellites
Risk posed by debris	0.310	3.85	2.46
Transfer energy cost	0.213	3.08	3.69
Raw material return	0.180	3.08	1.23
Mission complexity	0.201	1.54	5
Debris availability	0.096	3.08	2.46
	Total score	3.00916	3.01113

3.3. Final Space Debris Target Characteristics

In order to get a fundamental baseline of space debris target characteristics, the space debris database generated within the literature review part of this study was referenced [18]. The analysis performed in this literature review revealed that the space debris target class of Ariane upper stages in GTO is represented by three main vehicles. These are the ESC-A cryogenic upper stage used by Ariane 5 in its ECA configuration, the EPS upper stage used by several Ariane 5 configurations and the H10 upper stage, which was used by the Ariane 2, 3 and 4 launch vehicles. It was found that several H10 stages that were launched on Ariane 2 in the late 80's remain in orbit to this day. A summary of the most important characteristics for these three vehicles are given in Table 3.4. At this point it should be noted that some conflicting numbers were found in publicly available data regarding some of the masses and heights of these vehicles. In order to remain consistent with the analyses performed during the literature review, it was chosen to use the data published in the DISCOS database as the defining baseline. A detailed breakdown of the orbital characteristics for these objects will be given later in this report when discussing the orbital transfer design.

Table 3.4: Summarized information on the three highlighted Ariane upper stages in GTO.

	Ariane 5 EPS	**Ariane 4 H10**	**Ariane 5 ESC-A**
Mass	1190 - 2850 kg	1764 - 1920 kg	5000 kg
Orbital region	GTO	GTO	GTO
Number of objects	15	27	63
Cumulative mass	27.86 tons	48.39 tons	315.0 tons
Diameter	5.46 m	2.66 m	5.45 m
Height	3.30 m	14.1 m	7.00 m
Tank material	AA2219 [27]	AA7020 [28]	AA2219 / AA7020 [29]
Main jurisdiction	Europe	Europe	Europe

The mass ranges for the EPS and H10 reflect the different configurations in which these vehicles were used on their respective range of launch vehicles. From this overview it can be seen that within the Ariane upper stages in GTO, the bulk of the mass is represented by the ESC-A upper stage. At 5000 kg of individual vehicle dry mass, the ESC-A is the largest of the three identified vehicles and thus also has the potential for the largest return in terms of raw material mass. This combined with its high prevalence in GTO makes the ESC-A in principle the ideal target for a space debris recycling mission within the established mission context. Note however that its high mass could also be a detrimental factor specifically when looking at Lunar applications, as it could impart unachievable constraints on the mission such as for example large required propellant masses for high-impulse orbital manoeuvres like the Lunar injection. As such, the H10 was taken as a lower mass alternative alongside the ESC-A to make up the two baseline targets to be considered for the study. Note however that it is crucial to target H10 stages that were flown after 1993. This is because prior to October 1993, these H10 upper stages were not passivated after the deployment of their payloads and thus still carry an unspecified amount of residual propellant [30]. The presence of this unused propellant was considered too dangerous for a potential recovery and recycling mission due to the risk of explosion. It was chosen not to target the EPS at this point, given the low number of objects in GTO and the subsequent low cumulative mass. Additionally, the EPS has a significantly different design in the sense that it is built more like a satellite, with a series of semi-spherical propellant tanks. Raw material mass yield could therefore be potentially lower than the 60% assumed to be typical for rocket upper stages. Note however that because the mass range of the H10 upper stage falls within that of the EPS, analyses done for the H10 will be representative also for the EPS to a certain degree.

One aspect that Table 3.4 does not capture is potential tumbling rates of these space debris objects. Tumbling is a dynamic phenomenon in which the attitude of an object in space moves in an uncontrolled manner due to residual momentum [31]. For launch vehicle upper stages, such tumbling behavior is potentially caused by off-axis passivation actions as well as numerous perturbing forces acting over prolonged periods of time, such as gravity gradients, Eddy currents, atmospheric drag, solar radiation pressure and even outgassing [32, 33]. During the literature review prior to this study, several feasible capture mechanisms were identified. Such capture mechanisms however can only handle moderate relative angular rates, with Nishida and Kawamoto [34] considering rotational rates below 3°/s able to be ”captured easily” while rates exceeding 30°/s are labeled as infeasible for a target to be considered for capture. Koch [9] however concludes rotational periods of up to 10 seconds are acceptable, which equates to a rate of up to 36°/s. A general lack of comprehensive information was found regarding the tumbling rates of objects in GTO. This lack of information is most likely a result of the lack of operational satellites in this orbital regime and the subsequent lack of incentive to study its tumbling dynamics. Alternatively, the Kazan Federal University publishes a catalogue of tumbling rates based on optical observations from its MiniMegaTORTORA (MMT) system [35, 36]. This catalogue lists a relatively wide range of rotational periods for Ariane 5 rocket bodies from 0.77 - 55.68 seconds, with a notable outlier of 475.36 seconds. However, it was found through analyzing the 86 Ariane 5 rocket body objects in the MMT catalogue that the rotation of effectively all of these stages is slowing down. Indeed, it seems that the forces acting on upper stages in GTO have a net breaking effect. Figure 3.4 shows the evolution of the rotational period of an ESC-A upper stage (NORAD 43176) using the data published in the MMT database[36], which highlights this phenomenon particularly well.

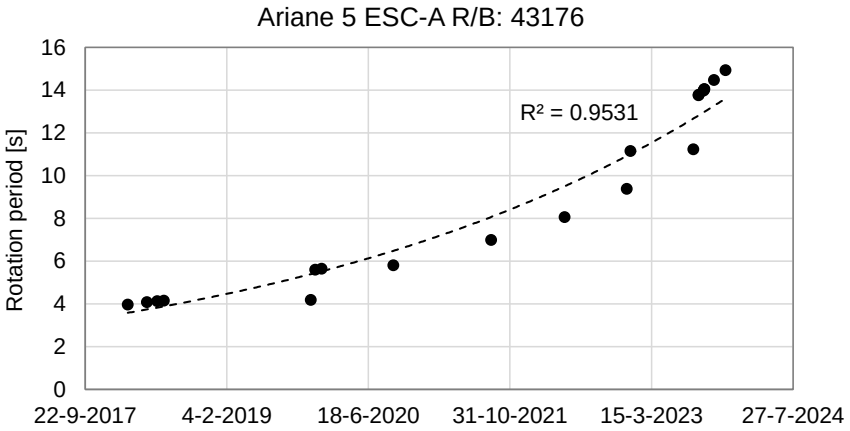

Figure 3.4: Tumbling behaviour over time for a selected ESC-A upper stage (NORAD 43176). Data from MMT database [36] with added exponential fit trendline.

A significant increase in the rotational period is observed for this particular upper stage, with a magnitude that nearly quadruples in a relatively short time frame of less than 6 years. Additionally, the behavior is shown to follow an exponential growth as indicated by the dashed trendline in the figure. It can therefore be reasoned that, even if rotational rates exceed what could be captured today, over time this observed breaking effect would reduce this constraining factor and widen the pool of objects that could be captured safely. The long orbital lifetimes of these stages in GTO exceeding decades or even centuries substantiate this as a practical consideration that could realistically be made. Accounting for the potential de-tumbling of debris targets in a preliminary mission study is difficult, as the dynamics are complex and warrant studies of their own. Several concepts have been proposed in literature, from the use of robotic arms with brushed end effectors [34] to using Eddy currents for de-tumbling large objects [37]. Additionally, it is likely that within the context of a debris recycling mission, it could be optimal to have a separate de-tumbling spacecraft to de-tumble several targets in GTO. Combined with the fact that upper stage tumbling rates seem to be slowing down exponentially, it was chosen not to further analyze the de-tumbling of debris objects within this study. However, it is recognized that this affects the overall feasibility of the space debris recycling mission as presented in this study, and should be looked at specifically upon further detailed study of a debris recycling concept mission.

Finally, some critical limitations regarding the MMT observations were also found. First, the data is ultimately limited. Many of the catalogued objects have less than 10 total observations. This results in many objects being labeled as having an aperiodic rotation or an uncharacterized rotation altogether, which is likely due to insufficient or incomplete measurements. Furthermore, since these observations are based on optical light curve measurements, they contain no inherent information on the axis about which the rotation occurs. This highlights the need for more powerful Space Situational Awareness (SSA) tools specifically for the characterization of tumbling motions, which would be useful not only for debris recycling missions but also for conventional debris removal. With the advancement of miniaturization technologies within the space industry, space-based assets in the form of CubeSats could potentially be leveraged to get up-close observations. Within the context of a space debris recycling missions, a CubeSat forerunner mission could be sent to GTO to validate the tumbling rates of upper stages and monitor their evolution over time.

4

Mission Architecture Definition

With the ideal space debris target defined, a number of mission-critical input variables are known. The debris orbit in particular is an important input for the Lunar transfer. This chapter details the conceptualization of a mission architecture, which will act as a throughline and guide the design of the individual mission phases. Specifically, a mission architecture is valuable as it defines mission interfaces which are critical for a space debris recycling mission. This includes a preliminary definition of the Space Debris Transfer Vehicle (SDSV) and the definition of an alternative mission scenario for the space debris mission concept to be compared against.

4.1. Concept of Operations

Given the lack of literature and generally the innovative and unexplored nature of space debris recycling as a concept, defining a clear overview and architecture of the mission is crucial. For this study, a space debris recycling mission was considered to consist of three main distinct mission phases. Each of these mission phases were defined primarily by the environments in which key parts of the mission will exist throughout its duration. These phases are represented as the Earth phase, the Space phase and the Lunar phase. By breaking down the mission into these three phases, a more comprehensive overview of what constitutes a space debris recycling mission can be achieved. While several different mission scenarios will be analyzed throughout this exploratory study, these mission scenarios share a basic underlying structure in terms of their architecture. In order to better understand this underlying structure, a Concept of Operations (CONOPS) was drafted to present a chronological overview of the mission and its three main phases connected together to form the complete space debris recycling mission targeting defunct rocket stages in GTO. Figure 4.1 and Table 4.1 present a visualization of this CONOPS along with a complementary mission sequence highlighting the most important steps of the mission concept.

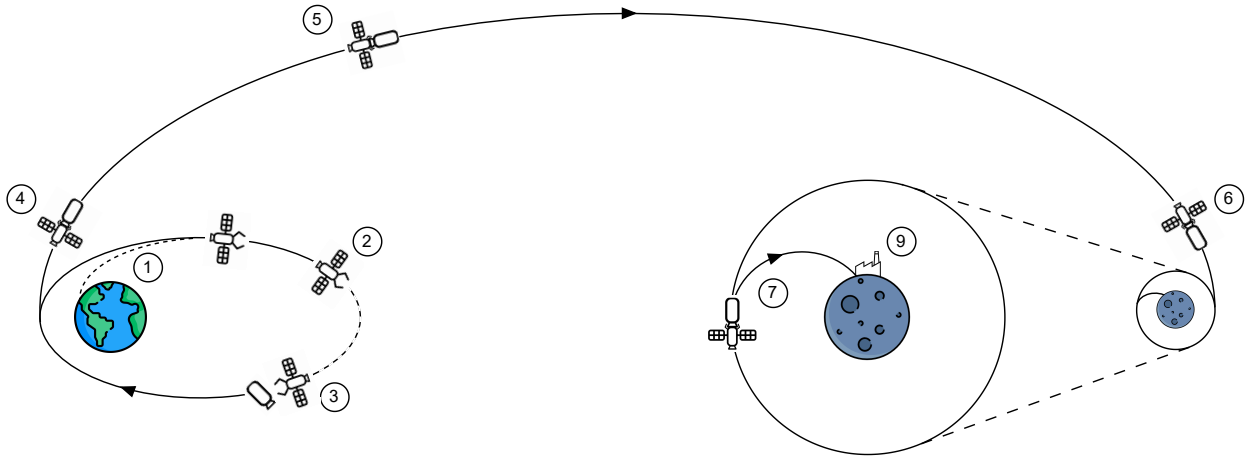

Figure 4.1: Simplified overview of the concept of operations for the space debris recycling mission to the Moon.

Table 4.1: Space debris recycling mission sequence.

Order	Event
1	Launch of servicing vehicle into GTO
2	Target phasing & long-range rendezvous
3	Close-range rendezvous & capture
4	Trans-Lunar Injection
5	Lunar transfer
6	Lunar orbit injection
7	Descent to Lunar surface
8	Processing & recycling

It is important to note that the definition of these mission phases are different from the ”ground segment” and ”space segment” traditionally used for space missions [25, 38]. This latter segmentation is useful for the complete mission design of space missions with a more cyclic nature such as Earth observation missions. The ground segment for example generally consists of all ground-based parts of a space mission, many of which are used continuously by the satellite operators [25]. This includes ground stations, mission control and launch sites [38]. A space debris recycling mission to the Moon is characterized by a more linear mission architecture as the debris is captured, transferred and recycled. In this sense, a space debris recycling mission can also be seen from the perspective of a production process rather than a traditional space mission. As such, it was chosen to break down such a recycling mission into the aforementioned phases on a more conceptual level. Whereas the traditional mission segments represent different parts of a whole space system that operate in tandem throughout the mission lifetime, the mission phases defined for this study are characterized by distinct periods in time as the debris recycling mission travels from Earth to the Moon. This was considered beneficial within the context of this study which focuses primarily on the investigation of overall feasibility and viability through the assessment of a global mission energy analysis, for which these mission phases will form the foundation.

4.1.1. Earth Phase

The Earth phase was defined as the main relevant processes that happen on Earth up until the servicing spacecraft is placed into a stable orbit. Within this definition, the Launch and Early Operations Phase (LEOP) are considered as part of the Earth phase. Comparing this to the aforementioned mission segments often used in space mission design, a number of considerations can be elaborated upon. First of all, any processes regarding the main operations of the mission were omitted from the defined mission phases as it was assumed that associated differences between the debris recycling mission scenarios and the alternative mission scenario would be small enough that differences in such energy sinks would effectively be negligible. That is, with regards to for example ground station usage, launch facilities and mission control operations, no meaningful differences were assumed to be present. This was also a practical assumption within the context of a preliminary study such as the one presented in this report as the associated energy usages would be difficult to determine.

Every space mission starts with a launch, which is expected to be a large energy sink in the global mission perspective given the massive propellant masses being combusted in the process. Given the established ideal of operating a space debris recycling mission under complete European autonomy, Ariane 6 is envisioned as the launch vehicle of choice. In order to target the identified rocket upper stage debris targets, launching into GTO was considered a prerequisite. The large payload mass capacity of the Ariane 6 specifically to GTO makes it a strong option for a debris recycling mission. The other main European launch vehicle, Vega and its derivatives, lacks the capability to launch into GTO. Given the current geopolitical climate, using Russian launchers like the Soyuz-2, which is capable of launching 3250 kg into GTO [39], was not considered for this study. This makes Ariane 6 the only option for a European launch vehicle as of the writing of this report. It was assumed that a space debris recycling mission could be considered the primary client for an Ariane 6 launch and as such, dictate the desired characteristics of the GTO launch. Nevertheless, choosing a debris target with favorable conditions for a semi-conventional GTO launch was identified as a potentially important consideration in order to include a potential rideshare client should there be leftover launch vehicle payload margin. Launching directly into close vicinity of a space debris object, especially a large uncontrolled rocket stage was considered too dangerous. Hence, care should be taken to launch into an orbit close to the targeted debris GTO such that orbit phasing and rendezvous operations can be performed.

Earlier in this report, when elaborating on the potential tumbling rates of the Ariane upper stages in GTO, the option of a forerunner mission to characterize such tumbling rates and perform a visual inspection on the debris target was highlighted. With the advancement in capabilities of microsats or even CubeSats, a forerunner mission based on such small satellite platforms could be used to validate the condition of a particular space debris targets. Such decentralization is particularly advantageous as a specialized forerunner mission equipped with its own propulsion system could be operated over a relatively long period of time to inspect and validate the conditions of multiple upper stages in GTO. The orbits of these stages have shifted and rotated over time due to orbital perturbations, primarily in Right Ascension of the Ascending Node (RAAN) and Argument of Periapsis (AoP). This alignment issue will be elaborated upon in detail later in this report. Following the knowledge gained through this study, it is envisioned that by lowering its apogee, greater relative influence of the J2 effect could be leveraged to shift the orbit over time in order to reach upper stages with different orbital orientations. Additionally, it should be noted that such a forerunner mission would be of great value not just for a space debris recycling mission, but for any space debris removal or servicing missions. The analysis and design of such a forerunner mission however was considered beyond the scope of this study.

Besides the launch, the manufacturing of materials is the second key process for the relative assessment of a space debris recycling mission. While the manufacturing of materials, principally metals, is not directly a part of a space debris recycling mission, it is a key part of the alternative mission defined for direct comparison. This alternative mission, a direct delivery mission of metal feedstock material to the Lunar surface using a conventional Lunar lander, will be used as a benchmarking tool for the space debris recycling missions to be compared against. The manufacturing of these metals is an energy sink that cannot be forgotten, as it represents the counterpart of the recycling process on the Lunar surface for a debris recycling mission. Details about this alternative mission will be elaborated upon later in this chapter.

4.1.2. Space Phase

The space phase was defined to encompass everything from the moment the servicing spacecraft is injected into a stable orbit and is fully operational up until touchdown on the Lunar surface. The potential tumbling state of the upper stage debris targets was introduced in the previous chapter, where it was found that effectively all upper stages in GTO are slowing down in terms of their rotational rate. Given that the lifetimes of these stages in GTO exceed hundreds of years in many cases, de-tumbling could potentially not be a required altogether. Nevertheless, while in-depth analysis on active de-tumbling of space debris targets was considered beyond the more broad mission scope of this study, several feasible options were still identified from literature. Two general strategies can be applied to reduce relative rotational velocities. The first of these is for the chaser vehicle to synchronize its own rotation to that of the target through active manoeuvres. [31] Such attitude synchronization is always required to some degree since a space debris object will never have a zero rotation rate [31]. The second is to actively de-tumble debris, for which various methods have been proposed. These include but are not limited to the use of brushed end effectors on robotic arms, plume impingement, laser-based systems and Ion Beam Shepherds (IBS) [31, 9]. Particularly interesting is the contactless de-tumbling method of Eddy current breaking. A study performed by Gómez and Walker [37] highlight Eddy current breaking as a potentially suitable option for the detumbling of an H10 upper stage, which was also referenced by Kumar et al. [40] for the removal of EPS upper stages from GTO. Similarly to the proposed forerunner debris identification mission, decentralization could be applied here as well. Given the natural slowdown of upper stages in GTO, a separate de-tumbling vehicle could be launched prior to a space debris recycling mission to actively de-tumble several upper stages. Assessing the need for de-tumbling and how best to approach such a dynamic problem however requires substantial additional analysis, starting with the need for a better understanding and validation of debris characteristics as concluded in the previous chapter.

Referencing Figure 4.1, the space phase begins with the servicing spacecraft performing the rendezvous operations and capturing the targeted piece of debris, in this case one of the defunct Ariane upper stages in GTO. Several technologies were identified already within the literature review part of this study, in which it was concluded that a stiff connection capture mechanism is a necessity for a space debris recycling mission [18]. The high degree of control over the target after capture is essential for a subsequent docking and to facilitate high-impulse orbital transfer manoeuvres for the transfer vehicle and the captured debris object. This is especially true for out of plane manoeuvres, which cannot be performed with proposed flexible capture mechanisms such as tethers or nets [18]. Generally, it was found that two suitable grappling fixtures are universally present on rocket stages, these being the rocket engine nozzle at the bottom and the payload mounting interface at the top (shown in Figure 4.2 and 4.3 for the Ariane 5 ESC-A).

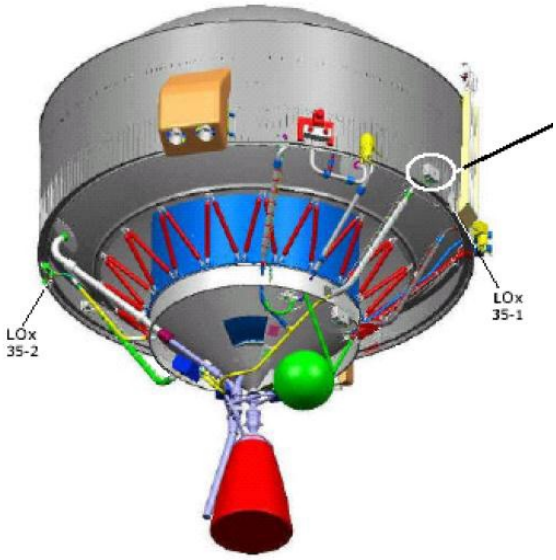

Figure 4.2: Ariane 5 ESC-A upper stage model. [41]

Figure 4.3: Ariane 5 payload adapter and interface. [42]

The use of robotic arms as well as nozzle probes were concluded to be suitable options for the recovery of large space debris items for a space debris recycling mission. Within the context of capturing defunct launch vehicle upper stages in particular, the use of nozzle probes was regarded as the desired capture mechanism. Upper stages are defined by the presence of a large rocket engine. This rocket engine is directly connected to the main structural elements of the rocket stage in order to sustain the large thrust forces and thus could also withstand the thrust forces applied by the servicing spacecraft. The validity of such a capture mechanism was proven by the Northrop Grumman MEV missions, which used a nozzle probe to capture a large Intelsat satellite in GEO [43, 44]. Such a nozzle probe could also be a weak point when considering the large masses of rocket stages compared to satellites. Looking at the primary identified space debris target, the Ariane 5 ESC-A in Figure 4.2, it can be seen that the vehicle is very top-heavy. A nozzle probe would have to be long and very robust to prevent snapping especially during rotational motions. The use of robotic arms to capture the payload mounting interface could potentially alleviate this issue. Such interfaces were designed to sustain heavy launch loads. Looking at Figure 4.3, it can be seen that the payload adapter is hollow and could potentially be grappled inside and out not unlike a nozzle probe for a subsequent docking procedure to lock the capture in place. However, various different payload adapters were used on the Ariane launch vehicles, making this option potentially problematic in terms of flexibility [42]. Ultimately, both options could be considered and require further analysis to determine absolute feasibility.

Upon capturing the target, the space debris servicing vehicle and the space debris target form a combined stack and effectively make up a single vehicle. Following this capture, a Trans-Lunar Injection manoeuvre is performed to put this combined stack of the transfer vehicle and the space debris target into a Lunar Transfer Orbit (LTO). Determining suitable orbital transfer trajectories is a key part of assessing the feasibility of a space debris recycling mission, specifically due to the inherent dependence on the debris orbit as a starting point for the transfer. Several ”paths” can realistically be taken and will be explored and analyzed accordingly throughout this study. This includes traditional quasi-impulsive manoeuvres as well as more novel low-thrust manoeuvres. The combination of such technologies in a hybrid propulsion system will also be considered as a potential solution. When the servicing vehicle reaches the Lunar vicinity, a Lunar capture manoeuvre is performed. This manoeuvre serves to put the servicing vehicle and the captured space debris target into a stable orbit around the Moon. Instead of directly being put onto a ballistic trajectory with the Lunar surface, the inclusion of an intermediate parking orbit allows for the reduction of the orbital velocity as well as the potential for assessing a landing site and perform additional manoeuvres if necessary. Once in Lunar orbit, the space phase concludes with a final descent manoeuvre down to the surface, where the Lunar phase begins. Regarding the landing itself, two general strategies can generally be applied, these being a semi-controlled retro-propulsive crash and conventional a soft landing [18]. Both of these options were analyzed throughout this study. The location of a potential debris landing site is interesting not just for a space debris recycling mission, but for every mission to the Moon. The unstable nature

of most Lunar orbits make the use of a graveyard orbit, like the one used for GEO, an unsuitable option. As such, the primary end-of-life disposal method used for Lunar mission has been to simply let them crash into the surface [45]. As such, the establishment of a unified debris (crash) landing zone could allow a recycling site to leverage also the material from crashed Lunar satellites alongside the space debris material actively transferred from Earth orbit. The Lunar Resource Registry [46] proposes a so-called ”Space Debris Lunar Landing Zone” for a similar purpose, targeting the Gambart crater on the Mare Insularum. This crater and its location are shown in Figure 4.4.

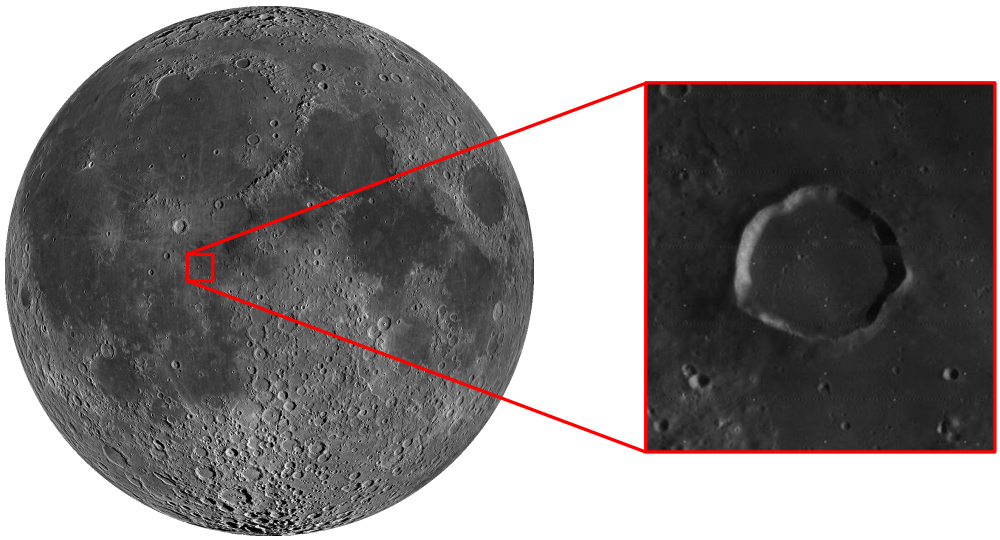

Figure 4.4: Gambart crater, located at N 0.9° W 15.2°.[(a)]

Utilizing a crater as a debris landing site has a number of benefits, the primary of which is the fact that the crater walls limit the spreading of ejecta when a shallow impact angle is used. The crater wall thus serves to contain the ejected material from the surface. When such a shallow impact is used, the Lunar Resources Registry argues that high-speed impacts won't rise above the 100 meter crater walls. While there are likely many craters that could potentially be used as a landing site, some criteria should generally be met. First, the crater should have one or multiple approach sites shallow enough for rovers to access the crater. Second, Permanently Shadowed Regions (PSR) should be avoided to prevent rovers from freezing. Finally, it was considered that low latitudes are the most flexible in terms of operational access for satellites and debris recycling missions, given that these inclinations are crossed by a wider range of orbital inclinations as compared to higher latitudes. This is likely why the Lunar Resources Registry opted for the Gambart crater, located almost on the Lunar equator. It should be noted however that this complicates utilization as the principle proposed location for a Lunar base is the Lunar south pole [7]. Hence, ideally a crater closer to the south pole should be targeted to decrease transportation needs after debris recycling.

4.1.3. Lunar Phase

The Lunar phase is the final defined phase of the space debris recycling mission and comprises of the debris processing and utilization stages. In terms of debris processing, several paths can theoretically be taken, though much of the potential assessment of their feasibility and practicality in basis is ultimately limited to qualitative measures and depends on numerous assumptions. Ideally, a recycling plant would operate at least semi-autonomously. The option of human intervention is a key benefit of having the recycling infrastructure on the Lunar surface compared to in orbit, but it should not be prerequisite for the infrastructure to function. This leaves the use of rovers as the only suitable substitute. The applicability of rovers and the design specifications required ultimately depend primarily on the state of the debris after entry onto the Lunar surface. For this study however, it was assumed that following the descent to the Lunar surface, space debris scrap of moderate size could be collected in a way that is suitable for rover transportation to the recycling site for further processing and final utilization. Following the collection of debris scrap, re-melting the debris is an important step in the recycling stage of the mission, drawing heavily upon well-understood terrestrial recycling processes for metals. As such, simple thermal re-melting processes are ideal. Within the constraints presented by the environmental conditions of the Lunar surface, two main suitable options for this were identified in the literature review part of this study, these being the use of inductive heating furnaces

[(a)] Moon images courtesy of Robinson [47] and Lunar and Planetary Institute [48]

or the use of concentrated solar energy through solar furnaces [18]. The latter of these options typically use Fresnel lenses to focus and concentrate sunlight [49, 9] and could be an ideal solution as concentrated solar energy could leveraged without the presence of an atmosphere attenuating the Solar flux on the Moon. However, such solar furnaces were found to depend on a number of critical disadvantages regarding their practicality for deployment on the Lunar surface. The ability to heat and melt large pieces of metallic scrap would require very large mirrors with precise alignment requirements in order to focus the light. Additionally, the focal point would likely have to be moved throughout the melting process, substantially complicating the system. Finally, the operation of large and delicate mirrors in direct vicinity of a space debris landing zone with a high probability of surface ejecta impacting the mirrors would greatly hamper reliability. Instead, the use of inductive heating furnaces was chosen as a much more reliable, well-understood and ultimately simpler alternative way of melting debris. Such inductive heating furnaces are widely used on Earth already and could be translated to the vacuum conditions of the Moon without fundamental changes [18]. Given the novel and relatively unexplored nature of space debris recycling, it was considered that a space debris recycling infrastructure should value simplicity whenever possible and practical. This ideal also extends to the utilization stage, for which the casting of metal feedstock material was chosen. The use of feedstock is incredibly common practice on Earth, as it represents a universal standard form of material which for use in numerous subsequent manufacturing processes [18]. The creation of feedstock is the simplest form of utilization but also has the potential to be the most flexible. This is especially the case in the early stages of a Lunar base, when recycling materials would be at its most valuable given the lack of ISRU activities. But even in later stages, feedstock could be used for numerous different applications as soon as the required manufacturing technologies and processes for those applications become available on the Moon. In this way, the feasibility and applicability of continuous space debris recycling could be inherently adaptable to the maturity of a Lunar base.

4.2. The Space Debris Servicing Vehicle

The proposed space debris recycling mission concept shown in Figure 4.1 employs an Orbital Transfer Vehicle (OTV) to capture the debris and facilitate the transfer from the debris orbit to the Lunar surface. Many different vehicles exist within the class of OTVs, though fundamentally an OTV is characterized by the main functionality of transporting a payload from one orbit to another using some form of propulsion. Within this definition, even cargo spacecraft such as ESA's ATV and even the Orion spacecraft instrumental to the Artemis program can be seen as OTVs. Within the context of a space debris recycling mission, the functionality of an OTV must be expanded with the capability to capture a piece of space debris, in this case a defunct rocket stage. With this added functionality in mind, the transfer vehicle for such a recycling mission was dubbed the "Space Debris Servicing Vehicle" (SDSV). While the design of the SDSV is not the primary focus of this study, a number of important aspects such as total mass budget and power consumption constraints were still be considered. Especially the wet mass of the vehicle is an important aspect that must be considered as it is constrained by the total payload capacity of the launch vehicle and thus heavily impacts mission feasibility.

In order to get a mass estimation for the vehicle, similarities were drawn to existing vehicles with similar purposes. It is important to consider that the estimated mass refers to the dry mass, as this will be used in combination with orbital mechanics and subsequent ΔV budgets to determine the propellant masses. One of the principle missions with shared heritage identified during the literature review are the Mission Extension Vehicle (MEV) missions performed by Northrop Grumman [18]. These vehicles were referenced for a mass estimation specifically because they were effectively launched without a payload, as they captured and docked with their target in orbit with their sole mission purpose being to extend the operational mission lifetime of the target satellite. This launch without a main payload is a key trait the MEVs share with a space debris recycling concept mission, which also captures its main payload mass in orbit. This consideration is important as it results in a lower required launch mass for an equivalent payload mass compared to a conventional satellite and more importantly, it allows for the reduction of the vehicle dry mass. Within this context, the capture mechanism could be regarded as the true payload for the MEVs and the space debris servicing vehicle alike. The MEVs effectively share all of the subsystems that a space debris servicing vehicle would need, including a propulsion system. The MEVs featured wet masses of 2330 kg and 2875 kg for the MEV-1 and MEV-2, respectively [44]. Since no dry mass information on the MEV-1 was found to be publicly available, it was chosen to use the dry mass of the heavier MEV-2 as a conservative baseline, which equals 1525 kg [50]. Given this information, a dry mass estimate of 1500 kg was chosen for the space debris servicing vehicle. Note that this does not include the debris mass. This is in line with a study performed by Koch [9], who outlines two rough estimates for vehicle concepts capable of transferring upper stages from GTO to the Moon with dry masses of 1500 kg and 1578 kg.

In terms of vehicle performance calculations for which the mass is an input (such as propellant mass), an overestimated dry mass is less dangerous than an underestimated one. As such, an analysis was performed to quantify the aforementioned mass saving due to not having to include a strict payload. Three main vehicles were identified for this analysis, these being the orbiters of the Chandrayaan-2 and Chandrayaan-3 missions as well as the European Service Module (ESM) of the Orion spacecraft. All of these vehicles are OTVs capable of transferring payloads of significant mass from Earth orbit to Lunar orbit. Mass data for these three vehicles has been tabulated in Table 4.2. Note that for the Chandrayaan vehicles, the ”payload” mass was defined as the wet mass of the landers it carried, as these (fueled) landers are the payload from the perspective of the transfer vehicle. For the ESM, the crew module was considered as the payload mass. The data presented in Table 4.2 refers to the published launch mass for the Artemis II mission [51].

Table 4.2: Dry mass and payload mass characteristics for representative missions vehicles.

Vehicle	Transfer vehicle dry mass [kg]	Payload mass [kg]	Transfer vehicle dry mass including payload [kg]	Payload to dry mass fraction
Chandrayaan-2 [52]	682	1498	2180	68.72%
Chandrayaan-3 [53]	448.62	1749.86	2198.48	79.59%
ESM [54, 51]	3500	10387.27	13887.27	74.80%

The difference between the Chandrayaan vehicles can be attributed to the fact that the Chandrayaan-2 transfer vehicle had a secondary mission as a Lunar orbiter and therefore an increased dry mass compared to Chandrayaan-3 transfer vehicle, which had no such secondary mission. Nevertheless, it can be seen that the payload makes up between 68.72% and 79.59% of the total vehicle dry mass to be carried from the perspective of the transfer vehicle. So by capturing payload in orbit, the launch mass of strictly the transfer vehicle can potentially be reduced significantly. A similar analysis can be made for the space debris recycling mission using the assumed 1500 kg dry mass to assess the validity of this assumption, taking into account the payload mass after capture in orbit. Table 4.3 shows the results of this analysis for two scenarios: one with the lowest mass H10 upper stage as a target and one with the heaviest ESC-A upper stage.

Table 4.3: Expanded dry mass and payload mass analysis for the SDSV.

Vehicle	Transfer vehicle dry mass [kg]	Captured payload mass [kg]	Total vehicle dry mass after capture [kg]	Payload to dry mass fraction
SDSV (H10)	1500	5000	6500	76.92%
SDSV (ESC-A)	1500	1764	3264	54.04%

It can be seen that for the 5000 kg ESC-A upper stage debris target, the payload dry mass fraction falls relatively well in line with the reference vehicles at 76.92%. When considering the lighter H10 upper stage as a target, the payload dry mass fraction falls to 54.04%, indicating that compared to the reference vehicle data, the dry mass is ”too heavy” for the payload mass. Hence the chosen 1500 kg dry mass would be a very conservative estimate for this case. Given these analyses, the 1500 kg dry mass assumption was considered adequate for a preliminary mission concept study like the one presented in this report.

4.3. The Alternative: Lunar Lander Material Delivery

When considering the idea of delivering raw materials to a Lunar outpost, recycling materials recovered from space debris is not the first concept that comes to mind. Rather, delivering such raw material directly to the Moon is a much more direct and readily accessible route. As such, a direct material delivery mission featuring a conventional Lunar lander was defined as the main alternative mission scenario and benchmarking tool for the space debris recycling missions to be directly compared against. In order to stay consistent with the vision of European autonomy, the Argonaut Lunar lander was chosen as the reference vehicle, shown in Figure 4.5. This choice also substantiates the comparative analysis as it is based on actual vehicle specifications rather than arbitrary ones. The Argonaut, previously designated as the European Large Logistics Lander (EL3), is a Lunar lander currently being designed by the European Space Agency and represents Europe’s vision for autonomous access to the Moon [55]. The Argonaut is designed with adaptability and flexibility in mind, and is capable of performing various mission types including science & exploration, technology demonstration, in-situ resource utilization support and cargo logistics, with latter being of principle interest for this study.

Figure 4.5: Rendering of the Argonaut Lunar lander. [55]

In terms of its overall mission profile, the Argonaut requires a dedicated launch of Ariane 64, which puts the Argonaut lander directly on a Lunar transfer orbit. The lander then performs its own Lunar capture followed by the descent and final landing manoeuvres. Since the casting of raw metal feedstock material was selected as the desired utilization method for the space debris recycling mission concept, it was chosen to also define such raw feedstock material as payload mass for the Argonaut in order to remain consistent. Additionally, this allows the full 2100 kg payload capacity to be realistically utilized. A set of specifications for the Argonaut lander are tabulated in Table 4.4. Note here that the information presented by ESA [55] lists only the ”mass on the Moon without cargo” as 1600 kg. Since the Argonaut has no ascent capabilities, it was assumed that the propellant tanks would be completely depleted after landing and in turn that this listed mass could thus be interpreted as the dry mass of the vehicle excluding the payload. Adding the 2100 kg of maximum payload mass results in the 3700 kg inferred dry mass shown in Table 4.4. Assuming that the launch mass presented by ESA [55] is the vehicle wet mass, a propellant mass of 6300 kg can be inferred from the presented data.

Table 4.4: Specifications for the Argonaut Lunar lander. [55, 56]

Argonaut specifications	
Launch vehicle	Ariane 64
Launch site	Kourou, French Guiana
Dimensions	Height: 6 m, diameter: 4.5 m
Propulsion system	Chemical bi-propellant
Propellants	MMH & MON-3
Launch mass	10 000 kg
Payload mass	2100 kg
Dry mass	3700 kg [(b)]

[(b)] Inferred from maximum payload mass and vehicle mass without cargo as given by ESA [55].

5

Planetary Phases: Earth & Moon

This chapter details the relevant mission analyses for the space debris recycling mission concepts as well as the alternative Argonaut mission concept. The Earth and Moon phases represent the starting and ending points for mission and as such they were assessed before the orbital transfer, which connects the two planetary phases.

5.1. Earth Phase: Manufacturing & Launch

The Earth phase, within the scope of the energy analysis that forms core of the study, is represented by two main processes. The first of foremost of these is the launch, which is expected to be the largest energy sink within the entire mission given the massive amounts of propellants being combusted. Secondly there is is the manufacturing of the raw material feedstock that forms the payload of the alternative Argonaut mission scenario. As this direct material delivery scenario does not have to perform any recycling operations, the inclusion of the energy cost of actually manufacturing this material is critical.

5.1.1. Aluminium Manufacturing

One of the primary ways in which a space debris recycling mission differs from an alternative, direct material delivery mission utilizing a Lunar lander is the way in which the the material is acquired. For a space debris recycling mission, metal is obtained from the targeted piece of space debris while for the alternative mission, material must be produced separately. The production processes for such metals add up to make a significant energy sink. Given that aluminium alloys were found to be the primary structural materials used within the space debris population [18], the process cycle for the refinement of conventional aluminium was assessed. Within the metal refining industry, two general production streams for metals can be defined. Primary production involves the production of metals from raw ore mined from terrestrial deposits, while secondary production involves specifically the recovery of metals from metallic objects that have reached the end of their primary life and other salvaged metallic scrap through a recycling process [57]. While the latter is important for the envisioned recycling of metals on the Lunar surface, evaluating the former is critical to estimate the energy sink made up by the manufacturing of the raw metals for the alternative mission scenario featuring the Argonaut Lunar lander.

Primary production is primarily facilitated through the refining of bauxite ore. The overall process cycle for this primary production is well understood and extensively documented in reports such as the one by Choate and Green [17] for the US. Given the lack of public data for global energy usages, these US values were considered representative for this study. For the energy analysis, it was chosen to use the actual energy used for aluminium production as opposed to the theoretical minimum energy required. This is because the primary production of aluminium knows significant efficiency losses across the production chain that must be accounted for to accurately capture the embodied energy. Additionally, a distinction is made between onsite production energy usage (i.e. the energy used within the production facilities) and ”tacit” energy. This ”tacit” or gross energy includes ”secondary energies” required for producing electric energy and raw material feedstock [17]. This is an important step considering that the generation of electricity required for some processes also requires energy. For the manufacturing of aluminium, the current US electrical grid was used to determine the tacit energy values used in the analysis. Accounting for sustainable energy generation, the current US grid consumes on average 3.01 kWh of chemical (fuel) energy to supply 1 kWh of electrical energy [17].

The primary production process for aluminium begins with the mining of bauxite ore from terrestrial deposits, which requires approximately 0.32 kWh of onsite energy in order to produce the 5.1 kg of raw bauxite required to produce 1 kg of aluminium [17, 58]. The mining is a primarily mechanical process which has an effectively negligible tacit component. This bauxite is then refined into alumina, which primarily consist of Aluminium Oxides (Al_2O_3), through the Bayer Process. This is an energy-intensive, caustic process that involves four main steps: digestion, clarification, precipitation and calcination [17]. The Bayer Process requires approximately 7.27 kWh of onsite energy to refine the 1.93 kg of alumina required to produce 1 kg of aluminium, with a total tacit energy usage of 7.87 kWh [17]. The alumina produced through the refining process are then used as inputs for the Hall-Héroult process, which involves the electrolytic reduction of alumina into aluminium [17, 59]. This process requires approximately 15.58 kWh per kg of final aluminium product [17, 58]. Because this electrolytic reduction requires a lot of electricity, the tacit energy value is a lot higher at 46.54 kWh per kg of aluminium [17]. Additionally, the Hall-Héroult process requires a carbon anode which is consumed throughout the reduction process. As such, the energy required to produce this carbon anode, equaling approximately 0.66 kWh per kg of final aluminium product with a tacit value of 6.02 kWh [17], must be added to the energy sum. Finally, considering the intention is to send aluminium as raw material to the Lunar surface, simple ingot casting was taken as the processing method. This casting of primary aluminium requires an additional 1.01 kWh of energy per kg of cast aluminium with a tacit value of 1.46 kWh.

In total, it can be concluded that approximately 24.84 kWh is required to produce a single kg of aluminium through primary production, with a tacit or gross energy required of over 250% at 62.26 kWh per kg of aluminium produced. This confirms the statement that the secondary energy components are crucial when considering total embodied energy. This analysis shows that the primary production of aluminium is a very energy-intensive process, with smelting being the largest energy sink in the cycle both in terms of on-site energy as well as tacit energy. A summarized breakdown of the primary production cycle of aluminium from bauxite ore with its on-site and tacit energy requirements is presented in Table 5.1. Additionally, it should be noted that various processes within the primary production cycle have significant environmental impacts and generate substantial waste products.

Table 5.1: Summary of the required energy for the primary production process of aluminium from bauxite ore.

Process	On-site energy	Tacit energy	
	[kWh/kg of Al]	[kWh/kg al Al]	[MJ/kg of Al]
Bauxite mining	0.32	0.34	1.22
Carbon anode production	0.66	6.02	21.67
Alumina refining (Bayer process)	7.27	7.90	28.44
Smelting (Hall-Héroult process)	15.58	46.54	167.54
Casting	1.01	1.46	5.26
Total	**24.84**	**62.26**	**224.14**

It should be noted that any tertiary energy, i.e. the energy used for the production of buildings, equipment and transport is not included within this analysis. Such energies would be excessively complicated to determine, especially considering the complex lifecycle of a satellite with all its additional mission components such as launch. Secondary production, by its nature of being a recycling process, does not require the elaborate, energy-intensive chemical processes that dominate the energy requirements of primary production. Generally speaking, the energy required for secondary production in practice ranges between 5% - 6% of the energy required for primary production [17, 59]. This required energy is driven primarily by the heat required to re-melt the scrap aluminium such that it can be cast into new feedstock. The major reduction in energy required is exactly the reason why the recycling of aluminium has been widely adopted by the world, and why such recycling practices could provide major benefits in terms of overall energy usage when translated to assets in space to establish a circular space economy. The exact energy required for the recycling process on the Lunar surface will be elaborated upon later in this chapter.

5.1.2. Launch on Ariane 6

Earlier in this report, the Ariane 6 was highlighted as launch vehicle of choice for a space debris recycling mission. Superseding the Ariane 5 after its recent decommissioning, the Ariane 6 will be Europe's principle heavy lift launch vehicle following its maiden flight scheduled for 2026. Ariane 6 follows a very similar

design language to previous iterations of the Ariane launch vehicle, with a set of solid propellant booster stages alongside a cryogenic core and upper stage. However, it also presents significant performance upgrades with a generally more streamlined approach through sharing common boosters with the Vega C launch vehicle. Two main launch configurations of the Ariane 6 will exist, these being the Ariane 62 and 64, which are characterized by their use of 2 and 4 solid P120C booster stages, respectively. In terms of performance, Ariane 62 and 64 have a maximum payload mass capacity of 4500 and 11 500 kg, respectively to the targeted GTO [60].

The launch is one of the primary energy sinks for any space missions. For this study, it was considered that all energy expended through the launch comes in principle from the combustion of the propellants used by launch vehicle. That is, the expended energy in basis is the chemical energy embedded in the propellants which is released upon combustion. A number of important specifications for the Ariane 6 and its component stages are presented in Table 5.2

Table 5.2: Specifications for the Ariane 6 and its main stages. [61, 62, 63, 64]

Launch vehicle stage	Booster	LLPM	ULPM
Propulsion type	Solid	Cryogenic liquid	Cryogenic liquid
Engine	P120C	Vulcain 2.1	Vinci
Vacuum thrust	4500 kN	1371 kN	180 kN
Propellants	HPTB 1912	LH2 & LO2	LH2 & LO2
Propellant mass	143 600 kg	150 000 kg	30 000 kg

Cryogenic liquid core stages

Previously in this report it was established that the space debris recycling mission concept shall be assessed within the context of a mission with European autonomy. As such, the Ariane 6 launch vehicle was selected as the baseline launch option. This works hand in hand with the assessment of the main alternative, the direct delivery of raw metallic material to the Lunar surface, as the European Argonaut lander also employs Ariane 6 to facilitate the launch towards cis-Lunar space, particularly in its Ariane 64 configuration. Ariane 6 uses a combination of liquid hydrogen (LH2) and liquid oxygen (LOX) as fuel and oxidizer for both its main core stage and the upper stage, respectively [63, 64]. The chemical reaction for the combustion of liquid hydrogen and liquid oxygen is given in Equation 5.1.

$$2H_2(l) + O_2(l) \rightarrow 2H_2O(g) \tag{5.1}$$

The energy liberated from the propellants through this combustion reaction can be found using thermochemistry. This total heat of reaction was assessed by determining the enthalpy change of the chemical reaction given above, which can generally be formulated as shown in Equation 5.2 [65].

$$\Delta_r H = \Sigma(n_{product} \cdot H_{product}) - \Sigma(n_{reactant} \cdot H_{reactant}) \tag{5.2}$$

Sutton and Biblarz [66] detail that this heat of reaction represents the available chemical energy within the propellants and as such, it was considered an adequate tool for the determination of energy expended in a rocket launch. But rather than assessing the total enthalpy of a specie, it is common to use the standard enthalpy of formation in a series of standard formation reactions. This standard formation reaction is a reaction in which 1 mole of a compound is formed from its elements in their standard states. Here, the standard state is defined commonly as 1 bar of pressure at a temperature of 298.15 K [65]. Making use of this formulation is particularly powerful since the values for standard enthalpy of formation are well documented and extensively tabulated by various sources such as the National Institute of Standards and Technology (NIST) and Joint Army-Navy-Air Force (JANAF). The standard heat of reaction can be determined as shown in Equation 5.3 [65, 66].

$$\Delta_r H^\circ = \Sigma(n_{product} \cdot \Delta_f H^\circ_{product}) - \Sigma(n_{reactant} \cdot \Delta_f H^\circ_{reactant}) \tag{5.3}$$

Where n is the amount of moles of a given specie, $\Delta_f H^\circ$ is the standard heat of formation and the superscript $^\circ$ indicates standard conditions. For the reaction for liquid hydrogen and liquid oxygen given in Equation 5.1 yields the total heat of reaction shown in Equation 5.4. The values used for the standard heats of formation were collected from the NIST Chemistry Webbook [67].

$$\Delta_r H^\circ = 2 \cdot \Delta_f H^\circ_{H_2O(g)} - (2 \cdot \Delta_f H^\circ_{H_2(l)} + 1 \cdot \Delta_f H^\circ_{O_2(l)}) \tag{5.4}$$

$$\Delta_r H^\circ = 2 \cdot -241.83 - (2 \cdot 0 + 1 \cdot 0) = -483.66\ kJ \tag{5.5}$$

Note here that a negative heat of reaction indicates an exothermic process, which is logical for a combustion reaction. Additionally, the heat of formation of an element in the standard state is by definition equal to 0, which is why the heat of formation on the right side of the equation is equal to 0. Note however that the reaction given in Equation 5.1 is the stoichiometric reaction, which means that complete combustion occurs between 2 moles of hydrogen and 1 mole of oxygen to form 2 moles of water. This equates to an oxidizer to fuel mass ratio of 7.94 when considering molar masses equal to 31.998 g/mol and 2.016 g/mol for O_2 and H_2, respectively. In reality, the Vulcain 2.1 main engine that powers the Lower Liquid Propulsion Module (LLPM) of the Ariane 6 operates at an oxidizer to fuel ratio of 6.03 [63], meaning that there is excess fuel flow. In terms of molar quantities, this results in an actual reaction which uses 2.632 moles of liquid hydrogen for every mole of liquid oxygen, rather than 2. As such, the combustion reaction factoring in the actual oxidizer to fuel mass ration is shown in Equation 5.6.

$$2.632\ H_2(l) + O_2(l) \rightarrow 2H_2O(g) + 0.632\ H_2(g) \tag{5.6}$$

Indeed, this means that almost a quarter of the hydrogen remains uncombusted. It should be noted however that this reaction represents the ideal combustion reaction. In reality, incomplete combustion results in a multitude of additional compounds that are formed within the violent combustion process due to the relative lack of oxygen, which have been ignored for this analysis under the assumption of ideal combustion. Under this assumption, this excess hydrogen remains uncombusted in the flow In reality, the actual energy released from the combustion of the propellants is lower as not all chemical energy can be extracted due to the incomplete combustion. However, considering the fact that the proposed space debris recycling mission concepts as well as the Argonaut utilize the same launch vehicle (Ariane 64), the assumption of ideal combustion does not influence the final outcomes of the study when comparing these mission scenarios directly to one another.

From Equation 5.5, a total energy release of 483.66 kJ was found for the stoichiometric reaction equation. This heat of reaction does not change with the changed oxidizer to fuel ratio, as the new reaction equation was defined in Equation 5.6 by changing the amount of hydrogen. As such, the amount of water created on the right hand said remains the same, which combined with the additional hydrogen being present on both sides of the reaction equation, results in the same total heat of reaction. However, this total energy release was computed in Equation 5.5 using the heat of formation under standard conditions. Liquid hydrogen and liquid oxygen are cryogenic propellants, which means that they are not in the standard condition at the start of the reaction. In order to account for the enthalpy needed to bring the propellants from their cryogenic state up to the standard state, Hess' law was used. This law states that a change in enthalpy for a reaction is independent of the amount of steps required so long as the total reaction is the same [65]. As such, it can be considered that a reaction occurs at standard conditions and subsequently correct for any changes to account for the actual state of the reactants.

This change in state is captured in the absolute enthalpy of the propellants, which is the amount of energy required to bring the propellants from their cryogenic temperatures to the reference standard state of 298 K for which the heat of reaction was determined. That is, it represents the heat required to vaporize the liquids and subsequently heat up them up to the standard 298 K [66]. Assuming a storage temperature of 20.27 K for liquid hydrogen and 90.18 K for liquid oxygen, this absolute enthalpy is equal to -9.018 kJ/mol and -12.987 kJ/mol for liquid hydrogen and liquid oxygen, respectively [68]. As such, the net heat of reaction was computed using Equation 5.7, where ΔH_{298K} represents the enthalpy used to bring the propellants into the standard state.

$$\Delta_r H = \Delta_r H^\circ - \Delta H_{298K} \tag{5.7}$$

$$\Delta_r H = -483.66 - (2.632 \cdot -9.018 + 1 \cdot -12.987) = 446.94\ kJ \tag{5.8}$$

This is the absolute heat released from the reaction under the actual oxidizer to fuel ratio as given in Equation 5.6. It should be noted that bringing the reaction products from the standard state to a new state is not required. Within the context of expended energy for a rocket launch, what this energy is used for after combustion is irrelevant, for the only thing of interest is the available chemical energy liberated from the combustion of the propellants. Using the molar masses of hydrogen and oxygen once more, this equates to a specific energy release of 11.981 MJ/kg of propellant reactants, which equal the reaction products due to the conservation of mass. The Lower Liquid Propulsion Module of the Ariane 6 launch vehicle carries in total approximately 150 000 kg of propellants [61], which results in a total energy expenditure of 1.797 TJ.

For the Upper Liquid Propulsion Module (ULPM), the exact same procedure was performed, though now using an oxidizer to fuel mass ratio of 6.1[(c)] for the Vinci engine that powers this upper stage of the Ariane 6 launch vehicle [64]. Indeed, this ratio is very close to the one used by the much larger first stage, which is reflected by the fact that accounting for the difference leads only to a change of 0.03 moles of liquid hydrogen on both sides of the reaction shown in Equation 5.6. Employing the same procedure for computing the energy expenditure as employed for the LLPM results in a net heat of reaction of $\Delta_r H$ = -447.21 kJ and a subsequent specific energy release of 12.008 MJ/kg of propellant reactants. The ULPM carries approximately 30 000 kg of propellants in total [61] which results in a total energy expenditure of 0.360 TJ. As such, the total energy expenditure of the entire Ariane 6 core rocket (LLPM & ULPM) equates to 2.157 TJ.

Solid rocket booster stages

Alongside the LLPM and ULPM core stages, the Ariane 6 launch vehicle also uses a number of P120C solid propellant booster stages. Depending on the configuration, 2 or 4 boosters are used for Ariane 62 and Ariane 64, respectively [61]. These booster stages employ HTPB 1912 solid rocket propellant. This particular propellant uses fine aluminium powder as a fuel and ammonium perchlorate (H_4ClO_4) as an oxidizer, held together in a solid grain by a binding agent called Hydroxyl Terminated Polybutadiene (HTPB) [69]. These boosters are key for facilitating the first part of the launch trajectory, where their massive 4.5 MN individual thrust levels provide up to 91% of the total thrust for the Ariane 64 configuration. The same general methodology was applied to determine the total energy release through combustion of the solid rocket booster as was used for the cryogenic liquid core stages.

The combustion reaction for HTPB 1912 was not readily found in literature. As such, a similarity was drawn to the Space Launch System (SLS) and the Space Shuttle, which both use solid booster stages with the same aluminium and ammonium perchlorate combination. Several reactions were found which vary slightly in terms of the reaction products involved. It was chosen for this analysis to use the same reaction as described by NASA [70] for the SLS booster stages. Note that a potential difference in oxidizer to fuel mass ratio will be accounted for later when determining the absolute total energy released. The balanced reaction equation for this combustion reaction is shown in Equation 5.9.

$$6NH_4ClO_4(s) + 10Al(s) \rightarrow 4Al_2O_3(s) + 2AlCl_3(s) + 12H_2O(g) + 3N_2(g) \tag{5.9}$$

The heat of reaction can be determined similarly as done before, by computing the total standard enthalpy of reaction using the standard heats of formation of the species involved, as shown in Equation 5.10[(d)]. The values for the standard heats of formation were once again taken from the NIST Chemistry Webbook [67].

$$\Delta_r H^\circ = 4\Delta_f H^\circ_{AL_2O_3(s)} + 2\Delta_f H^\circ_{AL_Cl_3(s)} + 12\Delta_f H^\circ_{H_2O(g)} + 3\Delta_f H^\circ_{N_2(g)} - (6\Delta_f H^\circ_{NH_4ClO_4(s)} + 10\Delta_f H^\circ_{Al(2)}) \tag{5.10}$$

$$\Delta_r H^\circ = 4 \cdot -1675.7 + 2 \cdot -705.63 + 12 \cdot -241.83 + 3 \cdot 0 - (6 \cdot -295.77 + 10 \cdot 0) = -9241.4\ kJ \tag{5.11}$$

Similarly to the reaction for liquid hydrogen and liquid oxygen in the core stages, the reaction given above represents an ideal combustion reaction. Aside from the neglection of incomplete combustion and dissociation effects mentioned before, it can be noted that HTPB is not featured in the reaction equation for the solid rocket propellant. This is because it was assumed that this binder agent does not contribute to the combustion and exists only to hold the main oxidizer and fuel. In reality, this binder will combust to some extent, but these effects were also ignored for the sake of avoiding an extremely complex reaction equation.

Because the solid propellant booster stages are not actively cooled in any way, it was assumed that the reaction occurs at the standard conditions. As such, the above computed heat of reaction can readily be used without having to account for bringing the propellant reactants to the standard state. The reaction given in Equation 5.9 equates to an oxidizer to fuel mass ratio of 2.613 when considering molar masses of 117.489 g/mol and 26.982 g/mol for NH_4ClO_4 and Al, respectively. The actual rocket booster however contains 69% ammonium perchlorate and 19% aluminium, which equates to an oxidizer to fuel mass ratio of 3.632. Hence the actual propellant combination is oxidizer-rich. Maintaining the ideal combustion assumption that was used in prior analyses, this additional oxidizer remains uncombusted in the flow and as such the total heat of reaction does not change, as explained before.

[(c)] This is the oxidizer to fuel ratio of the Vinci engine operating at maximum thrust. When throttled down, the oxidizer to fuel ratio can go down to 5.3. It was considered that operating at maximum thrust is the most probable scenario.

[(d)] The slightly different reactions found in literature were also assessed, from which it was concluded that the differences in the reaction resulted in a change of less than 3% in terms of heat of reaction.

In order to compute the total energy released from the combustion of an entire booster stage, consider that the heat of reaction determined in Equation 5.11 equates to a specific heat of reaction of 34.250 MJ/kg of aluminium. By determining the total expended energy based on the actual mass of aluminium fuel in the P120C booster stage, the change in oxidizer to fuel ratio is inherently accounted for considering that the actual propellant mixture is oxidizer-rich and thus contains less aluminium fuel than the stoichiometric case given in Equation 5.9. This is because in oxidizer-rich combustion, under the ideal combustion assumption, the heat of reaction and the amount of moles of fuel in the reaction equation do not change. Considering an aluminium mass percentage of 19% and a total booster propellant mass of 143.6 tons, each solid booster stage contains 27.284 tons of solid aluminium fuel. So a single P120C solid propellant booster stage has a total energy expenditure of 0.934 TJ.

Table 5.3 presents an overview of the propellant mass and the determined energy expenditures for the two cryogenic liquid core stages as well as the P120C booster stages. Additionally, the total energy expenditure of the Ariane 6 launch vehicle was determined for both the Ariane 62 and 64 configuration with 2 and 4 booster stages, respectively.

Table 5.3: Summary of propellant masses and energy expenditures for the Ariane 6 launch vehicle configurations.

Stage	**Propellant mass [kg]**	**Energy expenditure [TJ]**
Lower Liquid Propulsion Module	150 000	1.797
Upper Liquid Propulsion Module	30 000	0.360
P120C Booster Stage (1x)	143 600	0.934
Ariane 6 configuration	**Total energy [TJ]**	**Energy per kg payload to GTO [MJ/kg]**
Ariane 62	4.025	894.4
Ariane 64	5.893	512.4

5.2. Lunar Phase: Debris Processing & Utilization

Once the debris has been landed onto the Lunar surface, processing it and creating new, useful material out of it is the final step in the process chain. As it is for conventional metal recycling on Earth, re-melting is the primary energy sink within the process. Several potential melting technologies were identified in the Literature Study [18], with material melting through inductive heating presenting the most promising and potentially feasible option. Inductive heating is one of the primary aluminium recycling methods used on Earth and is characterized by high heating efficiencies, fast heating rates and instant start-up [71, 72]. Inductive heating is a contactless heating method, which is a key advantage when considering the (near) vacuum conditions of the Lunar surface. Fundamentally, inductive heating works by applying a rapidly alternating current to a conductive coil, which produces a rapidly oscillating magnetic field [71, 73]. When a metallic sample, or 'charge', is introduced within the coil, this oscillating magnetic field subsequently induces Eddy currents in the metal which in turn heat up the metallic charge material through the Joule effect [73, 72]. The fact that inductive heating does not require any combustion is a major advantage when considering its applicability on the Moon. Besides combustion not being a practical heating method due to the vacuum conditions, fuels would also have to be readily supplied from an external source. Induction heating however requires only electrical energy as input, which could readily be collected through the use of solar arrays. The lack of an atmosphere on the Moon would in turn allow for the leveraging of the complete incident Solar flux. These considerations paired with high furnace efficiencies of around 90% [17] make inductive heating an attractive option for a Lunar recycling infrastructure.

Several assumptions had to be made in order to assess the re-melting process. Most importantly, it was assumed that the required recycling infrastructure (furnaces, solar arrays etc.) is already present on the Lunar surface prior to the recycling mission. Detailing the process of establishing this infrastructure was considered beyond the scope of this study given the level of uncertainty in required size, utilization cycles and other aspects. Additionally, the assumption was made that scrap of reasonable size could be recovered as a result of the hard landing acting as a means of uncontrolled 'disassembly' of the space debris object. In order to assess the energy required for the re-melting of the salvaged metal scrap from the piece of space debris, Equation 5.12 was set up. This heat equation details the determination of the total theoretical energy required for heating and melting a material mass M from an initial temperature T_0 to a final pouring temperature T_{pour}. Note that this formulation neglects any adiabatic losses.

$$Q = M\left[C_{p_{solid}}\left(T_{melt} - T_0\right) + L_{fusion} + C_{p_{liquid}}\left(T_{pour} - T_{melt}\right)\right] \tag{5.12}$$

Where C_p is the specific heat capacity at a particular phase and L_{fusion} is the latent heat of fusion. The first term in this equation represents heating in the solid phase from a specified starting temperature up to the melting temperature T_{melt}. The second term, the latent heat of fusion, specifically represents the energy required to facilitate the phase change once the melting temperature has been reached. Finally, the last term in the equation represents the subsequent heating in the liquid phase from the melting temperature until the specified pouring temperature is reached. Note however that the specific heat capacity C_p is not a constant, but rather it varies with temperature, rising in the case of aluminium. In order to determine the specific heat capacity as a function of temperature, the Shomate equation was used. The Shomate equation, presented in Equation 5.13, describes the specific heat capacity based on a number of coefficients determined experimentally for various species [67].

$$C_p = A + B \cdot t + C \cdot t^2 + D \cdot t^3 + \frac{E}{t^2} \tag{5.13}$$

Where A, B, C, D and E are coefficients and t is the temperature (in K) divided by 1000. The values for these coefficients were retrieved from the NIST Chemistry Webbook for both the solid and liquid phase [67]. Due to the fact that these coefficients are determined experimentally for each species, values for the more exotic aluminium alloys used to make the upper stage space debris targets (Al7020 & Al2219) are not available. As such, it was chosen to use pure aluminium as a representative metal. This was considered an adequate assumption for the heat energy calculation due to the aforementioned aluminium alloys being predominantly composed out of aluminium, with weight percentages ranging from 91.2% to 94.7% [74]. Finally, Equation 5.13 returns the value of the specific heat capacity in J/mol-K. As such, the value was divided by the molar mass of aluminium (approximately 0.027 kg/mol) in order to yield the desired units of J/kg-K. Figure 5.1 shows the resulting specific heat capacity plotted as a function of temperature. The starting temperature in this graph is defined by the coefficients for the Shomate equation being given only down to 298 K at the lowest. It can be seen that the specific heat capacity varies significantly in the solid phase, but stabilizes into a practically constant value upon reaching the liquid phase.

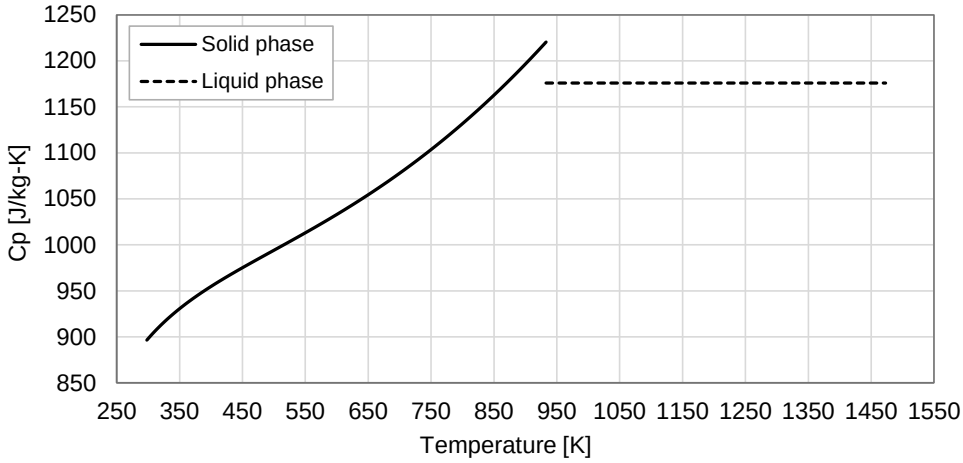

Figure 5.1: Specific heat capacity for solid and liquid phase aluminium obtained from the Shomate equation (5.13).

Several views can be had regarding the value for the initial temperature T_0. The temperature on the Lunar surface can range from 121°C in the daytime around the equator to −133°C in the night, with potentially even lower temperatures in craters or Permanently Shadowed Regions (PSR) [75]. Since the temperature on the Lunar surface effectively depends on the latitude, the main defining factor is the location of a recycling infrastructure. Given the fact that the Lunar south pole has been identified as the principle area for a Lunar base [7], it was chosen to use this same area as a baseline for the recycling infrastructure as well. The local temperature was recently measured in-situ by India's Chandrayaan-3 mission: the first mission to land near the south pole [76, 77]. Chandrayaan-3's Vikram lander measured a surface temperature of roughly 48.5°C during the Lunar day it was active. This value was determined from the graph shown in Figure 5.2 published by the Indian Space Research Organization (ISRO) [76].

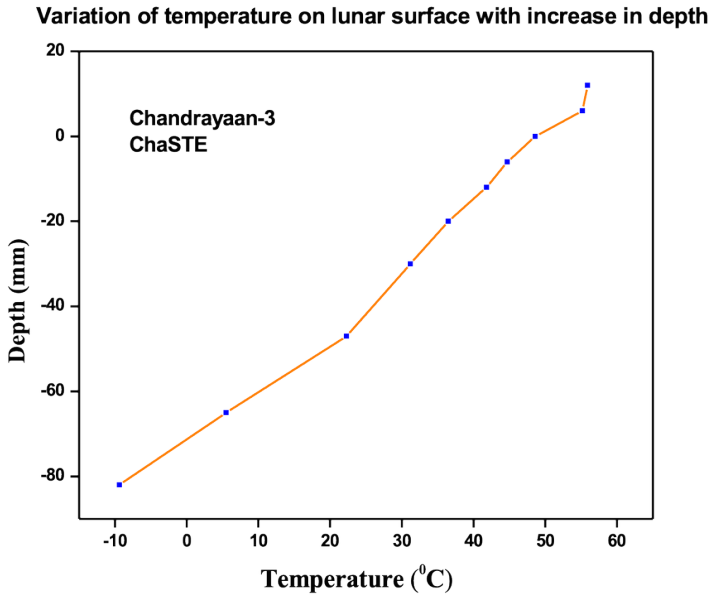

Figure 5.2: Temperature gradient in the Lunar soil at various depths. [76]

Given these observations, it was assumed that the space debris scrap recovered from the Lunar impact would have reached thermal equilibrium with the Lunar surface after being left on the surface for an undefined amount of time prior to recycling. As such, a surface temperature of 48.5°C was taken from Figure 5.2 at a depth of 0 mm as a baseline value for the initial temperature T_0 in Equation 5.12. In reality, other aspects such as differences in optical properties like absorbtivity and emissivity could also influence the temperature of metal scrap on the Lunar surface. While the low emissivity of the aluminium could potentially result in higher temperatures, the established 48.5° results in a conservative analysis considering a higher initial temperature would require less heating energy to be applied for re-melting the debris scrap. Note that the high Lunar daytime temperature of 121°C is still more than low enough to store the recovered scrap on the surface effectively indefinitely.

In order to complete Equation 5.12, the melting temperature T_{melt} and pouring temperature T_{pour} must be set. Values of 660°C and 960°C [17] were taken for the melting and pouring temperatures for aluminium, respectively. In order to account for the increasing value of the specific heat capacity, the energy required was calculated numerically for small steps in temperature dT and updating the specific heat capacity with every calculated step to compute the incremental step in required energy dQ. By omitting the mass multiplication at the start of Equation 5.12, a specific energy required for melting the material can be obtained per kg of material. This in turn allows for the determination of the required energy for different debris masses. Applying this method, a required melting energy of 1.394 MJ/kg is found from Equation 5.12. To stay consistent, the latent heat of fusion for pure aluminium was used at a value of 396 kJ/kg [78]. The evolution of the temperature as a function of the heating energy required for this remelting process is plotted in Figure 5.3.

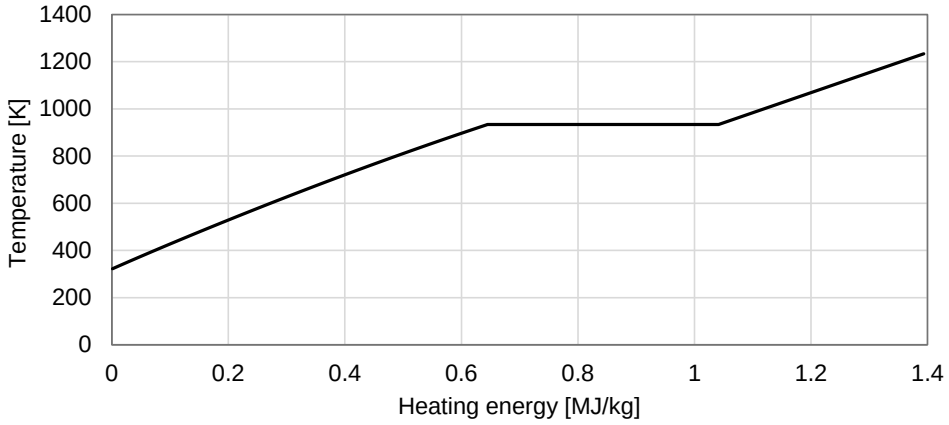

Figure 5.3: Evolution of the aluminium temperature and heating energy required for the remelting process

The horizontal segment of this graph represents the phase change from solid to liquid and corresponds with the defined magnitude of the latent heat of fusion. This however is only the theoretical energy required to melt the aluminium. The actual input energy required for the re-melting process depends on the efficiency of the electric induction furnace. Given a furnace efficiency $\eta_{furnace}$, Equation 5.14 can be used to determine the total specific input energy required for the debris re-melting.

$$E_{furnace} = Q \cdot \frac{1}{\eta_{furnace}} \tag{5.14}$$

Where Q is the heat energy as determined from Equation 5.12. Conventional induction furnaces used for aluminium recycling on Earth boast efficiencies of around 90% [17], which yields an energy requirement of 1.548 MJ/kg of aluminium. This is however only the energy required for the re-melting process. The casting of feedstock material completes the recycling process. Indeed, the creation of feedstock material is the most flexible and ultimately useful processing step considering such stock material can readily be stored on the Lunar surface and allows for a breadth of subsequent utilization techniques. This is especially so for the innovative mission that is space debris recycling, where simplicity is key whenever it can reasonably be achieved. Taking casting as the final processing step avoids uncertain approximations regarding transferring more complex manufacturing processes to the Lunar surface. Finally, the use of casting is consistent with the raw material provided by the alternative mission scenario delivering raw material directly to the Lunar surface detailed earlier in this chapter(see Table 5.1, for which simple ingots were also used. As such, the same 1.01 kWh (3.636 MJ) per kg of aluminium was used for the casting process [17], which leads to a total processing input energy of 5.184 MJ/kg of aluminium.

Comparing the energy required for this recycling process to the energy determined earlier in this chapter for the primary production of aluminium from bauxite (24.84 kWh, or 89.424 MJ per kg) reveals that the secondary production detailed in this section requires only 5.80% when considering the on-site energy required. Indeed, this is consistent with the 5% - 6% value found in literature [17]. The translation of the method to the Lunar surface, in terms of required energy, differs only due to the chosen starting temperature T_0. It was considered that in reality, the vacuum conditions potentially lower the heating energy required due to the lack of atmospheric pressure ”resisting” the free motion of molecules specifically for the liquid phase and the melting at the fusion point. However, characterizing this was determined to be beyond the scope of this study and as such, the applied analysis was taken as a conservative baseline.

While this electric energy for the inductive heating furnace is supplied by various sources including the burning of fossil fuels on Earth (which leads to the higher tacit energy usages as detailed earlier in this chapter), this is not suitable on the Lunar surface. Indeed, as explained before, sunlight is the prime source of energy to be used. The energy conversion efficiency of such solar arrays is the defining efficiency loss for a recycling plant on the Lunar surface. This thematically can be compared to the tacit energy used for the analysis of aluminium manufacturing on Earth, though it should be noted that they are not the same, considering that solar energy is sustainable and effectively free. It is embodied energy but does not represent an energy investment or ”cost”. While in the future a scenario could exist in which the entire electrical grid consists of sustainable energy which would not represent an energy ”cost”, the energy analysis for the aluminium manufacturing was based on the current situation in which 3.01 kWh of chemical (fuel) energy is required to generate 1 kWh of electrical energy [17]. Factoring in the efficiency of solar cells η_{cell}, Equation 5.15 can be used to determine the total input energy used by the recycling process.

$$E_{processing} = E_{furnace} \cdot \frac{1}{\eta_{cell}} \tag{5.15}$$

Plugging the previously found value of 5.184 MJ/kg into this equation with an assumed solar cell efficiency of 30% yields a total specific recycling energy of 17.28 MJ/kg of aluminium. Hence, in order to melt the estimated 3000 kg of raw material provided by an ESC-A upper stage, a total energy of 51.845 GJ of solar energy is required. This recycling energy required is 7.71% of the 224.14 MJ/kg tacit energy required for primary production of aluminium on Earth. This increase compared to the on-site energy is a result of the added relative inefficiency of solar arrays compared to the average efficiency of conventional fuels used on Earth as a means of generating electricity used to establish the tacit energy for the primary production of aluminium as presented earlier in this chapter.

6

Space Segment: Orbital Transfers & Trajectories

With the planetary phases and their respective key processes detailed, this chapter is dedicated to the analysis and design of the main orbital transfers. This chapter follows an exploratory approach in which several critical complexities are discovered and subsequently solved through the definition and analysis of various mission scenarios.

6.1. Orbital Characteristics Input Data

Before any transfers and trajectories can be considered, let us first solidify the starting conditions. The ideal target for a space debris recycling mission were identified earlier in this report to be European rocket stages, primarily defunct Ariane upper stages drifting in Geostationary Transfer Orbit (GTO). The fact that these objects exist primarily in the same orbital region simplify the initial characterization of the starting conditions for the orbital transfers in terms of the orbital elements. That is, the target rocket stages all share a very similar set of primary orbital elements, which are shown in Table 6.1.

Table 6.1: Range of orbital elements shared by the European rocket stages in the space debris target set, along with the standard Ariane GTO.

Orbital element	Symbol	GTO debris range	Ariane GTO [42, 60]
Semi major axis	a [km]	20 000 - 26 000	24 474.6
Perigee altitude	h_p [km]	200 - 400	250
Apogee altitude	h_a [km]	27 000 - 37 000	35 786
Eccentricity	e [-]	0.67 - 0.74	0.73
Inclination	i [°]	0.71 - 8.04	6
Mean motion	n [rev/day]	3.04 - 1.95	2.27

It can be seen that many of these orbital elements have remained relatively consistent with the standard orbital elements employed by ArianeGroup for GTO launches. These launches are based on low inclination (< 6°) with a perigee radius of 250 km and an apogee radius touching the Geostationary ring at 35 786 km. Of course the specific launch parameters change on a per-launch basis, but these standard parameters set a solid baseline for further use which simultaneously represent the actual orbital elements of the rocket stages making up the space debris population adequately. As such, it was chosen to use these standard parameters as a set of starting conditions for the orbital transfer analysis.

With the baseline set of orbital elements of the debris determined, several important physical and orbital parameters of the Moon are required to complete the input data for the orbital transfer analysis. A summary of this data, retrieved from NASA's "Lunar Constants and Models" document [79], is presented in Table 6.2.

Table 6.2: Important physical and orbital parameters of the Moon [79].

Parameter	Value
Mean radius	1738.0 km
Gravitational parameter	4902.8 km^3/s^2
Mean semi-major axis	384 400 km
Sidereal orbital period	27.32 days
Mean eccentricity	0.05490
Inclination	18.28° to 28.58°
RAAN	−13.36° to 13.36°

Given that the Moon's shape closely resembles a perfect sphere [79], excluding variations in local topography, the assumption of a perfectly spherical Moon with a global radius equal to the mean radius was made. The Moon's orbit however is much more complex than most Earth satellites due to the principle perturbation on its orbit being the third body gravitational force of the Sun [79]. Key orbital elements, such as the orbital inclination and the RAAN, vary significantly over time, as shown by Figure 6.1 and 6.2. To simplify the orbital transfer analysis, the assumption of a circular Moon orbit was made, setting the eccentricity to 0 with an orbital radius equal to the semi-major axis of 384 400 km. This is a common assumption in preliminary Lunar transfer studies which does not have a major impact on the transfer analysis [80], given the Moon's naturally low eccentricity. This assumption also removes the influence of variations in argument of periapsis.

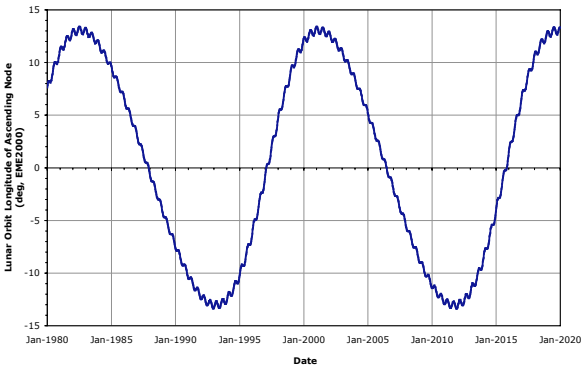

Figure 6.1: Moon orbit inclination w.r.t Earth's equator [79].

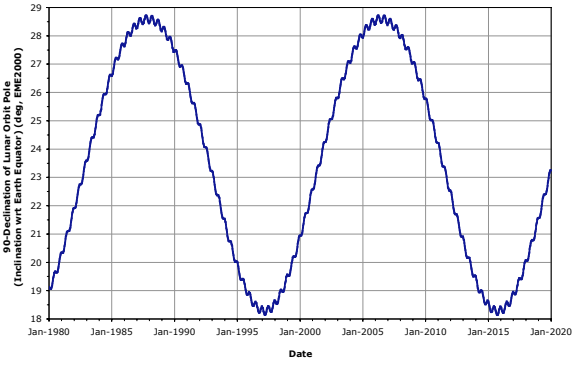

Figure 6.2: Moon orbit RAAN in the EME2000 frame [79].

6.2. Baseline Direct Lunar Transfer

When reviewing Lunar transfer trajectories used in the past, a direct, impulsive transfer from a low-Earth parking orbit is a common occurrence. The most commonly applied historical Lunar transfers employ a single or multiple subsequent elliptical transfer trajectories to reach the Moon. The parking orbits that function as the starting points for these trajectories can be both circular or elliptical. Considering that it was concluded earlier in this report that the ideal target space debris objects are defunct rocket stages residing in GTO, it makes sense to use this GTO as the baseline parking orbit. As such, it was assumed that the launch vehicle can inject the space debris servicing vehicle directly into the GTO orbit of the targeted rocket stage. After all, GTO is a very common launch trajectory typically used for the deployment of GEO satellites, which is why these stages continue to drift in GTO in the first place. It should be noted that this capability to launch the vehicle into GTO is a critical factor that must be accounted for in the design phase by continuously evaluating the payload mass capacity of the Ariane 6 launch vehicle. After being launched into the targeted GTO, the space debris servicing vehicle will perform a rendez-vous with the target and subsequently capture it using the nozzle probing mechanism discussed in the previous section.

As a first order analysis, an impulsive Trans-Lunar Injection (TLI) manoeuvre based on the minimum energy Hohmann transfer was used to determine the ΔV required for such a transfer. Performing the transfer injection at the perigee of the GTO is instrumental in order to make maximum use of the Oberth effect and allow for a minimum ΔV investment [81] to put the combined stack of servicing vehicle and the rocket stage space debris target onto a Lunar Transfer Orbit (LTO). The overall transfer geometry for this initial Lunar transfer is visualized in Figure 6.3. Note here that the inclination of the Moon was taken as the maximum naturally oscillating inclination of 28.58° [79].

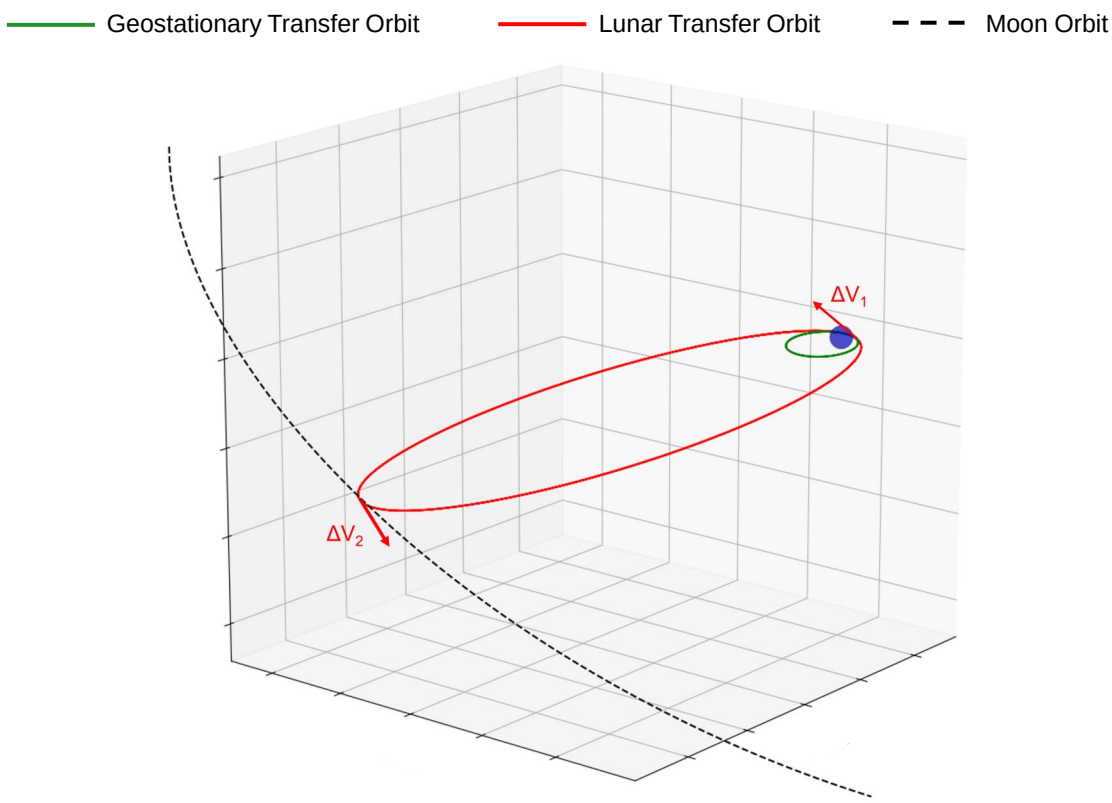

Figure 6.3: Transfer geometry for the direct, impulsive transfer from GTO to the Moon (to scale).

The figure above also displays the two impulsive manoeuvres ΔV_1 & ΔV_2 for TLI and Lunar capture, respectively. The exact orientation and size of these vectors is for indication purposes only and will be elaborated upon later in this section. One or multiple intermediate elliptical phasing orbits with a lower apogee may be used to ensure an encounter with the Moon at the final apogee passage point, as well as to perform any potentially necessary mid-course corrections. Instead of performing a single large transfer, the use of multiple successive smaller Hohmann transfers is often employed in reality to limit gravity losses and excessive thrust requirements associated with a single transfer, thus spreading out the total impulse over several consecutive manoeuvres performed in perigee. However, the assumption of impulsive manoeuvres means that gravity losses are not a factor and thus are neglected accordingly. The addition of one or multiple subsequent intermediate elliptical orbits does not equate to any additional ΔV costs compared to a single manoeuvre when considering impulsive Hohmann transfers [81]. Considering this knowledge, any phasing orbits were omitted and a single Hohmann transfer was considered moving forward. However, it should be noted that in reality, manoeuvres are not impulsive. As the required burn time increases, gravity losses can become significant, which is especially true when considering the large total vehicle mass for a debris recycling mission due to the captured debris object. As such, the use of multiple successive smaller Hohmann transfers should be used in a real mission scenario to limit these gravity losses.

Before assessing the ΔV requirements of the Lunar transfer, the phasing and rendez-vous manoeuvres must be addressed. Modelling these complex manoeuvres was considered beyond the scope of this research however, so instead values from literature were taken. A study by Koch [9] details the preliminary mission analysis for a smallsat mission that aims to rendez-vous with a rocket stage in GTO, presenting a total ΔV budget of 172.92 m/s. Instead of directly adapting this number, a value of 165.65 m/s was used, which is equal to the value presented by Koch after subtracting the ΔV of 7.26 m/s required for an inclination changing manoeuvre. Koch includes this inclination change to account for a deviating launch orbit due to the assumption of the smallsat mission not being the primary client. This assumption also causes the phasing orbit in which the satellite is deployed to be chosen very liberally, with a difference of over 3500 km in apogee altitude. For this study however, a space debris recycling mission was assumed to be the primary client for a launch considering the large expected vehicle mass. This means that a launch orbit much closer to the actual target orbit can likely be achieved. As such, the value of 165.65 m/s was considered a conservative estimate for the phasing and rendez-vous manoeuvres.

6.2.1. Zero-patched conics method

In order to assess the ΔV requirements for the two given impulsive manoeuvres, the method of "zero sphere of influence" or "point to point patched conics" was used, as presented by Uphoff [80]. This concept is a simple yet powerful method for the analysis of a non-coplanar Lunar transfer for which a simplified 2D analysis is not possible. This non-coplanar nature is critical, as a debris recycling mission is inherently dependent on the orbit of the debris, which exists in an orbital plane substantially different than the Earth-Moon plane. The method is commonly used in preliminary Lunar transfer studies [80], as well as interplanetary transfer problems [80, 81], capable of assessing the most critical part of the transfer, the planetary encounter hyperbola, within a few percent accuracy in terms of excess velocity. The zero-patched conics method works in basis by approximating the transfer trajectory as an ellipse that goes to the center of the Moon. By applying this method, the magnitude of the two required impulsive manoeuvres can be determined analytically. The first impulsive manoeuvre, ΔV_{TLI} can be computed by considering a purely coplanar transfer between GTO and LTO, subtracting the two perigee velocities as shown in Equation 6.1.

$$\Delta V_1 = \Delta V_{TLI} = V_{p_{LTO}} - V_{p_{GTO}} \tag{6.1}$$

Where V_p refers to the orbital velocity at the perigee point, respectively. A potential conversion between a vector and scalar subtraction is not required here since the manoeuvre was assumed to be impulsive and in line with the GTO velocity vector in pericenter. These two perigee velocities can readily be computed using the Vis-Viva equation, which allows for the determination of the orbital velocity at any point on an orbit, as shown in Equation 6.2 [81].

$$V_r = \sqrt{\frac{2\mu_E}{r} - \frac{\mu_E}{a}} \tag{6.2}$$

Where μ_E is the gravitational parameter of Earth (398 600 km^3/s^2 [82]), a is the semi-major axis of the orbit and V_r is the velocity at a point along the orbit with radius r. The Moon-relative excess velocity of the transfer vehicle at apogee passage where the encounter occurs can then be computed using Equation 6.3.

$$\overrightarrow{V_\infty} = \overrightarrow{V_M} - \overrightarrow{V_{a_{LTO}}} \tag{6.3}$$

Where $\overrightarrow{V_M}$ and $\overrightarrow{V_{a_{LTO}}}$ are the velocity vectors of the Moon and the transfer vehicle at apogee, respectively. A vector subtraction is necessary to account for the difference in orbit inclination. Determining the magnitude of this excess velocity can be done by using the cosine law, according to Equation 6.4.

$$V_\infty = \sqrt{V_{a_{LTO}}^2 + V_M^2 - 2 \cdot V_{a_{LTO}} \cdot V_M \cdot cos(\Delta i)} \tag{6.4}$$

Where Δi is the difference in inclination between the initial GTO and the orbit of the Moon. Again, the worst case scenario of a 28.76° should be used to ensure transfer feasibility over the range of naturally occurring Lunar inclinations. Note that within the zero-patched conics method, this relative velocity V_∞ is taken as the hyperbolic excess velocity in the selenocentric reference frame. By equating the Vis-Viva equation within the selenocentric frame once at an infinite distance (i.e. where the excess velocity is the only term) and once at the desired pericenter altitude of the hyperbolic entry trajectory around the Moon, Equation 6.5 can be set up. This operation is allowed because the orbital energy is constant within an orbit [81].

$$\frac{V_\infty^2}{2} = \frac{V^2}{2} - \frac{\mu_M}{r} \tag{6.5}$$

Where μ_M is the gravitational parameter of the Moon (4902.8 km^3/s^2 [83]). For this first order analysis, it can be assumed that the transfer orbit was targeted for a certain periapsis approach distance r_p around the Moon. Equation 6.5 can then be transformed into Equation 6.6 to yield the velocity at periapsis of the hyperbolic entry orbit.

$$V_p = \sqrt{V_\infty^2 - \frac{2\mu_M}{r_p}} \tag{6.6}$$

Assuming that the desired orbit is spherical in shape and coplanar to the hyperbolic entry orbit, the second impulsive manoeuvre ΔV_2 can be determined. This Lunar capture manoeuvre ΔV_{cap}, performed at periapsis of the hyperbolic selenocentric entry orbit, is equal to the subtraction of the periapsis velocity and the circular orbital velocity in the desired target orbit, as shown in Equation 6.7. Where V_c is the orbital velocity in the circular Lunar target orbit.

$$\Delta V_2 = \Delta V_{cap} = V_p - V_c = \sqrt{V_\infty^2 - \frac{2\mu_M}{r_p}} - \sqrt{\frac{\mu_M}{r_p}} \tag{6.7}$$

Validation of zero-pathed conics
To verify the validity of this method, a number of test scenarios were calculated and compared with numbers obtained from literature. Adapting the described procedure of the zero-patched conics method into a Python script allowed for the straightforward adaptation to several different transfer scenarios with varying initial and final orbit conditions. Wakker [81] presents a more detailed application of the patched conics approach which accounts for Lunar gravity and patches the two conic sections at the Lunar sphere of influence. It should be noted that this method assumes the transfer orbit to be coplanar with the Moon, restricting the analysis to 2D. Regardless, when considering a transfer from a 200 km circular parking orbit to a 500 km circular Lunar orbit, Wakker shows that the minimum-energy transfer results in ΔV values of 3.130 km/s and 0.732 km/s for the TLI and Lunar injection manoeuvres, respectively. Applying the zero-patched conics approach as detailed in this section for the same coplanar transfer conditions yields ΔV values of 3.131 km/s and 0.772 for the TLI and Lunar injection manoeuvres, respectively. These values correspond very closely to the ones presented by Wakker for the more detailed application of the patched conics approach, with only the Lunar injection manoeuvre showing a 40 m/s greater ΔV requirement. Additionally, Parker and Anderson [84] detail a number of direct Lunar transfer orbits from a circular 185 km parking orbit to a 100 km circular Lunar orbit. Applying the zero-patched conics method to this problem resulted in ΔV_{TLI} = 3.135 km/s and ΔV_{cap} = 0.822 km/s. These values match up very well 3.138 km/s and 0.828 km/s given by Parker and Anderson [84], respectively. Finally, Biesbroek and Janin [85] present a total ΔV requirement of 1.530 km/s for the MORO candidate mission, which launched from GTO to a 200 km Lunar orbit. Using the zero-patched conics method results in a value of 1.50 km/s for the total ΔV. The difference lies primarily in the first manoeuvre, where a difference of approximately 40 m/s is observed. This could be attributed to a number of variables, as the exact input parameters are not given, nor are any potential margins. Nevertheless, the result is within 6% and therefore was not considered a critical shortcoming given the circumstances.

6.2.2. Lunar descent & landing

Subsequently to the capture manoeuvre into the circular Lunar parking orbit, a descent manoeuvre down to the Lunar surface must be performed. Such a manoeuvre is relatively simple and as such it may readily be approximated by conic sections [84]. That is, the descent manoeuvre consists of an impulsive manoeuvre that places the periapsis point at zero altitude, followed by a second termination burn in order to cancel out the required surface-relative velocity. This is effectively a Hohmann transfer to the surface level combined with a larger second burn to slow down relative to the Lunar surface. Using such a Hohmann transfer, the descent injection ΔV_1 can be computed using Equation 6.8.

$$\Delta V_1 = \Delta V_{descent} = V_{c_{park}} - V_{a_T} = \sqrt{\frac{\mu_M}{r_{park}}} - \sqrt{\frac{2\mu_M}{r_{park}} - \frac{\mu_M}{a_{descent}}} \tag{6.8}$$

Where $a_{descent}$ is the semi-major axis of the Hohmann -like descent transfer. As mentioned before, this first manoeuvre puts the spacecraft on a trajectory with a 0 km altitude at periapsis, thus 'grazing' the Lunar surface [84]. The velocity at this point can be computed once again by employing the Vis-Viva equation and setting the radius equal to the (mean) radius of the Moon, as shown in Equation 6.9.

$$V_{p_{descent}} = \sqrt{\frac{2\mu_M}{R_M} - \frac{\mu_M}{a_{descent}}} \tag{6.9}$$

This orbital velocity at 0 km altitude must be reduced to the targeted impact velocity in order to approximate the actual landing. This is captured in a second impulsive burn, denoted here as a 'termination' burn. The required velocity increment for the termination burn is equal to:

$$\Delta V_{terminate} = V_{p_{descent}} - V_{impact} \tag{6.10}$$

Selecting an impact velocity is difficult, given that little is known about the behavior and dynamics of hyper-velocity impacts and how they influence large bodies impacting the Lunar surface. While the velocity should ideally be high enough to disintegrate and fragment the debris into scrap pieces that can be collected, it should not be so high that the material vaporizes. The study performed by Koch [9] concludes that velocities between 800 and 1600 m/s are an acceptable range for the impact of space debris onto the Lunar surface. Additionally, one of the mission concepts presented utilizes a Lunar impact velocity of 1332 m/s.

For the study presented in this report, it was chosen to set the impact velocity in the middle of the suggested range at 1200 m/s as a baseline. It should be noted that when crashing onto the Lunar surface, other effects will reduce the impact energy transferred to the crashed debris. This includes aspects such as deformation of the Lunar surface and the impact energy absorbed by the transfer vehicle, which impacts the surface first after performing the retro-propulsive termination burn, acting not dissimilar to the crumple zone in a car.

It should be noted that while this method is suited for a 'hard' (i.e. non-zero velocity) landing, a soft landing can be analyzed using the same procedure by setting the impact velocity V_{impact} to 0. From this equation it can immediately be seen that a hard landing has significant potential for ΔV savings. For a traditional Lunar mission (like the Argonaut lander), a soft landing is a hard requirement which, due to its very costly nature in terms of ΔV historically results in slim payload margins. For example, consider a descent and landing from a 152 km circular Lunar parking orbit, which was an altitude commonly used by the Apollo missions [86]. This yields $\Delta V_{descent}$ = 0.0341 km/s and $\Delta V_{terminate}$ = 1.725 km/s for a total ΔV of 1.759 km/s if a soft landing is targeted. This value corresponds closely with the 1.742 km/s given by Wilhite et al. [86] for the optimum theoretical descent from an identical parking orbit. However, Wilhite et al. also show that landing on the Lunar surface is subject to substantially more losses than other transfer manoeuvres, predominantly gravity losses and thrust vectoring losses. So much so that the nominal ΔV used by the Apollo missions was 2.081 km/s [86]. Factoring in additional margins used by NASA for dispersions, contingencies and manual manoeuvres raised the total budgeted ΔV up to 2.261 km/s to ensure a safe landing for the astronauts [86].

To highlight the "cost" of a soft landing, the influence of the chosen Lunar impact velocity was analyzed. Figure 6.4 shows the theoretical ΔV computed using the method presented above, as well as the associated propellant mass, for which the calculation will be elaborated on in the next section. A target mass of 5000 kg (ESC-A) and transfer vehicle dry mass of 1500 kg were used. It can be seen from this figure that indeed, a soft landing is excessively costly, requiring nearly 5000 kg of propellant even when considering only the optimum theoretical ΔV. Moreover, since landing is the last manoeuvre in the mission sequence, it increases the required propellant mass for all previous manoeuvres (Lunar capture, TLI etc.). As such, it was concluded that a soft landing is infeasible for a space debris recycling mission, and instead a controlled crash with a 1200 m/s Lunar impact velocity was set as the baseline moving forward.

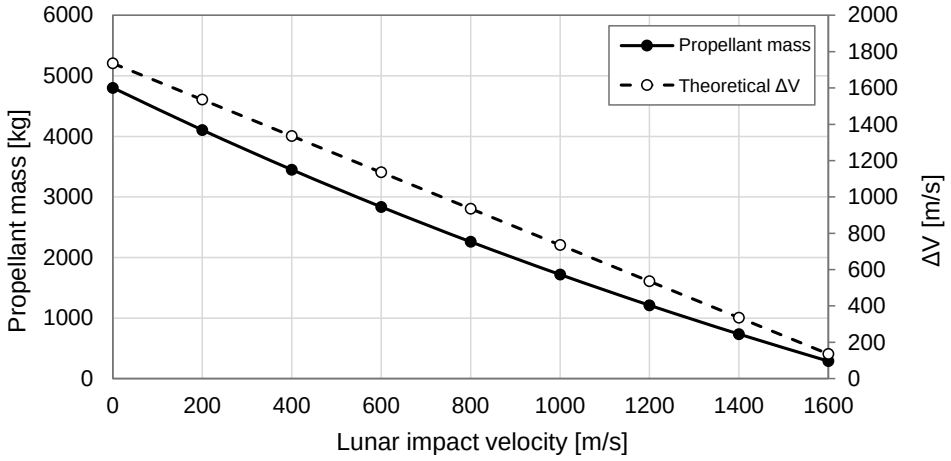

Figure 6.4: Landing ΔV and propellant mass as a function of Lunar impact velocity for a 5000 kg debris target.

This completes the full analytical definition of the four required impulsive transfer manoeuvres for the direct Lunar transfer mission scenario. As such, a complete ΔV budget can readily be determined for a defined set of orbital parameters. A Python script was written in order to ensure a structured implementation of the defined calculations and to allow for rapid iteration and re-evaluation.

6.2.3. Orbital transfer energy analysis

In order to determine the actual energy expenditure of the orbital transfer, the general procedure shown for the launch vehicle energy was used. That is, the total energy expenditure is represented by the chemical energy released from combusting propellants. As such, this metric represents the energy investment that has to be made in order to realise a particular orbital transfer manoeuvre, which is representative of the 'cost' of that specific manoeuvre. The procedure for the orbital transfer energy calculation has three main

steps. First, determining the ΔV through analytical implementation of the zero-patched conics approach, followed by determination of the propellant masses using the rocket equation and finally computing the energy expenditure through chemical energy released from those combusted propellants. The starting point for this analysis is thus a ΔV budget, which encompasses all required manoeuvres in a given mission sequence and details their respective required ΔV.

Using the standard Ariane GTO detailed earlier in this report (Table 6.1) as the starting point for the orbital transfer, a target circular Lunar parking orbit was set at a 100 km altitude. This altitude is by no means a hard requirement, as it is merely a staging point considering the mission has no additional operational or scientific mission prior to the descent and landing phase. For the landing, a crash velocity of 1200 m/s was set as a baseline. While this may be considered high, it is lower than the feasible crash velocity of up to 1600 m/s considered by Koch [9] for a similar mission. Since the presented calculation procedure outlined in this section are based on several assumptions and simplifications, design margins for the resulting ΔV values were taken into account. Such margins account for uncertainties in the calculations and unforeseen manoeuvres such as (small) mid-course corrections. For ΔV budgets, ESA accounts for a margin of 5% for "accurately calculated manoeuvres" [87]. In order to capture the simplification presented by the zero-patched conics method, it was chosen to double this margin to 10% for this analysis. Consequentially, the resulting ΔV budget for the baseline direct transfer is presented in Table 6.3.

Table 6.3: ΔV budget for the baseline direct, impulsive transfer from GTO to the Lunar surface.

Manoeuvre	ΔV [km/s]	Including margin [km/s]
Rendez-vous	0.166	0.182
TLI	0.679	0.747
Lunar capture	0.827	0.910
Descent injection	0.023	0.025
Landing termination	0.513	0.564
Total	**2.207**	**2.437**

From this point onwards, all ΔV budgets and calculations will include this 10% margin unless stated otherwise. The Tsiolkovsky rocket equation forms the basis of the procedure used to determine the required propellant. Presented in Equation 6.11, the rocket equation relates the required ΔV to the mass ratio of the transfer vehicle before and after the impulsive manoeuvre.

$$\Delta V = I_{sp} \cdot g_0 \cdot \ln\left(\frac{M_0}{M_F}\right) \tag{6.11}$$

Where M_0 is the initial mass, M_F is the final mass, g_0 is the standard gravitational acceleration on Earth (9.80665 m/s^2 [82]) and I_{sp} is the specific impulsive of the rocket engine. By noting that the initial mass M_0 is equal to the sum of the final mass M_F and the required propellant mass M_P, this propellant mass can be solved for according to Equation 6.12.

$$\Delta V = I_{sp} \cdot g_0 \cdot \ln\left(\frac{M_F + M_P}{M_F}\right) \qquad \rightarrow \qquad M_P = M_F\left(e^{\frac{\Delta V}{I_{sp} \cdot g_0}} - 1\right) \tag{6.12}$$

In order to determine the total required propellant mass, Equation 6.12 can be applied for the last manoeuvre in the sequence and subsequently moving backwards through the sequence to determine the propellant mass for each of the manoeuvres. This particular methodology works by noting that the final mass M_F for the last manoeuvre can be set equal to the sum of the dry mass of the transfer vehicle and the mass of the captured space debris target. That is, assuming that the propellant tank is depleted after the last manoeuvre is executed. The propellant mass determined for this last manoeuvre can then be added to the dry mass to form an updated final mass M_F for the manoeuvre preceding it. This procedure can then be repeated until the first manoeuvre is reached, and the final wet mass of the vehicle can be determined. Note that for the very first manoeuvre, the rendez-vous and capture, the target mass must not be included in the dry mass since the target is not yet captured.

A critical aspect of most space missions is the need for propellants that are long-term storable. Using cryogenic propellants like the ones used by the Ariane 6 is generally not suitable due to the cryogenic temperatures being very difficult to maintain over long periods as well as present boil-off losses. For launch vehicles, with operational lifetimes generally in the order of hours, this is not an issue. For spacecraft

that must function for much longer periods of time however, different solutions are required. A number of propellants have historically been used, but Hydrazine is by far the most common one. While inherently toxic and therefore difficult to handle, it presents numerous benefits that has made it the chemical propellant of choice for the majority of space missions and is still being used heavily in the space industry. For this analysis, it was chosen to use a bipropellant system as a baseline, using the common combination of Monomethyl Hydrazine (MMH) and Nitrogen Tetroxide (NTO) as fuel and oxidizer, respectively. These are both liquid at room temperature. Considering Hydrazine-based propellants are highly hazardous and toxic, which is why the space industry has seen a significant strive towards alternative, so-called "green" propellants. The main green propellants that have been developed are Hydroxyl-Ammonium Nitrate (HAN) based such as AF-M315E, Ammonium Dinitramide (ADN) based such as LMP-103S, and Hydrogen Peroxide [88, 89]. However, the engines developed for these propellants are limited to low thrust levels. Within the current industry, the highest thrust engine that was found is the ECAPS 220N HPGP engine, though this engine only has a Technology Readiness Level (TRL) of 3 [90]. Given the large debris masses that must be moved, high-thrust engine(s) are a necessity. Since the propulsion system definition was based on the current state of the space industry, the propellant combination of MMH and NTO was chosen, as the associated thrusters can readily achieve kN levels of thrust [91]. However, in the future, it is likely that green propellants will replace hydrazine-based propellants if comparable performance can be achieved. Just like what was done for the Ariane 6 launch vehicle, the energy liberated from these propellants can be determined using thermochemistry. The combustion reaction for this propellant combination is given in Equation 6.13 [92].

$$4CH_3NHNH_2(l) + 5N_2H_4(l) \rightarrow 9N_2(g) + 12H_2O(g) + 4CO_2(g) \tag{6.13}$$

The heat of reaction can be determined similarly as done before, by computing the total standard enthalpy of reaction using the standard heats of formation of the species and subtracting the reactants from the products, as shown in Equation 6.14 [93]. The values for the standard heats of formation were once again taken from the NIST Chemistry Webbook [67].

$$\Delta_r H^\circ = 9\Delta_f H^\circ_{N_2(g)} + 12\Delta_f H^\circ_{H_2O(g)} + 4\Delta_f H^\circ_{CO_2(g)} - (4\Delta_f H^\circ_{CH_3NHNH_2(l)} + 5\Delta_f H^\circ_{N_2H_4(l)}) \tag{6.14}$$

$$\Delta_r H^\circ = 9 \cdot 0 + 12 \cdot -241.83 + 4 \cdot -393.51 - (4 \cdot 54.14 + 5 \cdot -19.56) = -4790.31\ kJ \tag{6.15}$$

As mentioned during the analyses for the launch vehicle, this again represents the ideal, stoichiometric combustion reaction. Because both of the propellants are liquid at room temperature and therefore generally stored at such temperatures also within the spacecraft, it was assumed that the reaction occurs at the standard conditions. As such, the heat of reaction determined in Equation 6.15 holds. It can be noted from the reaction equation that the stoichiometric reaction occurs at an oxidizer to fuel mass ratio of 2.50 when considering molar masses of 46.072 g/mol and 92.016 g/mol for MMH and NTO, respectively. In reality however, the majority of rocket engines using MMH & NTO operate at an oxidizer to fuel ratio closer to 1.65 [91, 94]. This means that in reality, engines using MMH and NTO often run fuel rich, just like the core cryogenic liquid stages of the Ariane 6 discussed prior in this report. While this has performance benefits as highlighted before, this specific ratio is also the ratio of respective densities, leading to tanks of equal size [95, 96]. In order to determine the heat of combustion released under this actual oxidizer to fuel ratio, the same procedure can be followed as was done for the P120C booster stages of the Ariane 6. Consider that heat of reaction shown in Equation 6.15 equates to 10411.91 kJ/kg of NTO. By determining the actual expended energy based on the real oxidizer mass, the fuel rich combustion is accounted for. The oxidizer mass for a given total propellant mass can be determined from the oxidizer to fuel ratio, as shown in Equation 6.16.

$$OF = \frac{M_{OX}}{M_{FUEL}} = 1.65 \qquad \rightarrow \qquad M_P = M_{OX} + M_{FUEL} = M_{OX}\left(1 + \frac{1}{OF}\right) \tag{6.16}$$

Where OF is the oxidizer to fuel mass ratio, M_{FUEL} is the fuel mass and M_{OX} is the oxidizer mass. Note that this is effectively the same as updating the reaction equation with additional MMH on either side and then computing the heat of cumbustion per kg of total reactants. This is because this additional MMH remains uncombusted in the flow under the ideal combustion assumption and therefore does not increase the total heat of reaction, as explained before.

With this knowledge, a complete procedure for determining the total energy expenditure for each of the orbital transfer manoeuvres has been established. Using the same general mission scenario characteristics as established prior in this section when determining the ΔV budget (Table 6.3), the analysis results for the baseline direct transfer scenario from GTO to the Moon are given in Table 6.4. Both the ESC-A (5000

kg dry mass) and the H10 (1764.12 kg dry mass) were analyzed as space debris targets. Note that for the propellant mass calculations, a specific impulse (I_{sp}) value of 320 seconds was taken as a representative value for a bipropellant propulsion system using MMH& NTO [91, 94].

Table 6.4: Performance metrics for the baseline direct transfer scenario, including both the ESC-A and H10 as space debris targets.

Manoeuvre	∆V Budget [km/s]	Propellant mass [kg]		Energy cost [GJ]	
		H10	ESC-A	H10	ESC-A
Rendez-vous	0.182	294.89	496.16	1.912	3.217
TLI	0.747	1414.03	2815.83	9.167	18.255
Lunar capture	0.910	1325.40	2639.34	8.593	17.111
Descent injection	0.025	31.64	63.01	0.205	0.409
Landing termination	0.565	643.30	1281.04	4.170	8.305
Total	**2.429**	**3709.26**	**7295.37**	**24.047**	**47.297**

From these results, it can be seen that the overall energy expenditure for the orbital transfer is approximately 2 orders of magnitude lower than the energy expenditure for the launch. This substantial difference in energy however makes sense, as launch vehicles are first and foremost substantially larger and therefore carry much more propellant, but they are also a lot less efficient. Launch vehicles require a lot of energy to combat Earth's gravity and suffer from substantial drag losses as they go through the atmosphere. It can also be seen that the smaller H10 stage requires approximately half of the energy investment as compared to the heavier ESC-A, but this increase is disproportional to mass difference.

Considering the large influence of the launch, evaluating the payload mass margin is critical. Figure 6.5 visualizes the payload mass margins for the Ariane 62 & 64 configurations using the determined total masses for both the H10 and the ESC-A mission scenarios.

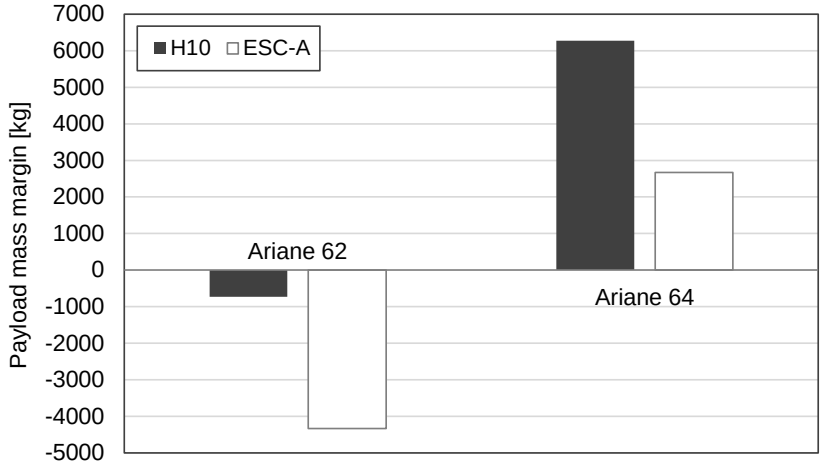

Figure 6.5: Ariane 62 & 64 payload mass margins for the baseline direct transfer scenario

It can be seen that the required launch mass exceeds the payload capacity of Ariane 62 to GTO for both considered space debris targets. The Ariane 64 however has significant payload margin leftover, which is predominantly caused by the fact that the main 'payload' mass is captured in orbit in the form of the space debris target, and thus does not have to be launched. The difference in payload margin is instead entirely due to the additional propellant required. As such, this is the first indication of a significant benefit of a space debris recycling mission as compared to a direct material delivery mission.

6.2.4. Direct raw material delivery using Argonaut

When considering the direct material delivery mission using a conventional lander, a direct transfer is the predominant transfer of choice. So too does the Argonaut employ a direct transfer to the Moon. The mmain difference between a conventional lander mission and the space debris recycling concept is the fact that there is no capture involved. As such, the established ΔV for the rendez-vous manoeuvres does not have to be accounted for. Since the Argonaut is facilitated by a dedicated launch of Ariane 64, the established

launch calculations hold also for this alternative. The only main difference in terms of orbital transfers is the fact that the Argonaut does not need to perform a TLI manoeuvre, as the launch vehicle puts it directly on a Lunar transfer orbit that encounters the Moon at apoapsis. Since the exact transfer trajectory is not known as of the writing of this report, it was assumed that the Argonaut's LTO uses the same perigee altitude of 250 km as the conventional GTO orbit. As such, the established direct transfer analysis featuring the zero-patched conics approach can be used again, though this time without the TLI manoeuvre, to facilitate a suitable comparison. This method was favored as apposed to directly inferring the Argonaut's propellant mass from public data in order to maintain consistency with the other analyses performed and thus ensure an adequate comparison. Another key difference as compared to the debris recycling concept is the fact that the direct delivery of metals through the use of a Lunar lander requires a soft landing.

Because the Argonaut also features a chemical bi-propellant system with MMH as fuel, the same performance characteristics (I_{sp} & H_r) that were used in the baseline direct transfer scenario were used here. While the Argonaut's main engine is set to use MON-3 as an oxidizer instead of NTO [56], the performance difference due to the 3% added nitric oxide was assumed to be negligible for this analysis. With this knowledge, the resulting performance metrics of the Argonaut mission scenario are given in Table 6.5.

Table 6.5: Calculated performance metrics for the Argonaut mission scenario.

Manoeuvre	ΔV Budget [km/s]	Propellant mass [kg]	Energy cost [GJ]
Lunar capture	0.910	2288.03	14.833
Descent injection	0.025	54.62	0.354
Landing termination	1.885	3045.35	19.743
Total	**2.820**	**5388.00**	**34.930**

While the final Lunar termination burn was based on the ideal minimum ΔV as detailed in subsection 6.2.2, using the previously established 2.081 km/s used as a nominal value for the Apollo missions to account for various margins applied by NASA [86] leads to a total required propellant mass of 5975.23 kg and a subsequent vehicle launch mass of 9675.23 kg. This corresponds closely with the reported 10 000 kg launch mass of the Argonaut as reported by ESA [55], further verifying the validity of the applied analysis.

Since it was determined that launch on the Ariane 62 configuration was unsuitable for the respective payload masses required, the three scenarios evaluated so far can readily be compared by considering all of them use the Ariane 64 launch vehicle configuration. It can be seen from these results that the total transfer energy expenditure for the Argonaut alternative mission scenario sits almost directly in between the energy expenditures of the two space debris recycling transfers of the H10 and ESC-A upper stages, respectively. The substantially larger final landing termination burn is balanced by the lacking of a required TLI manoeuvre, which is performed by the Ariane 6 instead. However, looking at only the total transfer energy expenditure as a means of quantifying the energy investment required for the orbital transfer does not capture the complete picture. This is because each of the mission scenarios, while differing in their energy expenditure, also fundamentally differ in the amount of material they bring to the Moon. As such, a "specific" transfer energy cost was defined as the energy cost per kg of raw material delivered to the Moon. Using the raw material fraction of 60% for the rocket stages as elaborated prior in this report, Table 6.6 details the proper comparison between the three scenarios considered thus far. Note here that the payload mass for the recycling scenarios was defined as the dry mass of the captured rocket stages.

Table 6.6: Breakdown of the specific transfer energy cost for the debris recycling scenario and the Argonaut scenario.

Mission scenario	Recycling: H10	Recycling: ESC-A	Argonaut
Payload mass [kg]	1764.12	5000	2100
Raw material mass fraction	60%	60%	100%
Raw material yield [kg]	1058.47	3000	2100
Transfer energy cost [GJ]	24.165	47.530	34.930
Specific transfer energy cost [MJ/kg]	**22.830**	**15.843**	**16.633**

A number of conclusions can be made from this analysis. First, when looking strictly at the transfers required for the rocket stages, it can be seen that the larger mass return of the ESC-A outweighs the increased propellant required in terms of overall energy efficiency. All the while the increased propellant mass required for the ESC-A does not prevent it from being launched, as was seen in the previous section. Comparing this with the Argonaut transfer scenario reveals that the necessity for a soft landing is the dominant factor that results in the large transfer cost for the Argonaut. Ultimately, the energy investment required per kg of delivered material is very similar for the ESC-A recycling mission scenario and the Argonaut mission scenario. This indicates that in terms of transfer efficiency, the additional mass delivered by capturing debris effectively makes up for the additional manoeuvres required. Note however that this analysis only shows the orbital transfer. The addition of the other mission segments such as material manufacturing and debris processing on the Moon will change the total numbers. An analysis on the complete mission cycle will follow later in this report.

6.2.5. The alignment problem

The baseline direct, Lunar transfer is a common trajectory for traditional Lunar missions. However, within the context of a debris recycling mission, the required optimal transfer geometry is not a given. This is because a debris recycling mission is inherently dependent on the orbit of the targeted piece of space debris. While the Ariane upper stages were originally launched into orbits with very similar characteristics, over time, various perturbations have shifted the orbital elements of these stages. Such perturbations include the gravitational effects of the non-spherical Earth (J2 effect), Solar radiation pressure, gravitational effects of other celestial bodies and even atmospheric drag. In order to visualize this alignment problem, consider Figure 6.6, which shows the actual orbit of three Ariane upper stages from the generated dataset along with the potential transfer orbit from perigee.

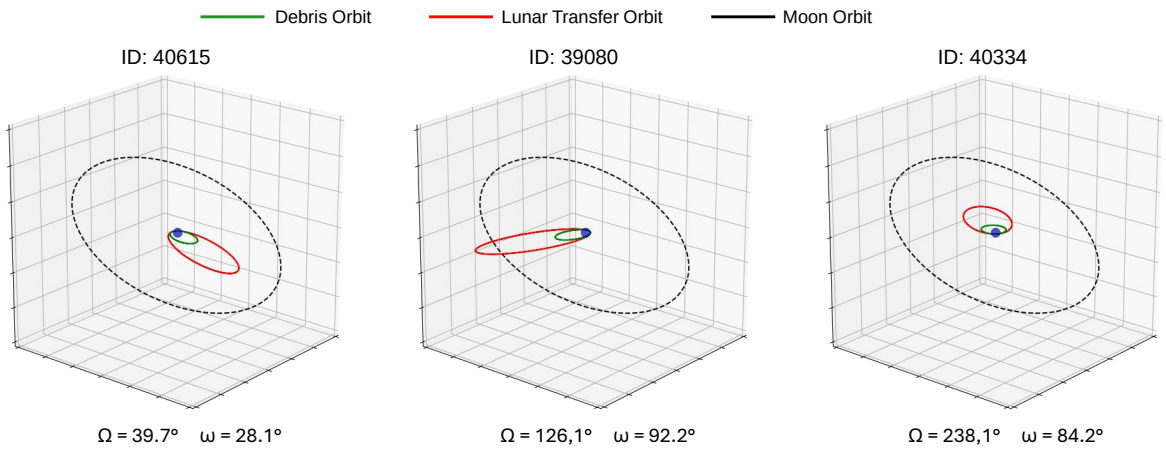

Figure 6.6: Orbital plane orientation of three samples from the dataset of Ariane upper stages in GTO.

Comparing this with the ideal transfer geometry highlighted in Figure 6.3, the issue becomes apparent. Indeed, in all of the presented cases, the transfer geometry is misaligned with the orbit of the Moon. Because the Argonaut mission scenario is facilitated by a direct, dedicated launch, this alignment problem is not an issue, for the planar alignment can readily be targeted for by choosing a specific launch day and time in order to place the apogee of the transfer orbit in the required position for a Lunar encounter. Looking at the orbital alignments presented above, it can be seen that the most prominent perturbing motion is rotational about the polar axis. The orbital elements extracted from the TLE's for the dataset of Ariane upper stages in GTO confirm this, as other elements like the inclination remain relatively unchanged from their original value. This observed rotation is governed by secular changes in the argument of periapsis (ω) and the Right Ascension of the Ascending Node (Ω), as indicated also in Figure 6.6. The distribution of these two orbital elements for all objects in the aforementioned dataset is plotted in Figure 6.7.

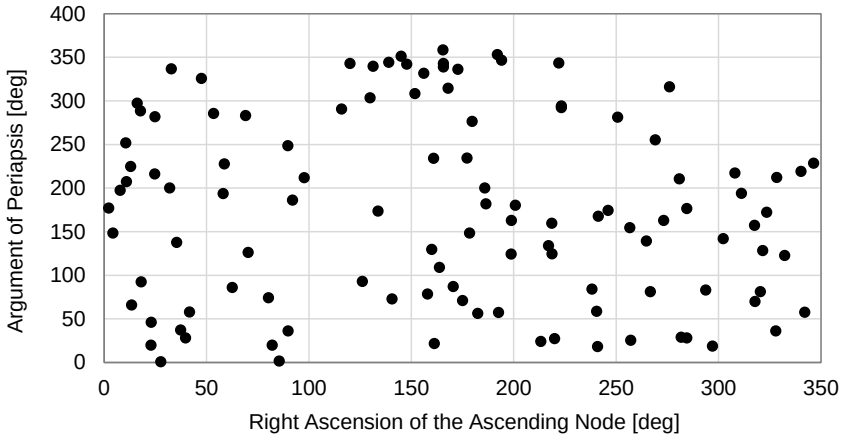

Figure 6.7: Distribution of argument of periapsis and right ascension of the ascending node for the Ariane upper stages in GTO.

From this figure, it can be seen that there is a very wide distribution over the full range (0° to 360°) of angles. Note that while each of these stages have been launched to orbits with very similar shapes and characteristics, their launch date and subsequently the time spent in GTO is the key difference. This difference in lifetime is what causes this wide distribution, as perturbing forces have acted longer on older stages. The dominant of these forces in GTO is the perturbation due to the non-spherical gravity field of Earth, often denoted as the J2 effect. This non-spherical gravity field is caused by the Earth's non-spherical shape and irregular mass distributions. The average secular rate of change in argument of periapsis and right ascension of the ascending node can be determined analytically using Equation 6.17 and 6.18, respectively [97, 80].

$$\dot{\bar{\omega}} = \frac{3}{4}\bar{n}J_2\left(\frac{R_E}{\bar{p}}\right)^2\left(4 - 5\sin^2(\bar{i})\right) \tag{6.17}$$

$$\dot{\bar{\Omega}} = -\frac{3}{2}\bar{n}J_2\left(\frac{R_E}{\bar{p}}\right)^2\cos(\bar{i}) \tag{6.18}$$

Where n is the mean motion, J_2 is the J2 coefficient of Earth's gravity field (1.083×10^{-3} [82]) and p is the semi-latus rectum of the orbit. Note that these are first order relations, but since the J2 term is approximately a thousand times larger than the other J_n and $J_{n,m}$ Legendre polynomial coefficients [81], this first order analysis was considered valid. Plugging in the corresponding values for the standard GTO yields values of $\dot{\bar{\omega}}$ = 0.824°/day and $\dot{\bar{\Omega}}$ = −0.415°/day. This is means that a full rotation in each element is completed in approximately 437 and 868 days, respectively. Considering the rather drastic consequences in terms of orbital alignment, this is considered rather fast in terms of motion, especially the change in argument of periapsis. Additional complexity is raised within the problem when considering the fact that the Moon's orbit also shifts over time. While this motion of the Moon's orbit is slow, it is another factor that should be considered.

In order for the transfer geometry for the baseline, direct transfer to be aligned properly, a number of conditions must be satisfied. For the sake of comprehensibility, let us define these conditions with respect to an arbitrary Moon orbit with frozen orbital elements. In basis, the transfer can only occur when the line of apsides (the line connecting the periapsis to the apoapsis) of the debris orbit lies in the Earth-Moon plane. When this occurs, the apogee of the Lunar Transfer Orbit touches the Moon's orbit. In the principle case, shown also in Figure 6.3, this happens when the debris and the Moon cross the equatorial plane at the same time, such that their lines of nodes coincide. In terms of orbital elements, this requires the RAAN of the debris to be equal to the RAAN of the Moon, as well as the argument of periapsis to be either 0° or 180°. This latter condition ensures that the apogee of the transfer orbit is at either the Moon's ascending node or the descending node.

Note that, given the distribution of RAAN and argument of periapsis shown in Figure 6.7, choosing a target stage that naturally approaches a particular desired value for either RAAN or argument of periapsis is considered possible, as a a debris recycling mission would have to be excessively planned ahead of time. However, because the rate of change for the RAAN and argument of periapsis is different in value as well as direction, orbital alignment is not guaranteed. Through analyzing the motion of the objects in GTO, it was found that the required orbital alignment for the 'perfect combination' of argument of periapsis

and RAAN, which aligns the line of nodes of the debris and Moon's orbit and positions the apogee of the transfer orbit at that intersection, does not naturally occur reliably under the given perturbations. While the situation does theoretically exist, it requires the three angular variables to be at a perfect condition, which exists only sporadically. Planning for such an alignment to appear would take an excessive time just to capture and recycle a single target, which was deemed a non-viable constraint for this study.

However, it was observed that given a set value for the Moon's RAAN, there are two unique combinations of RAAN and argument of periapsis for any particular debris orbit in GTO that lead to a suitable transfer alignment, though not in the equatorial plane. To highlight this, consider that the RAAN and argument of periapsis are effectively coupled and form the foundation of the orbital orientation for a piece of debris. To further analyze the behavior of these two variables within the context of this orbital orientation, the shift due to the J2 effect was modeled over time. Figure 6.8 shows a visualization of this analysis for an arbitrary debris orbit taken from the dataset of Ariane upper stages in GTO as it drifts over the span of 800 days. Note that this shows the possible transfer orbit after phasing for a set time in GTO, so phasing is not done in the LTO itself.

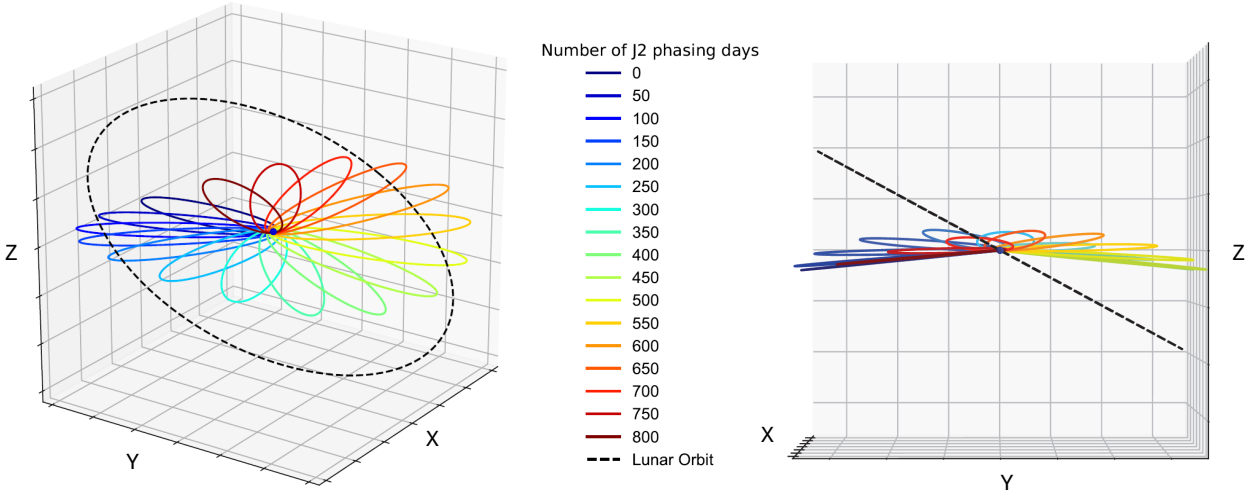

Figure 6.8: Visualization of Lunar transfer orbit orientation after J2 phasing propagation in GTO, timestep = 50 days.

As expected, the larger value of the J2 drift in argument of periapsis causes an overall Eastward motion over time. Combined with the influence of the RAAN drift, this results in a motion that takes on a saddle-like shape, as can also be seen in the figure above. The key thing to notice however is the fact that the apogee of the transfer orbit does seem to cross the Moon's orbit at two points, for the Moon's ascending and descending node, respectively. From the figure, a crossing between 200 and 250 days is observed, as well as one between 650 and 700 days. Figure 6.9 presents a second analysis, this time with a higher temporal resolution to show the drift in greater resolution.

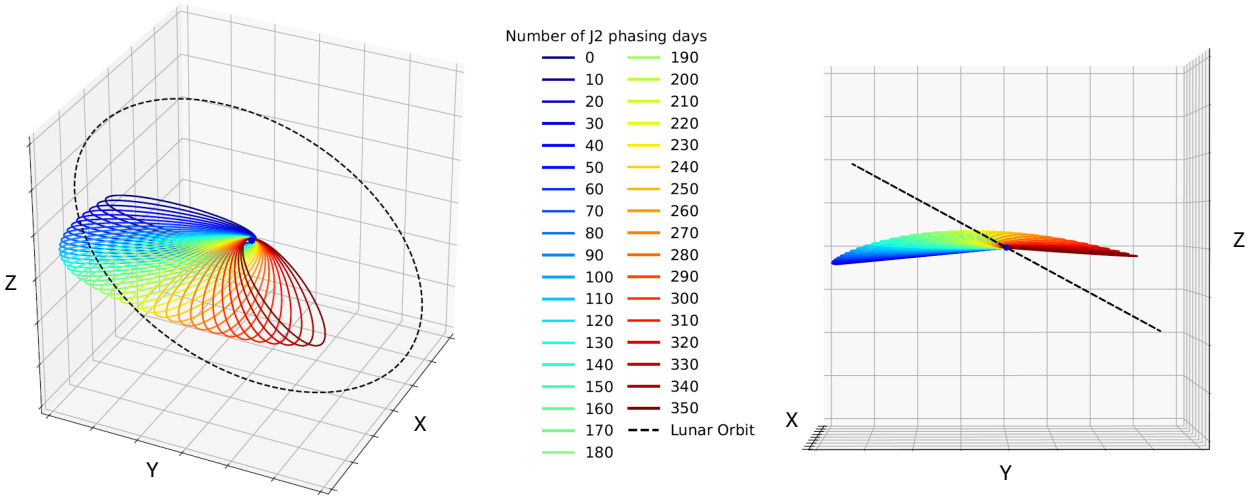

Figure 6.9: Visualization of Lunar transfer orbit orientation after J2 phasing propagation in GTO, timestep = 10 days.

Indeed, it can be seen that the apogee of the Lunar transfer orbit does touch the Moon's orbit after a phasing time in GTO of approximately 220 days. The actual phasing time required depends primarily on two factors. The first of these is the initial condition for the piece of debris itself,specifically in its RAAN and argument of periapsis. This reflects the initial orientation of its orbit at a particular point in time. The second factor is the position of the Moon. Due to the assumption of a circular Moon orbit, only its RAAN remains as an independent variable. Looking again at Figure 6.8, it can be seen that for any other orientation of the Earth-Moon plane in terms of RAAN, a moment exists for which the two identified unique combinations of argument of periapsis and RAAN of the debris orbit facilitate a transfer opportunity. This thus confirms that J2 phasing enables the use of the baseline direct orbital transfer strategy also for the space debris recycling concept. It should be noted that in reality the Moon's orbit is not stationary during this phasing time. However, given that the main shifting orbital element for the Moon which influences the orbital alignment, the RAAN, moves with a periodicity of 18.6 years, it was assumed that this shift is negligible in the proposed timeframe of the phasing. Under this assumption that the motion of the Moon can be neglected, the maximum potential phasing time for the required alignment to occur from any initial condition is characterised by the time needed for the debris orbit to precess through half of its complete and combined revolution shown in Figure 6.8. It was found that regardless of initial orbit conditions (ω & Ω), the time required to complete this motion equals approximately 380 days.

Additionally, the angle between the orbital plane of the debris and the orbital plane of the Moon shifts as well due to the J2 drift, which can be seen especially in the side projection in Figure 6.9. This means that the inclination difference as required for Equation 6.4 also varies. The angle between two orbital planes is equal to the angle between their respective angular momentum vectors. By conducting a grid search approach between the given GTO orbit and the Moon's orbit for various RAAN values, it was found that the maximum angle between the two orbital planes is approximately 35°. Indeed, this maximum is bound by the sum of the two inclinations. This maximum angle occurs when the RAAN values of the Moon and the debris differ by exactly 180°. As such, this 35° inclination difference was taken as a worst case scenario for the baseline direct orbital transfer for the debris recycling mission scenario to ensure feasibility for any natural occuring alignment geometries. Using this maximum inclination difference, Table 6.7 presents the final performance metrics for the baseline direct transfer scenario.

Table 6.7: Final performance metrics for the baseline direct transfer scenario, including both the ESC-A and H10 as space debris targets.

Manoeuvre	ΔV Budget [km/s]	Propellant mass [kg]		Energy cost [GJ]	
		H10	ESC-A	H10	ESC-A
Rendez-vous	0.182	294.89	498.32	1.912	3.231
TLI	0.747	1417.88	2823.48	9.192	18.305
Lunar capture	0.919	1339.72	2667.84	8.685	17.296
Descent injection	0.025	31.64	63.01	0.205	0.409
Landing termination	0.564	643.30	1281.04	4.170	8.305
Total	**2.437**	**3727.43**	**7333.69**	**24.165**	**47.544**

Comparing this with the results from the ideal analysis shown in Table 6.4 highlights only minor differences. In terms of ΔV, the larger maximum angular difference between the orbital planes of the Moon and the debris results in approximately 10 m/s of additional performance required. While plane changes are conventionally expensive [81], the presented case is limited due to the Lunar capture manoeuvre being performed at apogee, very far away from Earth. The subsequent increases in propellant mass are similarly small, totaling as most approximately 38 kg (0.5%).

While phasing for a defined length of time in GTO does help solve the alignment problem, it does also come with several downsides. The primary of these is the fact that after capturing the defunct rocket stage, the Space Debris Servicing Vehicle will spend a long time (up to the determined 380 days at worst) in the high-radiation environment defined by the Van Allen belts. These Van Allen radiation belts are zones of charged particles trapped by the Earth's magnetic field, generally torroidal in shape. The high amounts of radiation in these zones is dangerous to various satellite systems, particularly electronics, sensors and photovoltaics. There are two main Van Allen belts, the inner belt stretching from about 6000 km to 12 000 km and the outer belt stretching from about 25 000 km to 45 000 km [98]. As such, the standard GTO orbit crosses both the inner and the outer Van Allen belts. This makes GTO an orbit particularly precarious in

terms of radiation, though by far the most dangerous of these belts is the lower one, with particle energies as high as 10 MeV [98]. While studying the implications of waiting potentially over a year in this high-radiation environment was considered beyond the scope of this study, it is recognized that this could be a substantial risk to the servicing vehicle and the mission as a whole. Performing an initial periapsis raising manoeuvre after capture of the targeted piece of debris in order to escape the lower belt was considered, but found to be a non-viable solution. For alongside the additional propellant requirements, the larger semi-major axis after the manoeuvre would cause the natural J2 drift to decrease exponentially (see Equation 6.17 & 6.18), thus increasing the total phasing time required to an unreasonable degree.

6.3. Introducing Intermediate Orbits

One of the ways to prevent such excessive time spent in the Van Allen belts is through the introduction of intermediate orbits. Additionally, such orbital elements can be chosen to potentially facilitate a faster transfer without the need of large phasing times to create the proper orbital alignment between the debris and the Moon. However, the introduction of such orbits require additional manoeuvres and thus additional propellant and energy investment. Indeed, such orbits are very similar in nature and application to parking orbits. Given the elliptical shape of the GTO orbit in which the Ariane upper stages drift, two primary options were analyzed. These are circularizing at apoapsis into GEO, or at periapsis into LEO. Moving forward, these orbits will be denoted as ”staging orbits”, as they represent a staging point prior to the Trans-Lunar Injection manoeuvre. The choice of circular orbit was taken as a baseline, as it presents the simplest orbit but it also critically removes one of the complicating variables, namely the argument of periapsis ω. This is because the argument of periapsis is undefined for circular orbits. The main orbital elements of interest for the analyzed staging orbits are given in Table 6.8. In reality, the achievable circular LEO and GEO altitudes depend entirely on the perigee and apogee altitude of any specific piece of debris, as these differ on a per-object basis (consider Table 6.1). For this analysis however, the standard Ariane GTO perigee and apogee altitudes were used in order to create a representative baseline for the global set of GTO targets.

Table 6.8: Orbital characteristics for the identified staging orbits.

Orbital element	GTO Debris orbit	LEO Staging orbit	GEO Staging orbit
Perigee altitude	250 km	250 km	35 786 km
Apogee altitude	35 786 km	250 km	35 786 km
Eccentricity	0.73	0	0
Inclination	6°	6°	0°

While the staging orbits effectively fulfill the same function, it can be seen that they differ in more than just their altitudes. Indeed, the GEO staging orbit requires an additional inclination change whereas the LEO variant does not. It was chosen to perform a strict apogee lowering manoeuvre for the LEO staging orbit because in the low-Earth circular orbit, the J2 phasing is substantially faster. Since only RAAN phasing matters in a circular orbit, plugging in the respective values for the LEO staging orbit into the J2 RAAN drift equation (Equation 6.18) results in a drift of -8.66° per day. Given the 180° relative RAAN shift required to wait for a potential transfer alignment, this results in a maximum phasing time of approximately 21 days. Combined with the fact that the low altitude of the LEO staging orbit is well beneath the inner Van Allen belt, this may be seen as an attractive option. As such, the ΔV required for injection into the LEO staging orbit can readily be determined using Equation 6.19. For the GEO staging orbit however, the high altitude results in a natural J2 RAAN drift that is far too slow at -0.01334° per day, resulting in a required phasing time of almost 37 years in the worst case. Additionally, long phasing times in an uncontrolled Geostationary Orbit are undesirable as they are subject to substantial Luni-Solar perturbations that add up over time. However, for a relatively small additional ΔV of around 20 m/s, the perigee raising manoeuvre can be combined with an inclination changing manoeuvre in order to equatorialize the circular GEO. Combining such a manoeuvre can be done according to the cosine rule, as shown in Equation 6.20 [81]. Note here that the inclination difference is equal to the GTO inclination considering the target inclination is 0°.

$$V_{staging_{LEO}} = V_{p_{GTO}} - V_{c_{LEO}} \tag{6.19}$$

$$V_{staging_{GEO}} = \sqrt{V_{a_{GTO}}^2 + V_{c_{GEO}}^2 - 2 \cdot V_{a_{GTO}} \cdot V_{c_{GEO}} \cdot cos(i_{GTO})} \tag{6.20}$$

The velocities in these equations can readily be computed using the Vis-Viva equation, as presented earlier in this report. Note that any impulsive inclination change can, by definition, only be applied at a point in the orbit that coincides with the old and new orientation of the orbit. Given that the inclination is

defined with reference to the equatorial plane, such inclination changes are in baseline done when passing this equatorial plane. For an elliptical orbit in particular, the apogee passage is ideal in order to reduce the overall magnitude of ΔV required due to the low orbital velocity at that point. Therefore, for such a combined manoeuvre to be applicable, the apogee must be placed in the equatorial plane. This occurs when the argument of periapsis is either 0° or 180°. Indeed, this is why launch vehicle GTO trajectories of almost exclusively target an argument of periapsis approaching 180°, which allows their client satellites to easily circularize into Geostationary Orbit. The choice to move into an equatorial orbit is crucial for facilitating a Lunar transfer opportunity. This is because the principle leftover dependent variable, the RAAN, is not defined for an orbit that moves only in the equatorial plane. For every complete revolution of the Moon in its orbit, it passes its line of nodes twice, which is by definition the point in which it crosses the equatorial plane. As such, a circular equatorial orbit in principle presents two transfer opportunities every draconic month (approximately 28 days). Recall however that a debris recycling mission is inherently dependent on the orbit of the targeted piece of debris. The only prerequisite for this GEO staging orbit therefore is the fact that a piece of debris must be chosen that naturally approaches an argument of periapsis of either 0° or 180°. The distribution of the argument of periapsis and RAAN for the Ariane upper stages in GTO was presented earlier in this report. Figure 6.7 shows strictly the distribution of argument of periapsis of this same dataset.

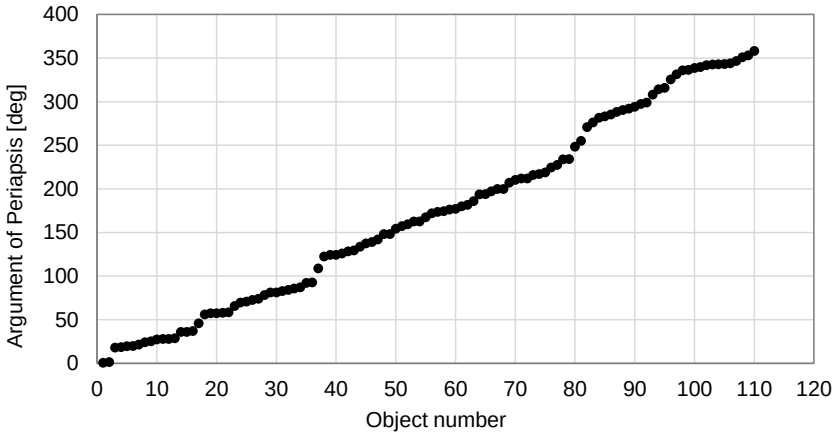

Figure 6.10: Distribution of argument of periapsis for the Ariane upper stages in GTO, in ascending order.

Considering the natural J2 drift in argument of periapsis of 0.824°/day previously found in this report, it is considered that indeed, targeting a rocket stage that naturally approaches a desired argument of periapsis value (particularly 0° or 180°) is a feasible and viable strategy. Though ultimately, this should be one of several considerations in terms of final target choice, with other critical aspects such as tumbling rate also being factors of importance.

In order to determine the ΔV, propellant masses and transfer energy for these additional mission scenarios, the same process for the complete transfer analysis as explained for the direct transfer scenario can be used with two minor changes. The first of these is the addition of the circularization burn from GTO to the respective staging orbit, for which the required velocity increment can be determined using the equations presented above in Equation 6.19 and 6.20 for the LEO and GEO staging orbit, respectively. Plugging in the defined orbital parameters yields a required velocity increment of 1.490 km/s and 2.440 km/s for an equatorial GEO and LEO staging orbit injection, respectively. Note that once again, a maximum potential inclination difference of 35° was used for the LEO transfer case to account for the worst case natural alignment where there is a 180° RAAN difference. Despite not needing any inclination changes, the LEO injection is significantly more costly due to the high velocities involved in such a low-altitude orbit. This can also be understood by recognizing that lowering the orbit significantly decreases the specific orbital energy, according to Equation 6.21 [81]. Energy that must ultimately be invested back into the orbit in order to raise it to the Lunar vicinity.

$$\epsilon = \frac{-\mu_E}{2a} \tag{6.21}$$

After injection into the staging orbit, the only remaining difference in the transfer analysis is the fact that the TLI manoeuvre now starts from a circular orbit rather than an elliptical one, which is reflected by the change in magnitude of ΔV_1 (as used in Equation 6.1) according to Equation 6.22.

$$\Delta V_1 = V_{p_{LTO}} - V_{c_{staging}} \tag{6.22}$$

It should be noted that the inclusion of a staging orbit does change the size and shape of the Lunar Transfer Orbit slightly, though this change is automatically captured within the applied transfer analysis and calculated through the written Python script. Given these changes, the complete transfer analysis was performed again for both of the additional mission scenarios with the defined staging orbits, for both the H10 and ESC-A upper stages as debris targets. The results of these analyses are presented in Table 6.9 and 6.10 for the LEO and GEO staging orbits, respectively.

Table 6.9: Performance metrics for the LEO staging orbit mission scenario.

Manoeuvre	ΔV Budget [km/s]	Propellant mass [kg]		Energy cost [GJ]	
		H10	ESC-A	H10	ESC-A
Rendez-vous	0.182	2109.58	4112.01	13.676	26.658
LEO injection	2.684	21299.01	42413.75	138.081	274.967
TLI	3.431	10473.57	20856.53	67.900	135.212
Lunar capture	0.918	1339.35	2667.10	8.683	17.291
Descent injection	0.025	31.64	63.01	0.205	0.408
Landing termination	0.565	643.30	1281.04	4.170	8.305
Total	**7.805**	**35896.45**	**71393.44**	**232.715**	**462.841**

Table 6.10: Performance metrics for the GEO staging orbit mission scenario.

Manoeuvre	ΔV Budget [km/s]	Propellant mass [kg]		Energy cost [GJ]	
		H10	ESC-A	H10	ESC-A
Rendez-vous	0.182	644.46	1194.44	4.178	7.744
GEO injection	1.639	5104.04	10163.92	33.089	65.892
TLI	1.162	2301.93	4583.95	14.923	29.718
Lunar capture	0.834	1198.88	2387.39	7.772	15.477
Descent injection	0.025	31.64	63.01	0.205	0.409
Landing termination	0.565	643.30	1281.04	4.170	8.305
Total	**4.407**	**9924.26**	**19673.75**	**64.339**	**127.544**

While the staging orbits may have seemed like an ideal potential solution at face value, their cost in terms of performance can immediately be realized from these results. Indeed, looking at the excessive propellant masses required alone already prevents their feasibility, as even for the lower mass H10 target, the required launch masses exceed the payload mass capacity of the Ariane 64. The ΔV required for the respective staging injections is the primary cause of this lack of performance, resulting in excessive required propellant masses due to the heavy target masses involved. Additionally, the substantial propellant masses required for the later manoeuvres result in early manoeuvres requiring an even larger amount of propellant as the propellant for later manoeuvres is effectively dead weight that needs to be carried along. The influence of the circularization on the ΔV magnitude of the TLI manoeuvre should not be overlooked, as the shift to a circular orbit substantially reduces the potential to leverage the Oberth effect through the high perigee velocity of the GTO which made the direct transfer so efficient. The poor performance of the staging orbit scenarios are further visualized in Figure 6.11.

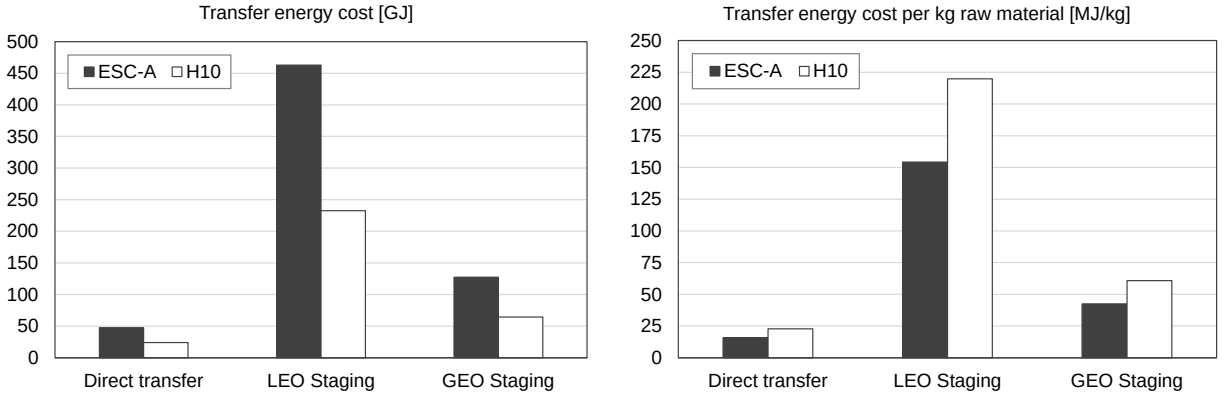

Figure 6.11: Transfer energy results of the LEO and GEO staging mission scenarios compared to the direct transfer scenario.

While the propellant masses indicate an infeasibility, the energy values presented in this figure highlight the unviability of introducing intermediate circular staging orbits. This is especially so when comparing to the baseline direct transfer mission scenario, which boasts significantly lower energy investments required. Additionally, it can be seen that while the absolute transfer energy cost is higher for the heavier ESC-A target scenarios compared to those using the H10, the transfer energy cost per kg of raw material delivered is substantially lower. This follows the trend indicated earlier for the direct transfer. So much so that there is no benefit to capturing the lower mass H10 as compared to the heavier ESC-A upper stage. Should the H10 scenario have fitted on an Ariane 62 instead, that would have been a significant advantage, but the performed analyses show that this is not an option. As such, it was decided to omit the H10 from any further analysis and use strictly the ESC-A as a baseline target. Should the ESC-A present infeasibilities or other problems, the H10 will be used as a second option.

6.4. Implementing Low-Thrust Electric Propulsion

Up until this point, the analyses performed have been limited to transfers consisting of strictly impulsive manoeuvres using chemical propulsion systems. However, the use of low-thrust electric propulsion systems has increased significantly in recent history. Such propulsion systems are widely adopted in the current state of the space industry and for all manners of manoeuvres from stationkeeping to orbit raising and even interplanetary flight. Typically, gaseous propellants are ionized by electric energy and then accelerated through electrostatic and/or electromagnetic fields to achieve very high exhaust velocities, far higher so than commonly achievable in chemical propulsion systems. As such, electric propulsion systems are characterized by a high efficiency in terms of specific impulse and therefore require significantly less propellant than chemical systems. However, thrust values are typically limited to a few hundred mN at most [89, 91]. This in turn leads to long flight times for manoeuvres of significant magnitude, as the propulsion system is operated for long continuous periods of time. While long flight times can generally be considered undesirable for space missions, as they effectively reduce the operational lifetime of a satellite due to degradation of electronics and other ageing effects, this is not in necessarily the case within the context of a debris recycling mission. Because it was found to be most suitable to perform the recycling operations on the Lunar surface, the mission as far as the transfer vehicle is concerned, consists only of transporting the targeted piece of space debris from its existing orbit to the Moon. The vehicle has no true operational lifetime once the transfer stage is concluded. Alternatively, one can consider that the spacecraft's operational lifetime *is* the transfer phase. Having a long flight time is therefore not especially detrimental to the performance of a space debris recycling mission.

ESA's SMART-1 mission, launched in 2003, was the first and only mission to the Moon using only low-thrust propulsion. Though the mission also started from GTO, it used a highly complex trajectory which employed several Lunar gravity assist manoeuvres to both raise the perigee as well as alter the inclination and argument of periapsis [99]. This trajectory is shown in Figure 6.12. While such a trajectory could potentially be used for a debris recycling mission, the mission planning and analysis involved would likely become highly complex and differ distinctly on a per-target basis due to the required Lunar gravity assists. For a debris recycling mission, it was chosen to instead explore alternative implementations of electric propulsion without these Lunar resonances that could readily be applied to a wide range of debris debris targets.

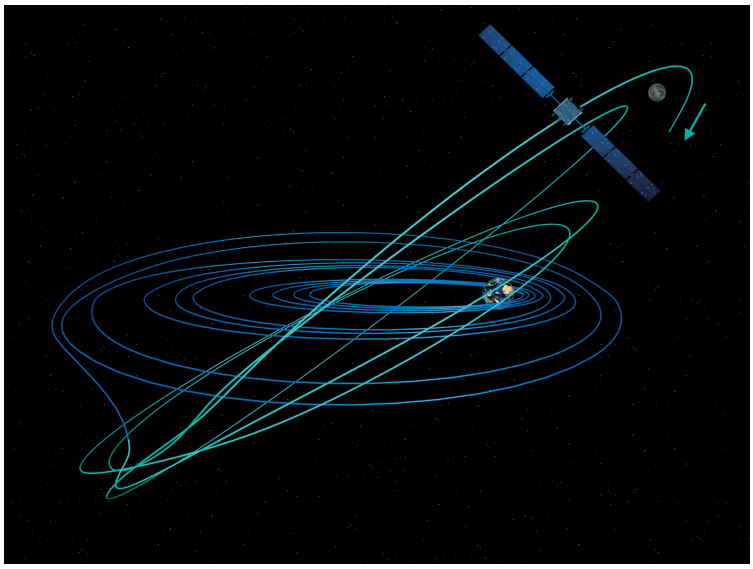

Figure 6.12: Trajectory of ESA's SMART-1 mission to the Moon. [99]

As such, a new mission scenario was defined in order to explore the potential of implementing electric propulsion for the space debris recycling mission concept. In order to determine what manoeuvres can be replaced by electric counterparts, the principle limitation of electric propulsion was used as a differentiator: the low thrust. The low thrust values of electric propulsion system brings forth the implication that a manoeuvre must be spread over a significant period of time to facilitate the compound impulse required. For several manoeuvres however this is not a practical option. Consider for example the Lunar capture manoeuvre at the end of the Lunar transfer orbit. In order for the transfer vehicle to inject itself into a stable orbit around the Moon, the required velocity increment must be provided in a short time such that the Moon isn't missed entirely. High thrust values are critical for achieving such an injection specifically for a space debris recycling mission, given the large mass of the captured debris target, as opposed to SMART-1, which only had a vehicle dry mass of up to 290 kg [100]. The final landing termination burn is another manoeuvre that requires high thrust to rapidly decrease the vehicle's velocity prior to Lunar impact. These manoeuvres effectively require a chemical propulsion system to be executed. This leaves the Trans-Lunar Injection as the primary manoeuvre to be adapted into a low-thrust one, making for a total vehicle propulsion that is hybrid in nature. That is, containing both chemical and electric side thrusters.

However, such an adaptation is not trivial. Low-thrust electric transfer manoeuvres are characterized by a spiral shape in which the spacecraft typically moves outwards in radial direction over time, as highlighted already in Figure 6.12. From this image alone it can be seen that implementing electric propulsion is significantly more complex than a conventional chemical manoeuvre, even without the Lunar gravity assists. Doing so analytically was not found to be a suitable approach for this study, given the complexity involved and the high degree of variance in low-thrust transfers, particularly starting from an elliptical parking orbit such as GTO. It was therefore chosen to use orbital simulation software to model the spiraling trajectory and evaluate its performance. For this study, the FreeFlyer software by A.I. Solutions was chosen as a suitable suite of powerful simulation tools with the capability to model low-thrust electric transfer trajectories. FreeFlyer was specifically chosen for its widespread adaptation in the space industry and its well-proven validity and applicability through numerous missions and studies. A FreeFlyer 'Engineer' grade license was courteously provided by A.I. Solutions through their FreeFlyer University program [101], which allowed the use of this highly capable and otherwise expensive software free of charge.

Before the simulation can be ran in FreeFlyer, the simulation environment must be set up. Since only the low-thrust manoeuvre modelling is of interest, many of the settings within FreeFlyer were left at their stock values. The basis for the propagator is a Runge Kutta 8 integrator, using a fixed step size of 300 seconds and a relative error tolerance of 1×10^{-9}. For this first-order analysis, it was chosen to limit the gravitational force model to only the Earth and the vehicle itself in a two-body problem to stay consistent with the zero-patched conics approach applied earlier. For the space debris transfer vehicle, in principle only the mass has to be set. FreeFlyer has the capability to implement numerous other physical properties like moments of inertia, but these are not important for the low-thrust manoeuvre modelling. Note that the vehicle mass in FreeFlyer is the vehicle dry mass. The direct transfer mission scenario results, as pre-

sented in Table 6.7, were taken as the baseline for determining this dry mass. Considering that the intent is to model a low-thrust orbit-raising manoeuvre, the 'dry' mass for the low-thrust manoeuvre was set as the sum of the previously estimated dry mass of 1500 kg, the 5000 kg ESC-A target and all propellant masses required after the TLI from the direct transfer scenario. Indeed, one can imagine that within the context of the electric propulsion system, the dry mass can be considered the mass of the vehicle after the low-thrust manoeuvre. What this mass is used for, i.e. chemical propulsion manoeuvres, is irrelevant. In total, this results in a dry mass of 10511.89 kg.

For the propulsion system itself, FreeFlyer requires the implementation of a Tank and Thruster object. For the thruster, it was considered critical to take an actual thruster that exists rather than a fictional one with baseline performance characteristics in order to add validity to the simulation results. Several electric thrusters exist on the market, though the vast majority of these boast very small thrust forces in the order of tens of mN. Such low thrust values however were considered to be insufficient for the recycling mission concept given the excessive mass of the rocket stage space debris targets involved. While flight time may not be an inherent issue, preventing it from becoming excessive is still considered important for operational feasibility. "High-thrust" electric thrusters were therefore given priority. Selecting an electric thruster becomes a balancing act of three main variables, these being thrust level, specific impulse and power consumption. The latter being important as the power must be provided using solar arrays. Given the need for relatively high thrust and high specific impulse in order to minimize propellant mass, the main two types of thrusters to be chosen from are ion thrusters and Hall effect thrusters [89]. Ultimately, it was chosen to use the Busek BHT-6000 thruster. This is a Hall effect thruster which is going to be used on the Power and Propulsion Element (PPE) of the Lunar Gateway [102]. The performance metrics of this thruster are given in Table 6.11.

Table 6.11: Specifications for the Busek BHT-6000 Hall effect thruster [103].

System specifications		**Mode**	**High Thrust**	**High Impulse**
Mass	12.5 kg	Discharge power	5 kW	6 kW
Total impulse	>8.5 MN-s	Thrust	325 mN	298 mN
Propellants	Xenon, Krypton, Iodine	Specific impulse	2029	2708

It was chosen to use a baseline number of 4 thrusters continuously for the simulation for a compound thrust value of 1.192 N. In tandem to the 4 BHT-6000 thrusters, the Gateway will also use 2 Advanced Electric Propulsion Systems (AEPS), which are larger, higher-thrust Hall effect thrusters designed by Aerojet Rocketdyne [102]. However, at over twice the discharge power requirement per thruster (12.5 kW [102]) and a lower specific impulse (2620 s [102]), the higher thrust value of 590 mN [102] was not considered a crucial benefit. Having a larger per-engine power consumption also reduces the flexibility for implementing multiple thrusters on the transfer vehicle as compared to the BHT-6000. For the Gateway however, with its immense mass, the high thrust values of the AEPS would of course be much more warranted. With the thruster defined, only the tanks remain. FreeFlyer requires the definition of a propellant mass for the tanks beforehand. As an initial condition, a propellant mass of 1500 kg was defined. Upon running the simulation, this propellant mass was then reduced in an iterative process until the defined manoeuvre could no longer be executed. This limit then defined the required propellant mass.

For the low-thrust orbit raising manoeuvre simulation, a complete mission sequence must be defined in FreeFlyer. The spacecraft is first stepped to its perigee position, after which the low-thrust manoeuvre is initiated. A while-loop is then used to continuously manoeuvre the spacecraft using the FiniteBurn object, setting the direction of the applied acceleration to the velocity direction until its apogee reaches the orbital radius of the Moon. Thrusting in the velocity direction is a common strategy for low-thrust manoeuvres, so this was taken as a simple baseline for the analysis as well. Burn objects in FreeFlyer operate in principle with the VNB coordinate system, which indicates the velocity direction, the normal direction and the subsequent binormal direction as its three base vectors. Once that condition is met, the spacecraft is again stepped towards its apogee, where it will have reached a radial distance equal to that of the Moon in its orbit. The resulting trajectory is presented in Figure 6.13.

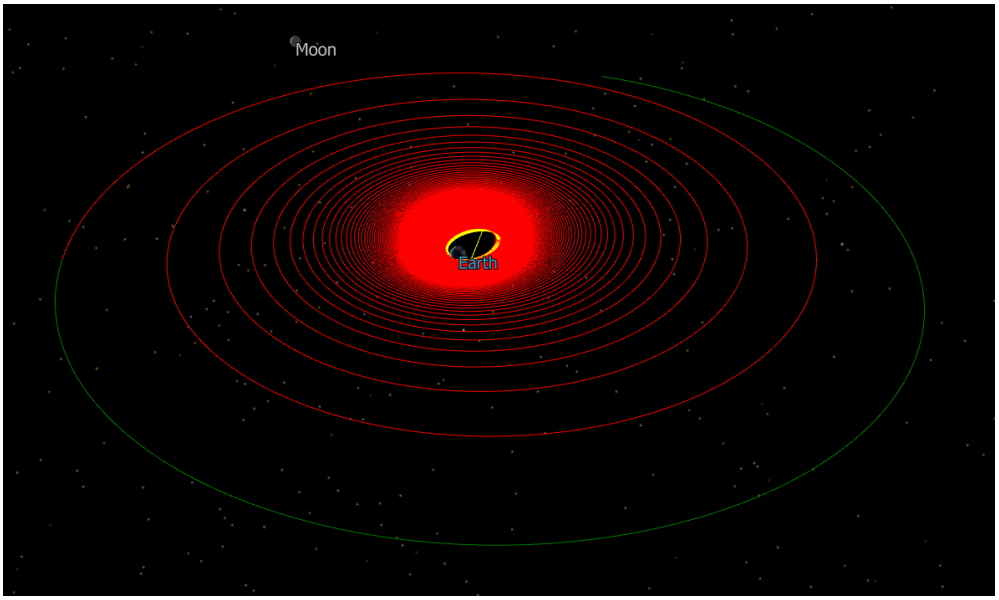

Figure 6.13: Render of the simulated low-thrust trajectory from GTO to Lunar altitude at apogee. Thrusting period shown in red, coast in green and parking orbit in yellow.

It can be seen that the trajectory approaches a more circular shape over time as the satellite continues to perform the low-thrust manoeuvre. Though ultimately even the final shape is still significantly elliptical in nature. The simulation results in a total time of flight of 343.09 days, during which it completes 318 total orbital revolutions and expends approximately 1320 kg of Xenon propellant. The total ΔV required to perform this manoeuvre was determined numerically by walking through the flight time and determining the acceleration of the transfer vehicle through dividing the thrust force by the total wet mass. This acceleration was then multiplied by a defined timestep dt to yield a velocity increment dV. Finally, the wet mass was updated by subtracting the mass expelled during the timestep dt. This process was ran through the entire flight time to yield the complete ΔV by summing the velocity increments dV. For the trajectory shown above, this yields a total ΔV of 3.248 km/s. Indeed, this is substantially larger than the 0.679 km/s found for the TLI manoeuvre of the direct transfer mission scenario. An increase of the ΔV required for manoeuvres can typically be expected when using low-thrust propulsion systems, as they cannot leverage the high velocity in perigee as a means of gaining additional efficiency. This increase is also shown by the ΔV analysis of ESA's SMART-1 mission, which has performance scenarios requiring between 3.6 and 4.5 km/s as shown by Racca et al. [100]. Considering that SMART-1 used a more elaborate trajectory and that these metrics are for the entire mission rather than just the orbit-raising manoeuvre, the 3.248 km/s obtained from the performed analysis was deemed representative.

Additionally, it was found that all the performance metrics do not change measurably depending on the position within the orbit at which the manoeuvre is started. This is due to the elliptical nature of the orbit in contrast to circular parking orbits, where the position does influence the orientation of the orbit due to its symmetrical nature. This means that timing the start of the manoeuvre such that the Moon is at the predicted apogee passage point is purely a phasing problem, which can be solved by simply waiting in the GTO after capturing the targeted piece of debris. However, looking at the figure shown above, a key issue presents itself once again as the Moon is not at the apogee passage point defined by the end of the green line. Indeed, the alignment problem was found to be an issue for the electric orbit-raising scenario just as it was for the chemical scenario. To highlight this issue particularly in the context of the low-thrust manoeuvre, consider the adapted representation of the geometry shown in Figure 6.14.

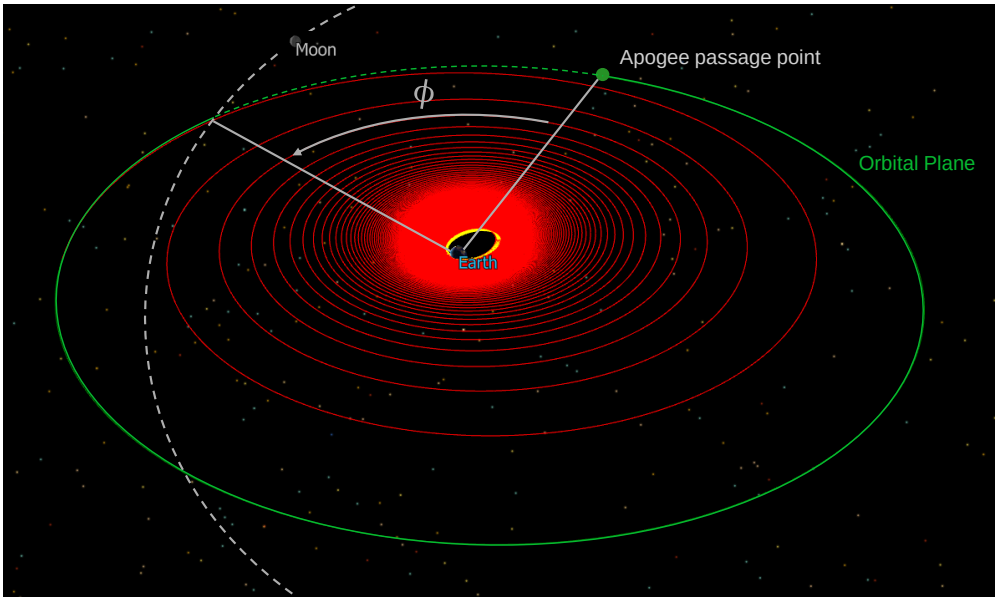

Figure 6.14: Render of the simulated low-thrust trajectory from GTO to Lunar altitude at apogee, adapted to show alignment geometry.

From this figure it can be seen that the apogee passage point lies well to the right of where the Moon crosses the orbital plane. So much so that in order to facilitate a proper alignment, the apogee point must be rotated or phased forward within the plane by an angle ϕ as shown in the figure. The actual value of this angle depends entirely on the specific RAAN of the Moon and the initial conditions for RAAN and argument of periapsis of the targeted piece of space debris. It is important to understand that this angle ϕ is not just either the RAAN or the argument of periapsis of the orbit. Like was shown for the J2 effect in GTO for the direct transfer mission scenario, the two variables are effectively coupled. Instead, consider that this 'phase' angle ϕ represents the orientation of the apoapsis. Therefore, in order to analyze how this angle potentially moves, let us define the longitude of periapsis $\bar{\omega}$ as a representative parameter, which captures exactly this orientation of the line of apsides. The longitude of periapsis is defined as the angular position of the perigee that would occur if the orbit's inclination were zero, and is therefore determined through Equation 6.23 [81].

$$\bar{\omega} = \omega + \Omega \tag{6.23}$$

In order to analyze the evolution of this new parameter, as well as the RAAN and argument of periapsis, their values were reported throughout the entire thrusting manoeuvre. An arbitrary object (NORAD 26612) out of the dataset of Ariane upper stages was used in order to visualize realistic initial conditions. It should be noted that the specific object does not matter as they all share the same GTO orbit which, as seen before, are subject to the same orbital perturbations. As the mission scenario will be designed for the worst case scenario orbital alignment, the choice of object for this analysis does not influence its outcomes. The results of this analysis are shown plotted in Figure 6.15.

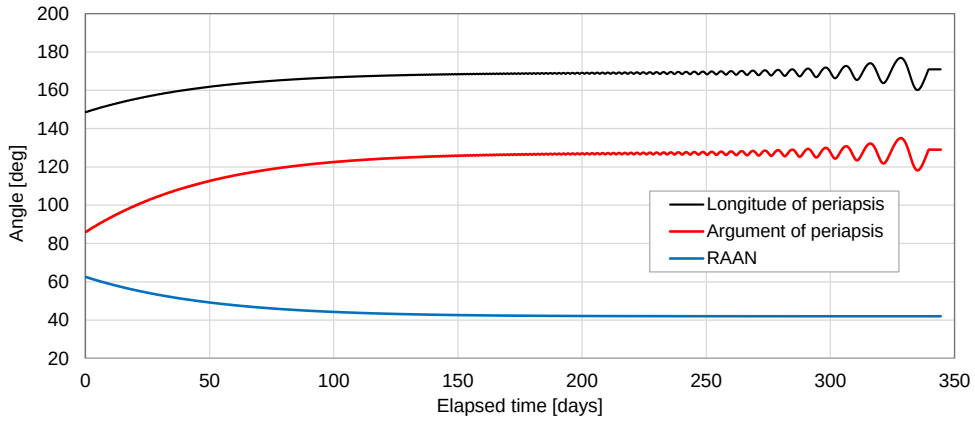

Figure 6.15: Evolution of RAAN, argument of periapsis and longitude of periapsis over the continuous thrusting period.

A number of observations can be made from this figure. first, it can be seen that the argument of periapsis and RAAN indeed move in opposite directions due the J2 effect, which was seen earlier when assessing the theoretical J2 drift. The longitude of periapsis as computed by FreeFlyer is also equal to the sum of the argument of periapsis and the RAAN, confirming Equation 6.23. The argument of periapsis however is shown to gain a substantial oscillatory motion as the secular increase slows down. It should be noted however that this oscillatory motion is present from the start, though it is invisible in the figure due to the scaling until the oscillations gain substantial magnitude. The RAAN on the other hand does not show this oscillatory motion and instead approaches a value roughly 32° below its starting value, dominated by the J2 effect. The growing oscillations in the argument of periapsis are caused by the constant thrust applied in the velocity direction having a more pronounced effect on the orbit as its size increases. Notably, it was found that the local minima and maxima correspond with the periapsis and apoapsis of the orbit, respectively. While this oscillation in the orientation of the spiraling orbit may seem like another issue, it is actually the key to solving the alignment problem.

Indeed, it was found that this oscillatory motion can be leveraged in a useful manner to 'steer' the apogee within the orbital plane. This is achieved by thrusting only in the first half of the orbit, i.e. the part of the orbit for which the true anomaly θ is between 0° and 180°. This part of the orbit corresponds to the region of each period in the oscillation featuring a positive slope in Figure 6.15. As a result, the orientation of the orbit is manipulated by stacking the positive growth in the longitude of periapsis while eliminating the negative. Leveraging the upwards slopes compared to the downwards ones was chosen specifically to compliment the natural upwards tendency of the longitude of periapsis in the initial part of the trajectory where the orientation change is influenced most by the J2 effect, as shown in Figure 6.15. The resulting trajectory features thrust-arcing phases in which the thrust is applied only in the first half of the orbit while coasting in the second half, which effectively phases the apogee forward in the orbital plane over time. It can be seen from Figure 6.14 that at most a shift angle ϕ of 180° must be achieved through the elaborated thrust-arcing approach in order to facilitate an orbital transfer alignment for any respective natural geometry between the debris orbit and the Moon. This thrust-arcing approach was adapted into the FreeFlyer simulation using this maximum shift angle of 180° in the longitude of periapsis with reference to its initial value. The resulting trajectory is rendered in Figure 6.16. The corresponding evolution of the longitude of periapsis, argument of periapis and RAAN is shown in Figure 6.17.

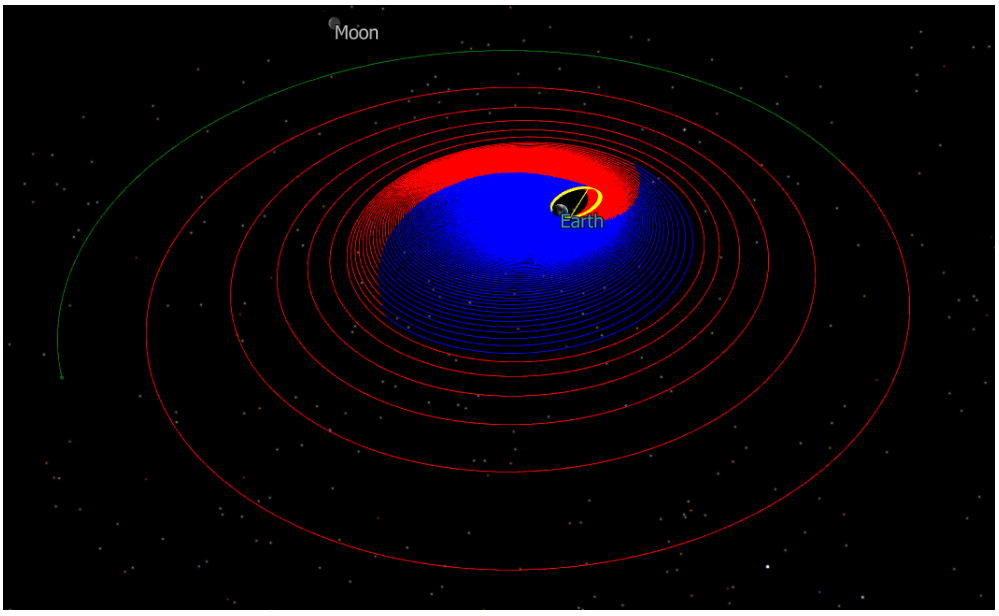

Figure 6.16: Render of the simulated low-thrust trajectory, showing the thrust-arcing approach to steer the apogee over 180°.

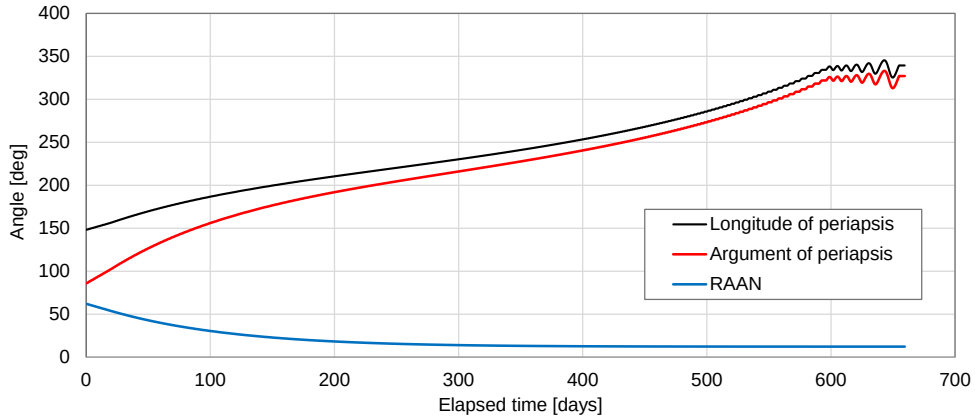

Figure 6.17: Evolution of RAAN, argument of periapsis and longitude of periapsis when applying the thrust-arcing regime.

From the rendered trajectory it can be seen that the thrust-arcing approach is indeed capable of shifting the apogee over the required 180° with reference to its initial value. In fact, there is significant room to spare within the trajectory, which can be seen by the continuous thrusting regime that is applied after the desired shifting angle is achieved. With this validating knowledge, it can be concluded that within the defined assumptions, employing low-thrust propulsion is indeed capable of facilitating the correct alignment geometry for a Lunar transfer using electric propulsion. For the presented initial conditions, the second figure shows that the RAAN stabilizes at approximately 12 degrees while the applied thrust-arcing method continuously increases the longitude of periapsis to the desired value which was set in this case at the previously defined 180° degrees above the initial value. The clear downside of this thrust-arcing strategy is the fact that the flight time is nearly doubled at 636.4 days. However, it was established earlier in this report that an increased flight time was not an inherent issue for a space debris recycling mission. Additionally, this increase in flight time represents the worst case scenario in which the apogee must be shifted over a complete angle of 180°. In reality this angle will likely be significantly smaller. The thrust-arcing approach yielded at most a performance penalty of approximately 25 kg more propellant required for the orbit-raising manoeuvre, which is a very marginal cost.

However, the low-thrust spiral orbit-raising manoeuvre does also in fact influence the Lunar injection manoeuvre. The apogee velocity of the impulsive transfer trajectory is significantly lower than the one of the low-thrust trajectory, which influences the injection ΔV required as defined earlier in this report (specifically Equation 6.4). It was observed through the simulation that the final apogee velocity for the low-thrust electric orbit-raising manoeuvre laid between 0.891 and 0.939 km/s depending on the amount of thrust-arcing applied and the exit conditions at the end of the trajectory, with the lowest value corresponding to the maximum required shift angle of 180°. This is substantially higher than the 0.187 km/s apogee velocity of the impulsive Hohmann transfer, and much closer to the orbital velocity of the Moon (approximately 1.02 km/s). The hyperbolic excess velocity for the Lunar approach (in the Selenocentric reference frame) is therefore substantially lower, which leads to a reduction in the injection ΔV required within the zero-patched conics methodology. This subsequently reduces the injection propellant mass and therefore also the vehicle mass input required for the FreeFlyer simulation. Adding this apogee passage velocity from FreeFlyer directly into the written Python code yields an injection ΔV of 0.748 km/s. Note that the Lunar injection is bound by a worst case situation in which the inclination difference is equal to the sum of the inclination of the Moon and the inclination of the debris orbit (in this case 35°), as was also explained for the direct, chemical transfer mission scenario. The injection ΔV value is larger than the difference between the velocity of the Moon and the vehicle's apogee velocity, as the larger apogee velocity results in an increase to the plane change component of the injection manoeuvre. However, this still results in a net lower injection ΔV. Adapting the FreeFlyer simulation with the updated input mass values, the simulation was ran in an iterative process once again until convergence to an optimal solution with minimal initial propellant mass was achieved. The resulting performance metrics for the electric propulsion mission scenario are tabulated in Table 6.12. In order to stay consistent with the applied margins, the ΔV of the low-thrust manoeuvre was determined and a 5% margin was added according to the ESA margin philosophy for electric propulsion manoeuvres [87]. The propellant mass including this ΔV margin was then computed through the Tsiolkovsky rocket equation (Equation 6.12). A sanity check was performed by computing the propellant mass without ΔV margin using the Tsiolkovsky equation, which yielded 1309.33 kg for the orbit-raising manoeuvre, which is nearly identical to the 1308.82 kg obtained from the FreeFlyer simulation.

Table 6.12: Performance metrics for the electric propulsion orbit-raising mission scenario.

Manoeuvre	ΔV Budget [km/s]	Propellant mass [kg]	Energy cost [GJ]
Rendez-vous	0.182	393.16	2.549
Low-thrust orbit raising	3.368	1379.04	2368.050
Lunar capture	0.823	2353.32	15.256
Descent injection	0.025	63.01	0.408
Landing termination	0.565	1281.04	8.305
Total	**4.963**	**5469.57**	**2394.569**
		Excluding Solar energy	**26.519**

Indeed, the significant reduction in propellant mass for the Lunar capture manoeuvre results in a propellant reduction also for the rendez-vous and low-thrust orbit raising manoeuvres. The high energy cost of the low-thrust orbit-raising manoeuvre immediately stands out from these results. This excessive energy usage is a direct result of the long thrust times combined with the fundamental principles of electric propulsion depending on large power requirements to create the required electric field that accelerates the ions. To compute the energy used by the thrusters throughout the orbit-raising manoeuvre, Equation 6.24 can be used.

$$E_{in_{thrusters}} = P_{thruster} \cdot n_{thrusters} \cdot t_{thrust} \tag{6.24}$$

Where $P_{thruster}$ is the discharge power of a single BHT-6000 thruster, $n_{thrusters}$ is the number of thrusters used (in this case 4) and t_{thrust} is the cumulative thrust time. This electric energy is captured by the solar arrays of the transfer vehicle. Accounting for a solar cell efficiency η (assumed to be 30%), the total required to operate the electric thrusters can be determined using Equation 6.25.

$$E_{total_{thrusters}} = \frac{E_{in_{thrusters}}}{\eta} \tag{6.25}$$

It is critical to realize that this energy represents a different kind of energy: electrical energy, contrary to the chemical energy used in combustion of chemical propellants. While these chemical propellants represent strictly an energy loss, i.e. an investment of energy to facilitate the orbital manoeuvres, this is not the case for the electric energy. This is because the electric energy is provided by sunlight and is therefore effectively ”free”. No actual investment of energy is required in order to access it as the source is completely sustainable. As such, the Solar electric energy cost does not contribute to the total energy cost and is to be omitted from cumulative energy calculations.

When looking at the angular orientation of the orbit along the simulated trajectory plotted in Figure 6.17, a growing oscillation can be seen at the tail end of the curves for the longitude of periapsis. This is a result of the continuous thrusting regime that was resumed after the orbital alignment was achieved through the thrust-arcing regime, as also seen in Figure 6.15. For a real transfer, such oscillations are undesirable and should ideally be prevented. Through further analysis and simulation, it was found that by thrust-arcing around perigee after orbital alignment is achieved, the angular alignment can be maintained while the apogee of the orbit is raised to the Lunar vicinity. The resulting trajectory when considering thrust-arcing around perigee between true anomaly values of −90° and +90° is visualized in Figure 6.18. The corresponding evolution of the longitude of periapsis, argument of periapsis and RAAN is shown in Figure 6.19.

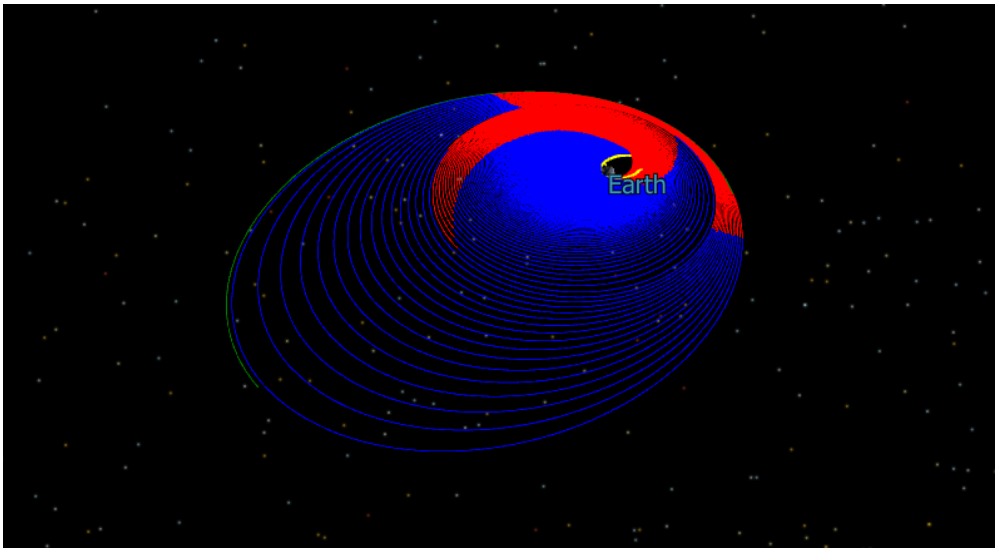

Figure 6.18: Render of the simulated low-thrust trajectory, showing the thrust-arcing approach to steer the apogee over 180° followed by thrust-arcing around perigee.

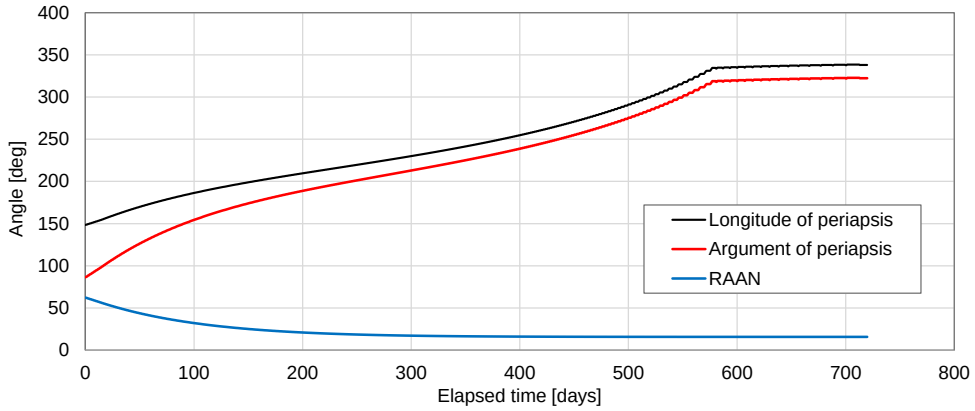

Figure 6.19: Evolution of RAAN, argument of periapsis and longitude of periapsis when applying the thrust-arcing around perigee to stabilize angular alignment.

It can be seen that the previously observed oscillations have been eliminated and indeed the orbital alignment is maintained, as the longitude of periapsis can be observed to remaining at a constant value after the desired 180° apogee shift angle is achieved for the worst case scenario. However, due to the fact that thrust is now only applied in smaller part of the orbit, an increased flight time of approximately 70 days is observed. In terms of propulsive performance however, thrust-arcing around perigee after achieving the desired apogee shift angle results in a reduction of propellant mass of approximately 114 kg for the entire low-thrust manoeuvre in the highlighted case. It should be noted however that this represents an ideal scenario as the ΔV required for the final portion of the apogee raising manoeuvre after achieving the orbital alignment limits the additional flight time. This additional flight time can become excessively large for smaller required apogee shift angles as a much larger part of the orbit raising must be done while thrust-arcing around perigee. In such cases, applying continuous thrust at the start of the trajectory could be applied to more quickly raise the orbit while applying the thrust-arcing approach later in trajectory to facilitate the smaller apogee shift angle and to reduce the added flight time. Ultimately, the specific thrusting strategy depends on the orbital orientation of the specific chosen piece of debris, and optimizing the trajectory any further was considered beyond the scope of this study. Additionally, the observed reduction in propellant mass was found to have only a very minor impact on the global mission energy analysis (< 2%). Given this knowledge, it was decided to use the results presented in Table 6.12 as a representative baseline for the low-thrust hybrid transfer mission scenario.

This results can be readily compared to the results obtained for the direct, chemical transfer mission scenario and the alternative Argonaut mission scenario. As discussed earlier in this section, the Solar electric energy usage does not represent an energy cost in the way that chemical energy does. The comparative analysis between the missions scenarios was therefore split into a total cumulative transfer energy and a

non-sustainable transfer energy metric that does not include the solar energy used. Figure 6.20 shows the transfer energy comparison between the direct, chemical transfer mission scenario, the electric hybrid transfer mission scenario and the alternative Argonaut mission scenario. Note that these figures have a logarithmic scale on the vertical axis.

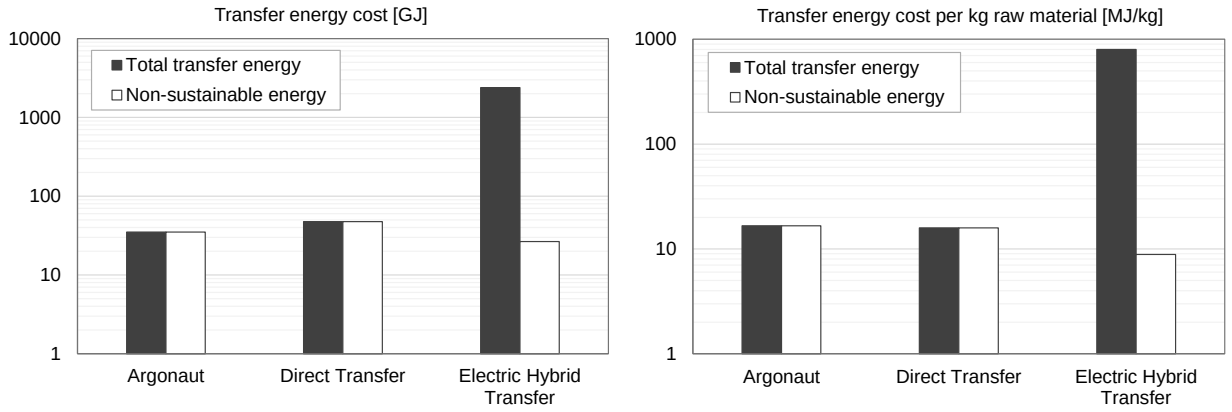

Figure 6.20: Transfer energy comparison of the electric hybrid transfer, direct transfer and the alternative Argonaut mission scenario.

When comparing the electric hybrid transfer mission scenario to the other scenarios, it can be seen that the former requires significantly more total energy for the orbital transfer. This can directly be attributed to the excessive energy requirements for the low-thrust orbit-raising manoeuvre. When accounting only for the non-sustainable transfer energy however, the electric hybrid transfer scenario becomes more efficient than the other two scenarios. This efficiency gain is maintained when looking at the specific transfer energy cost per kg of raw material.

While Solar electric energy does not directly contribute to mission-wide energy, the power consumption of the thrusters does contribute to the overall feasibility and practicality of a low-thrust orbit-raising manoeuvre. Excessive power requirements can create unrealistic design scenarios with excessively large solar arrays, especially for a vehicle that has a relatively short mission life and is completely lost upon impact with the Lunar surface. As such, different thruster configurations were explored and analyzed in terms of the performance consequences. It is important to note that the true thrust time and therefore the transfer energy cost were determined by running the FreeFlyer simulation again taking into account the margin on the TLI propellant mass. Using the same general thrusting regime as shown in Figure 6.16 with a defined maximum apogee shift angle of 180° to visualize a worst case scenario and an assumed average solar cell efficiency of 30%, the results of this analysis are tabulated in Table 6.13.

Table 6.13: Performance impact for different thruster configurations.

Number of thrusters	**4**	**3**	**2**
Total thrust [N]	1.192	0.894	0.596
Flight time [days]	636.38	838.14	1178.85
Thrust time [days]	342.64	459.72	679.93
ΔV [km/s]	3.236	3.258	3.210
Power usage [kW]	24	18	12
Total energy usage [TJ]	2.368	2.383	2.350

It can be seen from this table that the two main consequences of lowering the number of thrusters are an increased flight time and a lower power usage. Interestingly, the total ΔV and energy usage stay approximately the same for each of the analyzed thruster configurations. This reflects the observation from classical orbital mechanics in which the ΔV for a given manoeuvre is independent on thrust level or vehicle mass, as was previously highlighted in the zero-patched conics method. The difference that does exist in the shown ΔV values is likely a result of the slightly different shapes and exit conditions of the transfer orbits due to the differing thrust level. This also indicates that the total thrust time is effectively proportional to the total thrust level. Making a concrete choice in terms of number of thrusters is not a necessity at this early stage, though it is considered that using 3 thrusters provides a solid middle ground, boasting

acceptable flight times even in the worst case orbital alignment at feasible power requirements. However, should longer flight times be acceptable, there is no true downside to reducing the number of thrusters to 2 or even a single one as overall propellant mass and energy usage stay effectively the same.

6.5. The Continuous Moon Return Scenario

The analysis up until this point has been limited to single-target missions. That is, missions that aim to capture and transfer a single space debris target and are subsequently lost upon impact with the Lunar surface. This arguably wasteful aspect of a recycling mission can potentially be alleviated by establishing a mission that can be operated continuously. While single-target missions are undoubtedly the first step, operating a continuous mission scenario that returns multiple targets represents the ideal goal for a space debris recycling infrastructure. In basis, this means that the transfer vehicle returns to Earth orbit upon delivery of a space debris target in order to capture another one. A basic concept of operations is shown in Figure 6.21.

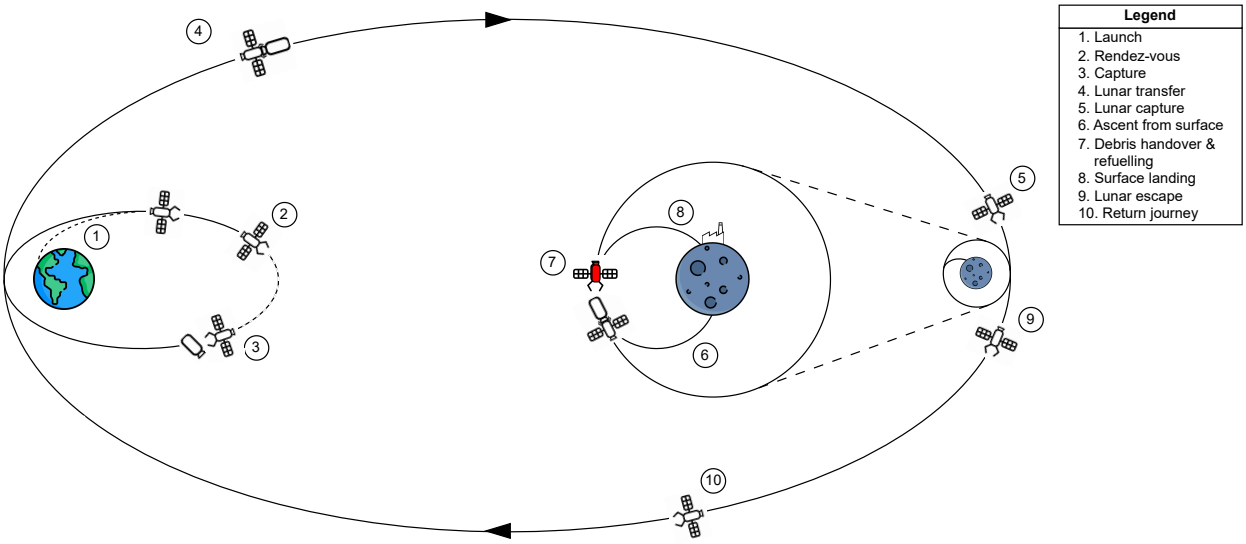

Figure 6.21: Simplified concept of operations for the continuous Moon return mission scenario.

This simple visualization already details some of the additional complexities involved for this continuous Moon return scenario. Most principally, it can be seen that this mission utilizes two distinct transfer vehicles. One that travels between Earth orbit and Lunar orbit (indicated in white in the figure), and one that travels between the Lunar surface and Lunar orbit (indicated in red in the figure). The choice to split the maneuverability demands over two vehicles was made deliberately upon consideration of the practical aspects of the mission as a whole. Principally, a soft landing is a necessity in order to operate the mission over multiple targets considering the transfer vehicle cannot be impacted into the Lunar surface. Carrying the large propellant masses required for the termination burn throughout the return leg to Earth and the subsequent Lunar transfer back to the Moon was found to bring excessively infeasible propellant mass requirements. While such propellant masses are infeasible in terms of vehicle design, one must also consider that these propellants would have to be shipped to Lunar orbit to refuel the transfer vehicle. In order to minimize the amount of propellant that would have to be shipped, it was chosen to take the hybrid electric mission scenario as a baseline for the continuous Moon return mission, as this reflects the most optimal scenario in terms of total propellant load. By operating a distinct vehicle, hereafter named the ”Debris Landing Vehicle”, that transports debris strictly from Lunar orbit to the surface, these problematic aspects are circumvented. A second vehicle, hereafter named the ”Debris Transfer Vehicle” therefore facilitates only the required transfer of the debris between Earth orbit and Lunar orbit, after which it hands over the debris target to the Landing vehicle. In terms of required infrastructure, two critical additional assumptions have to be made when considering a continuous Moon return scenario:

- **In-situ propellant production on the Moon:** The high-thrust requirement of the Lunar landing manoeuvre makes chemical propulsion a necessity. Transporting the large required propellant masses required for landing from Earth to the Moon would entail an entirely separate mission on its own, negating any energy efficiency benefits of a continuous Moon return mission. Instead, in-situ propellant production, mainly in the form of liquid oxygen and liquid hydrogen, presents a critical solution.

Considering these propellants are cryogenic, the debris landing vehicle will remain on the Lunar surface until the debris is in Lunar orbit. This allows the landing segment to be as short as possible while entirely leveraging the in-situ produced propellants.

- **In-orbit refuelling capabilities around the Moon:** The debris transfer vehicle however will have to be refuelled in Lunar orbit. Utilizing the liquid oxygen and liquid hydrogen produced on the Moon is not a feasible possibility considering that the long transfer times and intermittent waiting times to facilitate the orbital alignment make using cryogenic propellants infeasible. As such, the propellants used by the debris transfer vehicle must be shipped to the Moon and stored in an orbital refuelling depot to which the transfer vehicle docks prior to every return mission in order to replenish its propellant tanks. Note that in-orbit refueling around Earth would be unsuitable considering the wide range of potential orbital orientations for the subsequent upper stage space debris targets.

Its inherent reliance on these two major assumptions alone already push this continuous Moon return mission scenario far into the future in terms of potential feasibility. Additionally, a semi-permanent human presence would already be required to facilitate inevitable maintenance of the more complex infrastructure systems and the debris landing vehicle itself. Numerous other smaller assumptions and considerations are further tied to this advanced mission concept, such as the previously mentioned upkeep of a propellant depot in Lunar orbit, long-term radiation protection and transfer vehicle degradation, loss of solar array performance and advanced docking capabilities. Finally, the orbital alignment problem that was found to be one of the critical difficulties for a space debris recycling mission regardless of transfer strategy becomes exponentially more complex when considering multiple return legs not just back to Earth, but to a specific piece of debris. Attempting to solve the dynamics of these complex orbital alignments extrapolated over multiple return missions was considered beyond the scope of this research. Instead, the continuous Moon return scenario was analysed based on the assumption that orbital alignment could be achieved without major changes to the overall mission architecture. The already performed analysis for the electric orbit-raising mission scenario is therefore used as a representative baseline for the continuous Moon return scenario. While this is a major assumption, it was considered an warranted one given the complexity of the problem. This inherently limits the analysis of the Moon return scenario is to a higher level than the ones performed for the single-target missions. Though given the fact that the Moon return scenario already hinges on a large set of debatable assumptions such as the ones listed above, such a high-level analysis was considered warranted. Nevertheless, analyzing this continuous Moon return mission scenario was considered an important final addition considering that it represents an ultimate end goal for the concept of debris recycling for Lunar exploration as a whole. This high-level analysis is therefore a means of gauging potential energy efficiency gains that could potentially be achieved beyond the single-target missions, at least under the assumptions presented.

With the assumptions detailed, let us consider that a Moon return scenario effectively consists of two main mission phases: An initial phase in which the transfer vehicle is launched from Earth, captures a target and transports it to the Moon in a fashion very similar to a single-target mission, and a number of subsequent recurring phases. These recurring mission phases involve the debris transfer vehicle leaving the Moon, returning to Earth orbit to capture another debris target and subsequently transferring back to the Moon. For the initial mission, the performed analysis for the electric orbit-raising mission scenario was taken as a baseline and adapted accordingly to represent the additional manoeuvres for the continuous Moon return scenario. Indeed, for the debris transfer vehicle, this mission scenario is effectively identical and thus follows the same calculation steps in basis. Table 6.14 presents the calculated performance metrics for the initial transfer mission.

Table 6.14: Performance metrics for the initial mission of the continuous Moon return scenario.

	Manoeuvre	ΔV [km/s]	Propellant mass [kg]	Energy cost [GJ]
Debris Transfer Vehicle	Rendezvous	0.182	274.58	1.780
	Low-thrust orbit raising	3.368	1142.75	1967.900
	Lunar capture	0.823	1950.09	12.642
	Total	**4.3734**	**3367.42**	**1982.322**
Debris Landing Vehicle	Ascent from surface	1.884	5763.23	37.363
	Orbit injection	0.025	56.25	0.365
	Descent injection	0.025	95.62	0.620
	Landing termination	1.884	5439.94	35.267
	Total	**3.819**	**11355.04**	**73.614**

It can be seen from this table that indeed, the ΔV values for the debris transfer vehicle align with those of the electric orbit-raising mission scenario. While the ΔV for the low thrust orbit-raising manoeuvre was assumed to be equal to that of the corresponding manoeuvre in the single-target mission scenario, this cannot be said for the energy cost. To assess the energy cost, the orbit-raising manoeuvre was simulated individually in FreeFlyer having adapted the change in final vehicle mass for the lower required propellant mass of the debris transfer vehicle as it does not have to perform the descent and landing manoeuvres. This lower vehicle mass results in a lower required thrust time and therefore a lower energy cost. Additional care was taken to confirm that an apogee shift angle of 180° was still achievable in this lower thrust time, which was possible. As a sanity check, the ΔV applied in the FreeFlyer simulation was computed and compared to the assumed value, which yielded a difference of 1.56%. Accordingly, the computed propellant mass using the Tsiolkovsky rocket equation (without the applied margin) yielded a difference of 1.60% when compared to the propellant mass outputted by FreeFlyer.

For the debris landing vehicle however, the need for a soft landing results in a substantial increase to the propellant masses particularly due to the high-impulse ascent and landing termination burns. Combined with the large target mass of the ESC-A upper stage, this leads to a propellant mass of over 11 tons for the debris landing vehicle. This large propellant mass highlights the benefit of isolating the landing manoeuvres in a separate vehicle, as these excessive masses would have greatly impacted the required propellant mass of the transfer vehicle in a snowball effect, had only a single vehicle been used. While the propellant mass of the debris landing vehicle does not represent an inherent infeasibility, the magnitude of this value must not be underestimated. For reference, consider that the European Service Module (ESM) and the Apollo 11 Lunar Module feature a propellant mass of 8600 kg [104] and 10624 kg [105], respectively.

For the recurring missions, the mission sequence is expanded for the debris transfer vehicle while for the debris landing vehicle, the same performance metrics hold as for the initial mission, considering no changes are required. The calculated performance for each of these recurring missions is detailed in Table 6.15, which hold for every single subsequent space debris target that is retrieved following the initial mission.

Table 6.15: Performance metrics for the recurring missions of the continuous Moon return scenario.

	Manoeuvre	ΔV [km/s]	Propellant mass [kg]	Energy cost [GJ]
Debris Transfer Vehicle	Lunar escape	0.823	1657.77	10.747
	Low-thrust orbit lowering	3.368	658.24	1116.300
	Rendezvous	0.182	274.58	1.780
	Low-thrust orbit raising	3.368	1142.75	1967.900
	Lunar capture	0.823	1950.09	12.642
	Total	**8.565**	**5683.43**	**3109.370**
Debris Landing Vehicle	Ascent from surface	1.885	5763.23	37.363
	Orbit injection	0.025	56.25	0.365
	Descent injection	0.025	95.62	0.620
	Landing termination	1.885	5439.94	35.267
	Total	**3.821**	**11355.04**	**73.614**

Looking at the ΔV budget for the debris transfer vehicle, it can be seen that the magnitudes of the manoeuvres are mirrored about the rendezvous manoeuvre. This is a result of the assumption that identical but opposite manoeuvres are equal in their ΔV magnitude, which was adapted from classical orbital mechanics [81]. Hence, the previously calculated ΔV for the low thrust orbit-raising and the Lunar capture was 'reversed' in direction yet kept equal in magnitude and assumed as representative for the low thrust orbit-lowering and Lunar escape manoeuvre, respectively. Similar to what was explained for the initial mission, the energy cost was assessed by simulating the the low-thrust manoeuvres individually in FreeFlyer and implementing the change in final vehicle mass. It should be noted here that under the 'equal but opposite' assumption, the orbit-lowering was modeled as an orbit-raising manoeuvre. The same sanity check for the ΔV and propellant mass was performed once again, yielding differences of 0.31% and 0.15%, respectively. For the orbit-raising manoeuvre, the flight time and associated energy usage is identical to the initial mission case considering that they represent identical manoeuvres at the end of the mission sequence. The orbit-raising manoeuvre for the recurring mission scenario is therefore not impacted by manoeuvres that occur prior. Finally, it is key to highlight that for all manoeuvres up to the orbit-raising manoeuvre, there is no captured debris target which is part of the vehicle, which in the case of the ESC-A upper stage results in a mass reduction for the vehicle of 5000 kg. This is why, despite having to carry the propellant mass of all subsequent return manoeuvres, the propellant mass for the Lunar escape manoeuvre is lower than that of the Lunar capture manoeuvre for the same ΔV.

Comparing the continuous Moon return mission scenario as detailed in this section to the established feasible single-target mission scenarios, Figure 6.22 presents the performance comparison in terms of total energy cost and specific energy cost. That is, the transfer energy cost per kg of raw material returned. The values presented in this figure will change for different numbers n of returned targets. For this comparison, it was chosen to set the total number of returned space debris targets for the continuous mission to n = 3. Note once again the logarithmic scale used in this figure.

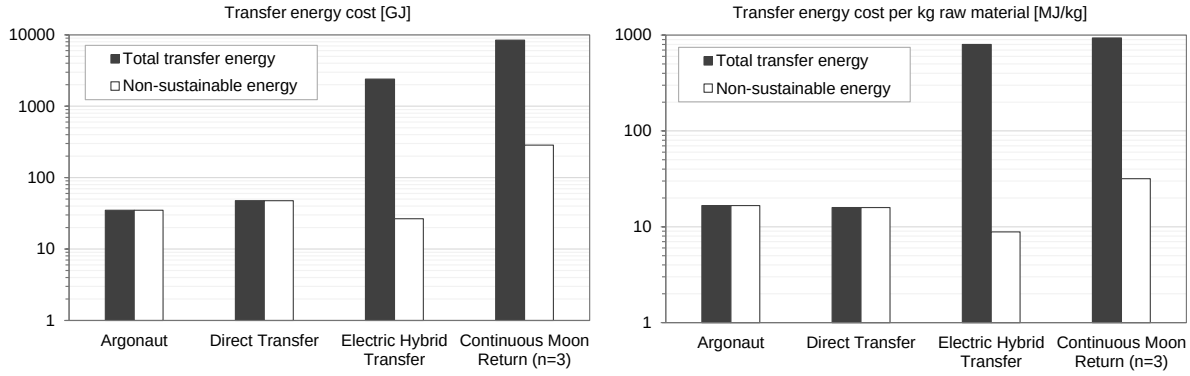

Figure 6.22: Transfer energy comparison of the continuous Moon return scenario, the single-target recycling missions and the alternative Argonaut mission scenario.

From this figure, it can be seen that the total transfer energy cost as well as the non-sustainable energy cost is substantially higher for the continuous Moon return scenario than it is for the single-mission scenarios. This makes sense, as the continuous scenario returns 3 ESC-A stages rather than the one for the single-target mission scenarios. Therefore, it makes more sense to compare the transfer energy cost per kg of raw material returned. It can be seen that despite the lower energy cost for each of its low-thrust manoeuvres, the continuous Moon return scenario has a higher total transfer energy cost per kg of raw material returned. This increase can be attributed to two factors. First, the need for an additional return manoeuvre in the recurring mission phase outweighs their lower individual energy cost. Second, the need for a soft landing significantly increases the energy cost. This can be seen especially when comparing the non-sustainable energy cost, which does not include the 'free' solar energy. Indeed, this non-sustainable energy cost represents the total energy investment that should ultimately be compared between the mission scenarios. This does not however mean that a continuous Moon return scenario is less efficient. The performance comparison shown in Figure 6.22 includes only the orbital transfers. The main advantage of a continuous Moon return scenario in terms of energy efficiency, which is not captured in this figure, is the fact that it only requires a single launch regardless of the amount of captured targets.

6.6. Transfer Scenarios: Conclusion

In this chapter, difficulties and constraints of a space debris recycling mission have been identified and several different orbital transfer scenarios have subsequently been explored and analyzed. Given the innovative nature of the mission, single-target missions were defined as the baseline. A zero-patched conics approach was used for the assessment of the orbital mechanics and determine the required ΔV required for the relevant manoeuvres. Within the identified target pool of Ariane upper stages in GTO, the H10 (1764 kg) and ESC-A (5000 kg) vehicles were both analyzed as the two space debris targets. However, it was found that since these targets area already in orbit, the larger raw material return mass of the ESC-A made it the ideal target with a significantly lower transfer energy per kg of mass delivered. The findings for the three analyzed main mission scenarios are summarized below.

- A conventional, direct, impulsive Lunar transfer was studied as a baseline option given the potential to leverage the high perigee velocity of the GTO debris orbit. However, the application of such a transfer is limited by the alignment between the orbital alignment between the targeted debris object and the Moon. However, it was found that given any initial conditions for the argument of periapsis and RAAN of a piece of debris and the standing of the Moon, two unique points exist which can be reached by using the natural J2 drift with little to no performance cost other than an increased mission time of at most 380 days.
- The introduction of intermediate circular ”staging” orbits was explored as additional mission scenarios in order to reduce the large potential waiting times in the Van Allen belts. However, neither circularizing into LEO at perigee or into GEO at apogee was found to be feasible due to the excessive propellant requirements for the staging orbit injection manoeuvres. The implementation of staging orbits also were found to have transfer energy costs significantly higher than the direct transfer scenario.
- The implementation of low-thrust electric propulsion for the main orbit-raising manoeuvre from GTO to the Moon was analyzed using the FreeFlyer orbital simulation suite. The significantly higher specific impulse of low-thrust electric propulsion systems allows for a significant saving of propellant mass though at the cost of a longer flight time. Through the analysis, it was shown that by using a thrust-arcing strategy, the apogee passage point can be shifted within the orbital plane to facilitate a Lunar encounter even in the worst case where a complete 180° shift is required.

As such, there are two main feasible single-target orbital transfer scenarios: the direct, chemical transfer and the low-thrust hybrid transfer. The key transfer characteristics for these scenarios as well as the alternative Argonaut mission scenario are summarized in Table 6.16 below.

Table 6.16: Summary of transfer characteristics for the two feasible single-target mission scenarios and the Argonaut.

	Argonaut	**Direct, chemical transfer**	**Low-thrust hybrid transfer**
Propulsion architecture	Chemical	Chemical	Hybrid (chemical & electric)
Total ΔV	2.880 km/s	2.437 km/s	4.963 km/s
Propellant mass	5388.0 kg	7331.5 kg	5469.6 kg
Total transfer energy	34.930 GJ	47.530 GJ	2394.6 GJ
Flight time	$\sim$ 5 days	< 385 days	< 636 days

Beyond assessing single-target missions, a preliminary analysis was performed for multi-target missions. It was chosen to spread the transfer functionality over two vehicles: a debris transfer vehicle to ferry the debris between Earth and the Moon, and a debris landing vehicle to safely land the debris onto the Lunar surface. Such a continuous mission is subject to numerous assumptions, but shows potential to return multiple debris targets in a continuous mission for marginal increases in transfer energy costs. The main advantage of such a multi-target mission scenario in terms of energy efficiency however is the fact that it only requires a single launch to capture several targets. This is in contrast to the single-target mission scenarios which require a launch for every captured target. In the following chapter, the impact of this will be explored in detail.

7

Global Mission Energy Analysis

With all of the mission phases and the various processes detailed, a number of complete space debris recycling missions concepts have been defined. In this chapter, all of the results from the energy analyses will be combined for each of these mission concepts, which will then be compared and analyzed to make up a single, global mission energy analysis.

7.1. Single-target Mission Scenarios

Given the novel nature of recycling space debris as a concept, the single-target missions are ultimately the baseline. They represent the most feasible and directly applicable approach to getting a space debris recycling mission off the ground. Throughout the mission design, two main mission concepts were shown to be feasible, which were discerned primarily by the use of either a direct, chemical transfer or a low-thrust hybrid transfer. Before compiling the energy analyses into a global energy expenditure, a summary of the two single-target space debris recycling mission concepts is given in Table 7.1 below. Note here that the flight time of the low-thrust hybrid transfer mission concept is based on the use of 4 Hall effect thrusters. The dependency of flight time on thruster configuration was highlighted in the previous chapter in Table 6.13.

Table 7.1: Mission characteristics for the two single-target space debris reycling mission concepts.

Mission Concept	Chemical Propulsion	Low-Thrust Hybrid Propulsion
Space debris target	Ariane 5 ESC-A	Ariane 5 ESC-A
Space debris target mass	5000 kg	5000 kg
Launch vehicle	Ariane 64	Ariane 64
Dry mass	1500 kg	1500 kg
Launch mass	8832 kg	6970 kg
Total ΔV	2.437 km/s	4.963 km/s
Propulsion system	Liquid bi-propellant	Liquid bi-propellant & solar electric
Propellant	MMH & NTO	MMH & NTO, Xenon
Flight time	< 385 days	< 636 days

7.1.1. Mission segment energy distribution

Across the three main identified mission phase, four distinctions have been made for the processes that govern the global mission energy analysis. These are material manufacturing and launch for the Earth segment, orbital transfer for the space segment and debris processing for the Moon segment. Each of these four processes consists of several underlying steps or components which have been analyzed in terms of their energy expenditure in the previous two chapters. These energy expenditures can be compared in terms of their individual magnitudes within a defined mission scenario as well as their relative magnitudes across the defined single-target mission scenarios. The overall distribution of the global mission energy across the main processes for each of the three single-target mission scenarios is presented in Figure 7.1. Note the logarithmic scale used on the horizontal axis of this figure.

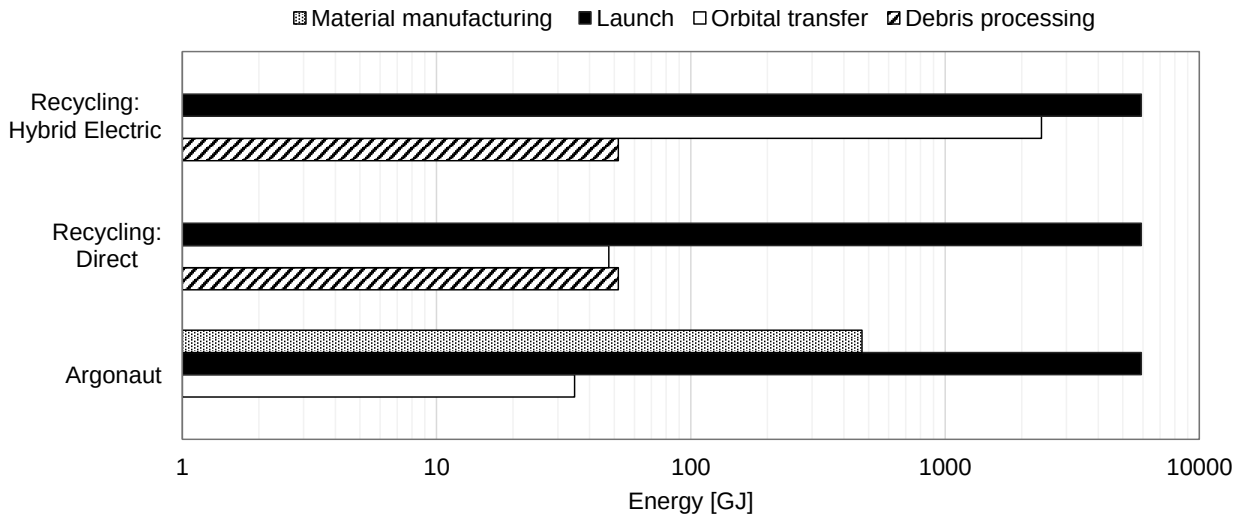

Figure 7.1: Single-target space debris recycling global mission energy cost distribution over key mission processes.

It can immediately be seen that the launch is the biggest energy sink across all segments by a substantial margin. This makes sense given the enormous amounts of propellant expended throughout the launch of Ariane 6. The launch energy is identical for all three mission scenarios as they all use the Ariane 64 configuration. At nearly 5.9 TJ, the launch is two orders of magnitude larger than the orbital transfers in terms of energy expenditure. This large energy expenditure highlights the launch as a crucial bottleneck given the strict limitation of launch mass not just for a debris recycling mission, but for any space mission. This is thus not only a conventionally practical limitation, but also the single dominant limitation in terms of total energy expenditure throughout the lifecycle of a mission. Hence,this comparison shows that the energy expended throughout the launch cannot be underestimated and highlights an important aspect of debris recycling as a concept. That is, by effectively capturing the payload mass in orbit, strain is alleviated from the launch as such mass does not have to be launched. The impact of this consideration will be elaborated on in detail within the next section.

It can be seen also that while the energy expenditure of the orbital transfer is similar for the direct chemical transfer mission scenario and the alternative Argonaut mission scenario, the low-thrust hybrid electric propulsion mission scenario has a substantially larger energy cost. This is a direct result of the low-thrust propulsion, which was seen earlier in this report to be characterized by large energy requirements due to the long thrust times during which the thrusters must be operated. Note however that, similarly to what was explained in the aforementioned section, this energy cost does not represent an actual energy ”investment” given that the energy is gathered effectively for free by utilizing solar energy. In terms of actual non-sustainable energy cost, i.e. the chemical energy invested through the combustion of propellants, the energy cost is similar to the direct transfer recycling mission scenario.

The major area in which the two recycling mission scenarios differ from the Argonaut mission scenario is the fact that they do not feature the energy sink related to the manufacturing of aluminium material. Instead they can leverage secondary production and its associated lower energy cost as material is recycled on the Lunar surface. Despite the larger raw material return mass of 3000 kg for an ESC-A upper stage that must be processed as compared to the 2100 kg of raw material to be manufactured for the Argonaut scenario, the processing energy remains substantially lower. Additionally, it should be noted that the energy used for the manufacturing of aluminium is non-sustainable, as explained in subsection 5.1.1. The tacit energy used to define the energy cost for aluminium manufacturing already accounts for the portion of electricity that is generated from sustainable sources. This is in contrast to the debris processing energy, which does not represent a true energy cost by virtue of solar energy being one of the only viable energy generation methods on the Moon. It should be noted however that even if the aluminium manufacturing was to be entirely done through sustainable energy and thus subtracted from the energy cost, this has only a marginal impact on the global energy analysis given that the launch dominates the energy cost.

7.1.2. Total mission energy analysis

With the single-target global mission energy usage distribution over the main mission segments defined, compiling the presented values into a total mission energy analysis forms the basis for the comparative analysis between the defined mission scenarios. Subsequently, this analysis is ultimately the foundation for the drawing of conclusions regarding the viability of recycling space debris for Lunar exploration activities. The results of the compiled energy analysis presented in this report are tabulated in Table 7.2 and visualized in Figure 7.2 for the single-target missions. Note that the distinction between total energy use and energy cost is made here once again. Earlier in this report, it was elaborated that solar energy does not represent an actual energy investment that has to be made and as such should not be considered as a strict energy cost since it is captured effectively for free. This is in contrast to other energy expenditures such as the combustion of propellants, which constitute to a strict energy loss. Hence, this definition of the total energy cost equates to the subtraction of the solar energy from the total energy use.

Table 7.2: Single-target space debris recycling global mission analysis results.

		Debris recycling:	
Mission Scenario	**Argonaut**	**Direct Transfer**	**Low-Thrust Hybrid Transfer**
Material manufacturing [GJ]	470.69	N/A	N/A
Launch [GJ]	5893.00	5893.00	5893.00
Orbital transfer [GJ]	34.93	47.53	2394.57
Debris processing [GJ]	N/A	51.84	51.84
Total energy use [GJ]	6398.62	5992.37	8339.41
Solar energy [GJ]	0.00	51.84	2419.89
Energy cost [GJ]	**6398.62**	**5940.53**	**5919.52**

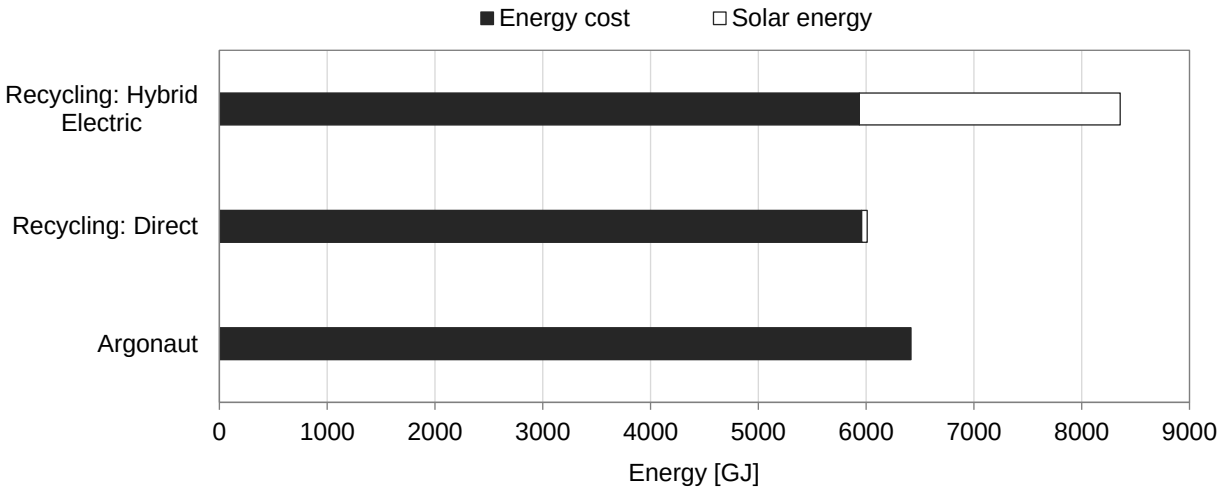

Figure 7.2: Global mission energy cost comparison for the single-target mission scenarios.

From these results, it can be seen that in terms of total theoretical energy cost, both recycling missions actually outperform a direct material delivery mission using Argonaut. The main defining difference is the material manufacturing energy cost compared to the associated energy with the debris processing, as was seen already in the global mission energy use distribution. The two recycling missions are practically identical in their global mission energy cost, with the low-thrust transfer mission scenario presenting a substantially higher solar energy usage as its defining trait as a direct result of the electric propulsion for the orbit-raising manoeuvre. Though as mentioned before, this does not constitute to an actual increase in energy cost. The direct, chemical transfer mission scenario features only a very marginal solar energy use which is dedicated only to the debris processing on the Lunar surface.

7.1.3. Specific energy analysis

Total energy however neglects one critical difference between the debris recycling mission scenarios and the Argonaut mission scenario in particular: the difference in raw material delivered. For a suitable comparison, a ”specific” energy cost was defined as the total energy cost divided by the delivered raw material mass. This is ultimately the defining parameter that must be used for an equivalent comparative analysis across the various mission scenarios as it represents the energy investment corrected for an analogous raw material mass. Table 7.3 is a direct continuation of the global mission energy analysis shown in Table 7.2 and highlights the determination of this specific energy cost, which is also visualized in Figure 7.3.

Table 7.3: Specific global mission energy cost analysis for the single-target mission scenarios.

Mission Scenario	**Argonaut**	**Debris recycling:**	
		Direct Transfer	**Low-Thrust Hybrid Transfer**
Energy cost [GJ]	6398.62	5940.53	5919.52
Raw material return [kg]	2100	3000	3000
Specific energy cost [GJ/kg]	3.047	1.980	1.973
Ratio Argonaut	100%	65%	65%

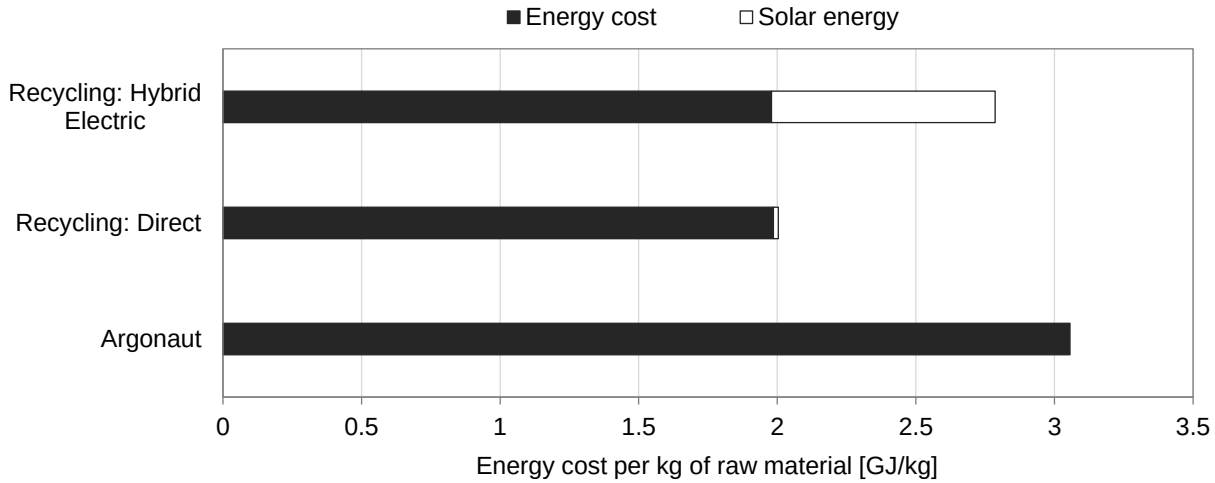

Figure 7.3: Specific global mission energy cost comparison for the single-target mission scenarios.

This analysis shows that the space debris recycling missions have a significantly lower specific energy cost principally by virtue of delivering over 40% more material than the Argonaut. So much so that even when accounting for the additional solar energy, which does not strictly contribute to the energy cost, the energy used per kg of raw material returned is still lower than that of the Argonaut mission scenario. The larger returned raw material mass is ultimately the biggest advantage of a space debris recycling mission compared to a conventional lander mission. Capturing payload mass in orbit circumvents the strict launch mass restrictions as a constraining factor which otherwise limit the payload mass as it has to be launched from Earth. For a space debris recycling mission however, the excessive energy associated with the launch of the captured material has already been provided by the original mission that left this material in orbit in the first place. Eliminating this launch energy is a proportionally much larger save in terms of global mission energy than the additional energy expenditure associated with the orbital transfer, especially when leveraging low-thrust solar electric propulsion.

Another direct consequence of capturing material in orbit is the fact that the overall launch mass in its entirety is reduced. Whereas the Argonaut requires a dedicated launch of Ariane 64 to put it directly on its Lunar Transfer Orbit (LTO), this is not necessarily the case for the debris recycling missions. Looking back at the single-target debris recycling mission overview presented in Table 7.1, it can be seen that the wet masses of the vehicles are 8832 kg and 6970 kg for the direct chemical transfer and the low-thrust hybrid transfer mission scenarios, respectively. While this exceeds the 4500 kg payload capacity of Ariane 62 to GTO, the corresponding 11 500 kg payload capacity of Ariane 64 leaves substantial payload mass margin. This payload mass margin could be made use of by introducing a secondary client in a rideshare

configuration, which is common occurrence within the space industry and can be facilitated directly on the Ariane 6 through Ariane's dual payload integration [60]. As such, the actual global mission energy expenditure for the space debris recycling missions is reduced by adapting the launch energy proportionally to the launch vehicle's payload mass capacity utilization. Considering that the conceptualized mission scenarios all must be launched into GTO, GEO missions are the primary candidates for inclusion as secondary clients. Given the launch masses determined for the recycling missions and especially their strict launch orbit requirements in order to rendez-vous with a targeted piece of debris, it was considered that these recycling missions would in principle be the primary customers. The potential to spread out the launch energy through the inclusion of a secondary rideshare client is another way to increase the energy efficiency of space debris recycling missions courtesy of the lower associated launch masses. The results of this adapted launch energy analysis are tabulated in Table 7.4 and further visualized in Figure 7.4.

Table 7.4: Specific global mission energy cost analysis for the single-target mission scenarios adapted for launch vehicle payload mass utilization.

Mission Scenario	Argonaut	Debris recycling:	
		Direct Transfer	Low-Thrust Hybrid Transfer
Ariane 64 payload capacity utilization	100%	77%	61%
Proportional launch energy [GJ]	5893.00	4525.58	3571.45
Adapted energy cost [GJ]	6398.62	4573.11	3597.97
Adapted specific energy cost [GJ/kg]	3.05	1.52	1.20
Ratio Argonaut	100%	50%	39%

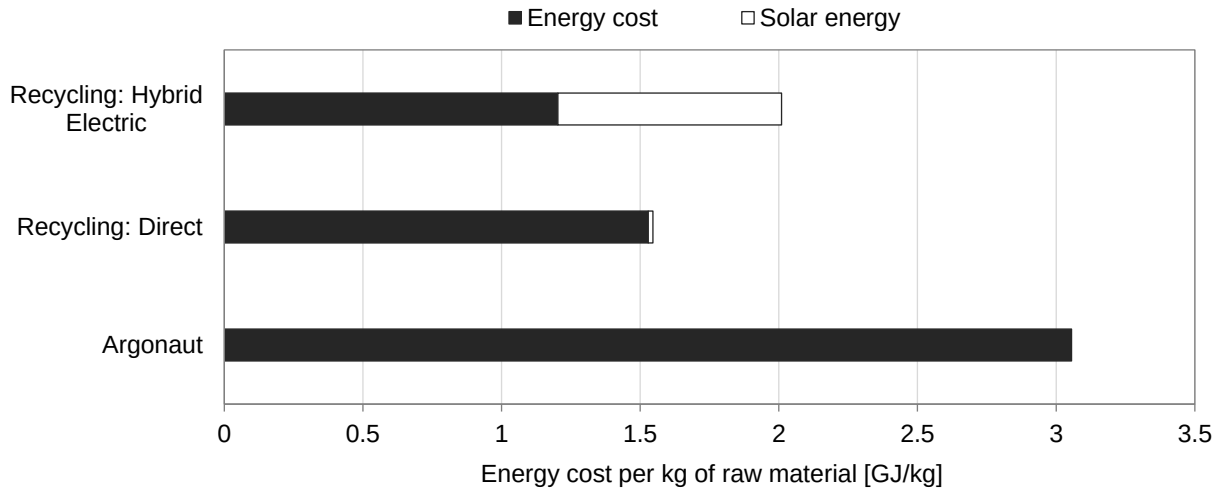

Figure 7.4: Specific global mission energy cost comparison for the single-target mission scenarios adapted for launch vehicle payload capacity utilization.

Comparing these results to the ones presented in Table 7.3 and Figure 7.3, it can be seen that the space debris recycling mission scenarios get a substantial increase in energy efficiency when accounting for the payload capacity utilization. This is especially true for the low-thrust hybrid mission scenario, for which the energy cost per kg of raw material delivered goes down to 1.2 GJ/kg, 60% less than the Argonaut. Though even the direct transfer mission scenario yields a substantial advantage over the Argonaut mission scenario with a specific energy cost half that of the Argonaut. This large impact in terms of total energy expenditure is a direct result of the fact that this analysis reduces the effective launch energy, which was found earlier to be by far the largest energy sink in the mission sequence. An important consideration to make here however is the fact that while adapting the launch energy based on launcher payload mass capacity utilization is in principle valid based on the potential for a rideshare, there is a lower limit to what leftover payload margin can actually be utilized realistically for a second client satellite. Missions to GEO are historically characterized by larger vehicle masses due to their longer mission lifetimes and their greater distance from Earth warranting more powerful hardware. This is substantiated by Figure 7.5, which presents the launch mass of all GEO satellites extracted from data published by the Union of Concerned Scientists (UCS) [106].

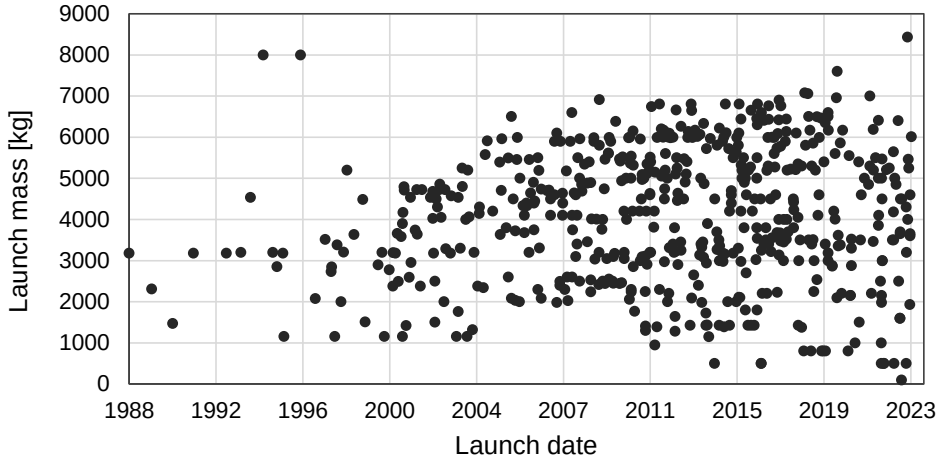

Figure 7.5: Launch mass distribution of GEO satellites since 1988. [106]

It can be seen that the vast majority of GEO satellites weigh in over 2000 kg, with an average launch mass of 4083.95 kg for all GEO satellites in the UCS dataset. Additionally, it can be seen that the overwhelming trend towards miniaturization for LEO satellites is not reflected to the same degree in the GEO satellite industry. In fact, a trend towards heavier satellites is observed within the dataset. The range of launch masses does increase over time, which shows that smaller GEO satellites are being developed alongside ever larger GEO satellites. The latter is enabled by the development of ever more powerful launch vehicles that push the boundaries of launch system capabilities. Nevertheless, the graph shows that client satellites exist within the leftover payload mass margins determined for the space debris recycling missions, with the low-thrust hybrid transfer mission scenario having the widest potential client base and therefore being most feasible. Finally, it should be considered that such secondary missions to GEO ideally launch on GTO trajectories that put the apogee within the equatorial plane. In terms of orbital parameters, this is reflected by an argument of periapsis value of 0° or 180°, where the latter is the baseline for Ariane launches [42, 60]. This is another consideration that should be taken into account to make the addition of a rideshare client a practical option. It was found earlier in this report that a wide distribution of argument of periapsis values exists within the dataset of Ariane upper stages in GTO, the motion of which is governed by the J2 effect. As such, it was already concluded that choosing a target that approaches a particular desired value (in this case 0° or 180°) is a practical option. Hence, the launch trajectory would be suitable for the space debris target capture and simultaneously facilitate the GEO injection opportunity for the secondary rideshare client. The only consequence for the debris recycling mission would be a longer potential phasing time for the direct, impulsive transfer mission scenario as it waits for the J2 effect to achieve the orbital transfer alignment. Or, within the context of the low-thrust hybrid transfer mission scenario, a longer flight time for the low-thrust orbit raising manoeuvre to achieve the required apogee shift angle. Neither of these consequences are inherently problematic and the analyses performed for these two recycling mission scenarios show these are feasible and viable options as the orbital transfers were designed for the worst-case conditions. Plenty of objects were also shown to exist in the pool of Ariane upper stages in GTO to establish flexibility in choosing semi-ideal targets with favorable orbital elements for faster orbital transfers. As such, the inclusion of a secondary rideshare client and the subsequent increase in energy efficiency for the recycling missions is a valid mission optimization.

Finally, it is recognized that the value set for the raw material mass fraction of these launch vehicle upper stages is a mission-critical assumption. The assumed value of 60% taken from literature is potentially high, as not all of this mass may be recoverable. However, the launch vehicle payload mass utilization for the single-target debris recycling missions shows that a significant margin exists for which lower raw material mass fractions still results in a favorable energy efficiency when compared to a traditional lander mission. Since the dry mass of the target does not change, only the total raw material mass yield is affected. To investigate the influence of the assumed value for the raw material mass fraction, a sensitivity analysis was performed. Figure 7.6 shows how the specific energy cost, i.e. the energy cost per kg of raw material delivered is impacted by the assumed value for the raw material mass fraction of a rocket stage.

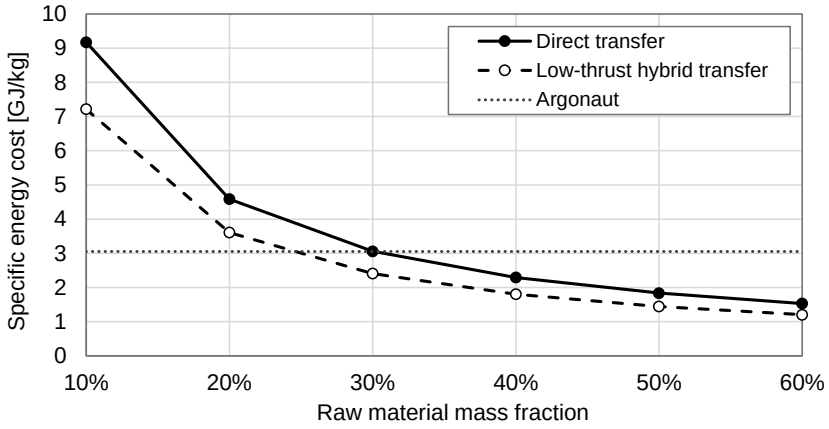

Figure 7.6: Specific global mission energy cost as a function of assumed raw material mass fraction for various mission scenarios.

From this figure, it can be seen that there indeed exists significant margin for this assumption to be lower while still maintaining a lower specific energy cost. To highlight this, the break-even point in which the specific energy cost is equal to that associated with the traditional lander mission (Argonaut) is plotted as the tightly dotted line in the figure shown above. The intersection of this line with the two plotted functions for the analyzed mission scenarios indicates the raw material mass fraction that must be recovered in order to break even. For the direct, chemical transfer mission scenario this break-even value is 30%, while for the more efficient, low-thrust hybrid transfer mission scenario this can go down to 23.6%. As such, there indeed exists significant margin to alleviate potential uncertainties in the raw material mass fraction while maintaining favorable energy efficiency.

7.2. Multi-target Mission Scenarios

For the multi-target mission scenario, the performed global mission energy analysis can be expanded. Because the continuous Moon return mission scenario inherently relies on substantially more assumptions and uncertainties, it was chosen to discuss the associated results separately in this section. This is in line with the argumentation given earlier in this report regarding the more high-level analysis performed for these multi-target mission scenarios, following the intent of gauging the energy efficiency gains that can potentially be achieved beyond single-target missions.

7.2.1. Total mission energy analysis

For the multi-target mission, the continuous Moon return scenario, a global mission analysis inherently depends on the number of upper stage targets that are returned across the total mission. For this analysis, it was chosen to asses two sub-scenarios with a number of total targeted space debris targets n = 3 and 5 to reflect potentially feasible return missions. It should be noted that for each of these missions, a single initial mission is followed up with a number $n-1$ of recurring missions, as explained in the orbital transfer analysis show detailed in section 6.5. The results of the total mission energy analysis, expanded from the previous section, is tabulated in Table 7.5 and further visualized in Figure 7.7.

Table 7.5: Multi-target space debris recycling global mission analysis results.

Mission Scenario	**Argonaut**	**Debris recycling:**			
		Direct	**Low-Thrust Hybrid**	**Moon Return**	
		Transfer	**Transfer**	**[n = 3]**	**[n = 5]**
Material manufacturing [GJ]	470.69	N/A	N/A	N/A	N/A
Launch [GJ]	5893.00	5893.00	5893.00	5893.00	5893.00
Orbital transfer [GJ]	34.93	47.53	2394.57	8421.90	14787.87
Debris processing [GJ]	N/A	51.84	51.84	155.52	259.20
Total energy use [GJ]	6398.62	5992.37	8339.41	14470.42	20940.07
Solar energy [GJ]	0.00	51.84	2419.89	8291.82	14563.90
Energy cost [GJ]	**6398.62**	**5940.53**	**5919.52**	**6178.60**	**6376.17**

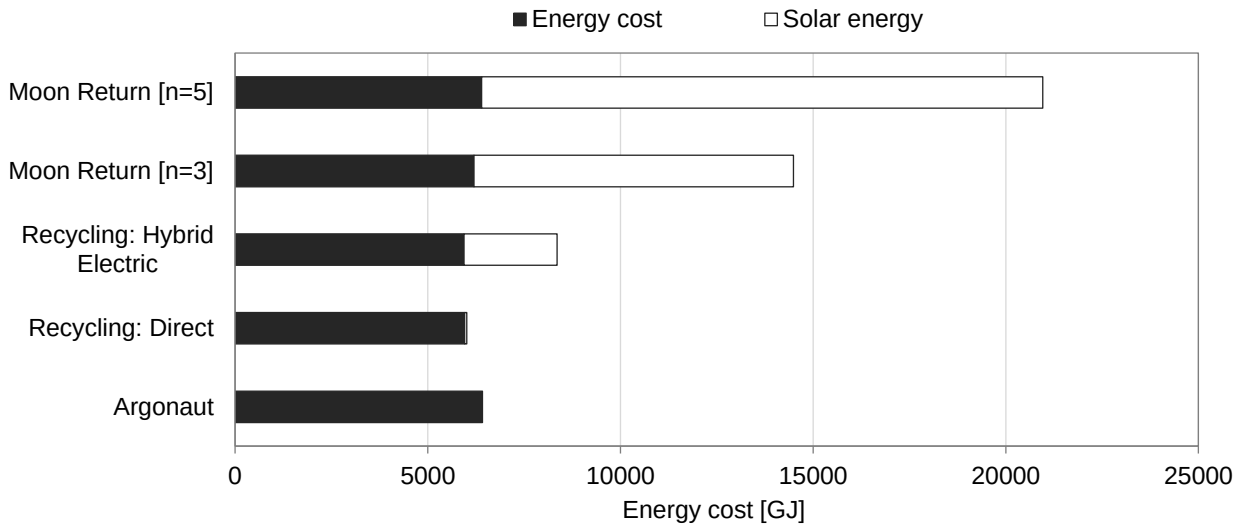

Figure 7.7: Global mission energy cost comparison for the single- and multi-target mission scenarios.

These results shown that, as one would expect, the total energy usage goes up with the number of space debris objects returned to the Moon. The actual energy cost however increases only marginally. This is a direct result of returning multiple space debris targets instead of a single one. The fact that these multi-target mission scenarios do not need to launch a new transfer vehicle for every target delivered to the Lunar surface is their greatest advantage. The figure particularly shows that the necessity of a soft landing results only in a small increase in total energy cost within the context of this global mission energy analysis, which as found earlier is dominated by the launch.

7.2.2. Specific energy analysis

In terms of comparison, the specific energy cost per kg of raw material must again be calculated. Given the marginal increases required in terms of total energy cost, the multiplicative nature of the increase in raw material mass returned for every recurring mission is expected to result in a substantially lower specific energy cost. Theoretically, returning more targets is better in terms of total energy cost per kg of raw material returned. This however neglects many practical limitations that would inevitably prevent the mission from being executed successfully. Several of these are directly tied to the assumptions made for this more advanced future mission scenario and include for example power generation loss due to solar cell generation and long-term radiation exposure over the cyclic journeys between the Moon and Earth. Given this knowledge, Table 7.6 and Figure 7.8 are direct continuations of the results shown in the previous subsection and highlight the results of the specific energy analysis.

Table 7.6: Specific global mission energy cost analysis for the multi-target mission scenarios.

Mission Scenario	**Argonaut**	**Debris recycling:**			
		Direct	**Low-Thrust Hybrid**	**Moon Return**	
		Transfer	**Transfer**	**[n = 3]**	**[n = 5]**
Energy cost [GJ]	6398.62	5940.53	5919.52	6178.60	6376.17
Raw material return [kg]	2100	3000	3000	9000	15 000
Specific energy cost [GJ/kg]	3.047	1.980	1.973	0.687	0.425
Ratio Argonaut	100%	65%	65%	23%	14%

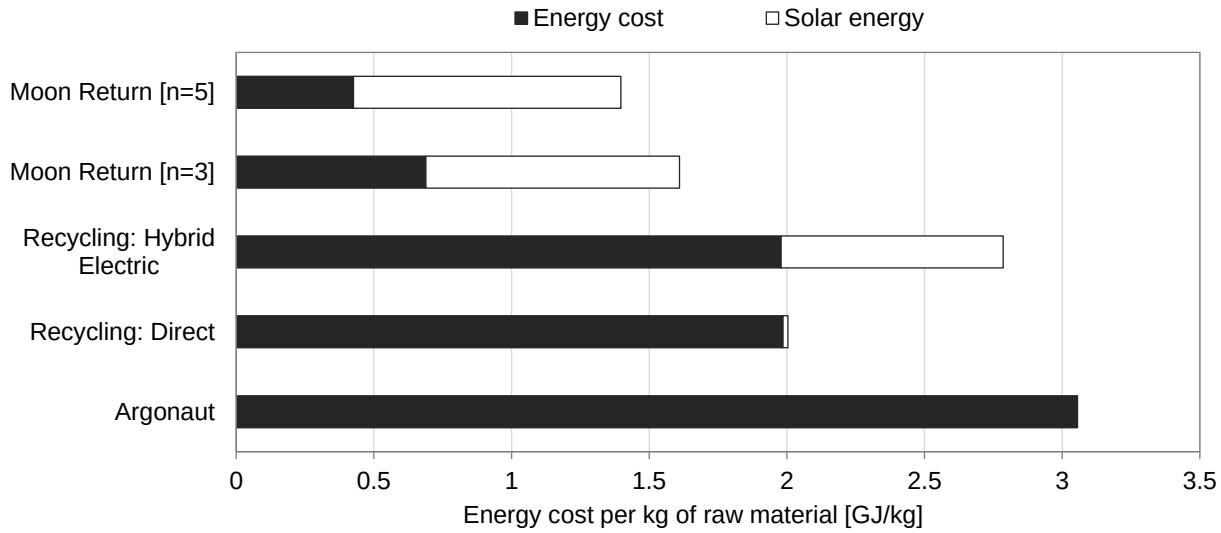

Figure 7.8: Specific global mission energy cost comparison for the single- and multi-target mission scenarios.

These results immediately show the significant reduction in specific energy cost resulting from the aforementioned multiplicative increase in raw material mass with the increasing number of space debris targets returned without needing additional launches. This is especially the case when compared to the single-target missions, for which the values here represent the results without taking into account the launcher payload capacity utilization and the potential for ridesharing. This was done to remain consistent with the analysis for the multi-target mission scenarios. For these scenarios, it was chosen not to perform a launcher payload mass optimization as, given the numerous assumptions involved, determining what infrastructure must be launched and what can be assumed to exist created an entirely new and rather subjective analysis of its own (e.g. differences between the debris transfer vehicle and the debris landing vehicle). Given the presented results in Figure 7.8 however, such an expanded analysis would not impact the conclusions in any way. Indeed, it can be seen that the multi-target mission scenarios are substantially more efficient than the single-target ones in terms of energy investment required per kg of raw material returned to the Lunar surface. Comparing the continuous Moon return scenarios to the low-thrust hybrid single-target mission scenario, diminishing returns are observed in terms of energy efficiency as the change in specific energy cost becomes progressively smaller from the single captured target, to 3 targets, to 5 targets. To highlight this further, Table 7.6 presents the specific global mission energy cost as a function of the number of captured targets n.

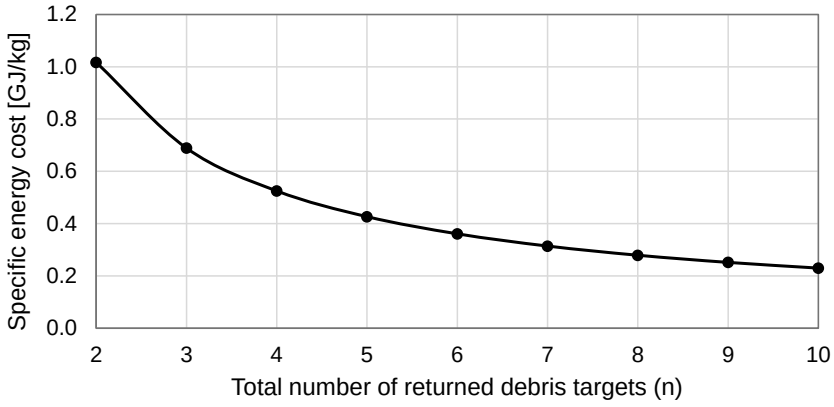

Figure 7.9: Specific global mission energy cost as a function of total returned debris targets n.

Indeed, while the specific energy cost continues to decrease, the magnitude of this decrease reduces in a curve not dissimilar to an exponential decrease. This means that while performing more return missions is better for overall energy efficiency, the advantage of capturing more debris reduces as the number of return missions increases. These diminishing returns can be attributed to the fact that the efficiency gain of only requiring a single launch becomes smaller when the launch is spread out over more return missions.

It should be noted that this global mission energy analysis for the multi-target missions does not include the energy cost required to provide the propellant to the in-orbit refueling depot, which would have to come from Earth due to the previously discussed infeasibility of utilizing cryogenic propellants for long-term storage aboard the transfer vehicle. As such, the actual process would yield a higher energy specific energy cost. Within the applied analyses, this uncertainty is not present for the single-target mission scenarios. Looking strictly at the numbers when making these aforementioned assumptions, the multi-target continuous Moon return missions are indeed the favorable option when striving for the maximum energy efficiency. However, in making this observation one must again be critical and review the numerous assumptions and simplifications made to the analysis. There is ultimately no single definitive answer, and while this analysis shows potential for the multi-target mission scenarios, they are reserved for a more advanced time in which these assumptions could potentially exist in reality.

7.3. Main Findings

The results presented in this chapter show that when comparing the space debris recycling mission scenarios to the Argonaut alternative mission scenario, the former show a greater energy efficiency across the board by virtue of having a substantially lower specific energy cost. The energy efficiency increase observed for the single-target mission scenarios upon inclusion of a secondary client in a rideshare configuration highlights the launch as the single most dominant energy sink in the global energy analysis. The fact that space debris recycling missions capture their principle payload mass in orbit and therefore save significant payload mass margin of the Ariane 64 launch vehicle is what ultimately defines their viability compared to a traditional Lunar lander like the Argonaut. Additionally, the mission design performed in previous chapters shows that the inclusion of such a secondary client is a feasible and viable option. Despite ultimately being a more preliminary global assessment, the observed comparative energy efficiency gains being as high as 61% for the low-thrust hybrid transfer mission scenario shows significant potential for space debris recycling to be a truly viable means of supplying raw material resources to the Lunar surface.

The analysis of the multi-target mission scenarios extend the potential gains in energy efficiency through the multiplicative increase of raw material returned with every subsequent return mission without requiring additional launches. In terms of relative performance however, the difference between the single-and multi-target mission scenarios gets smaller when considering the 77% higher energy efficiency for the n = 3 case compared to the 61% for the aforementioned low-thrust single-target mission scenario when considering the inclusion of a rideshare client. While this efficiency increases for the multi-target mission scenarios with increased number of targets captured, numerous practical limitations arise. Combined with the broad assumptions and simplifications made to analyze the multi-target mission scenarios in the first place, e.g. ISRU propellant production and in-orbit refuelling around the Moon, it is considered that the substantially simpler and more directly feasible single-target mission scenarios are the preferable choice.

8

Conclusions

Recalling all the acquired knowledge throughout the study, a number of conclusions are drawn in this chapter. First, a general conclusion to the entire study is given, after which the main research question and the defined sub-questions will be answered. Finally, a set of recommendations for further study are presented.

8.1. General Conclusion

With the continued and exponential growth of the space launch industry, the accumulation of space debris presents an ever larger threat to operational assets in space. Long-term sustainable debris mitigation strategies are an essential need for the future in order to combat this threat and prevent the risk of losing access to space entirely. Simultaneously, humanity has reaffirmed its commitment to return to the Moon. The establishment of a permanent human presence on the Lunar surface will be mankind's most ambitious endeavor in the history of space flight. Supplying the vast amount of raw materials required for the establishment of a Lunar settlement is one of the key problems yet to be solved. The concept of a space debris recycling and re-utilization mission presents a novel means of addressing both of these problems simultaneously. However, the concept of recycling space debris as a means of supplying raw material resources to the Lunar surface depends ultimately on the process being viable.

As such, the study detailed in this report addressed this innovative mission concept with the goal of establishing a fundamental baseline of understanding. By assessing the complete process chain, establishing a general mission framework and analyzing several different mission scenarios, a better understanding of the global mission energy expenditure was achieved. A prerequisite for mission viability is mission feasibility. Following the work performed in this study, it was concluded that strong potential exists for the recycling of space debris to be feasible, even from the viewpoint of complete European autonomy, without any critical showstoppers or roadblocks. While continuous, multi-target debris recycling missions show promise for the greatest energy efficiency, their inherent reliance on numerous assumptions and an the existence of an advanced Lunar infrastructure make these scenarios significantly less feasible within the foreseeable future. Instead, single-target missions were concluded to be the defining baseline for space debris recycling efforts. Based on a novel characterization of space debris in terms of resources and reserves, defunct Ariane upper stages in GTO were concluded to be prime targets for a recycling mission destined for the Moon. The concept of global mission expenditure used in this study as a novel tool for relative analysis also shows potential as an adequate means of analyzing space missions, especially those with multiple defining segments. The use of conventional, chemical propulsion as well as the implementation of solar-electric low-thrust propulsion were found to be feasible transfer strategies which yield a decrease in energy expenditure per kg of raw material delivered of 50% and 61% respectively when compared to conventional Lunar lander mission. This decreased energy expenditure shows that the mission is not only feasible, but viable as well. The feasibility of both transfer strategies allows for further trade-off between mission simplicity and increased energy efficiency. Uncertainties in mission-critical assumptions regarding raw material mass fractions and Lunar entry velocity can be alleviated at the cost of energy efficiency, for which significant margin was shown to exist. The advantage of a traditional Lunar lander mission however is its capability to not just deliver raw material, but complete end products. Indeed, a conventional lander mission is utilized much more effectively transporting rovers or other complex systems safely to the surface. This is why the creation of raw metal feedstock material presents the most suitable utilization strategy for a

space debris recycling mission specifically as a means to supply raw material resources. Such feedstock material could be accumulated ahead of time and serve as incredibly flexible input for subsequent manufacturing methods. Through this approach, the raw material recovered from space debris could serve as an instrumental stepping stone towards a permanent Lunar presence.

Ultimately, there is no single definitive conclusion that covers every aspect of a complex concept such as the recycling of space debris at this stage. However, this study has proven that strong potential exists for a space debris recycling mission to be both feasible and viable as a means of supplying raw material resources to the Lunar surface with substantially increased energy efficiency compared to a conventional lander mission. The findings presented in this study, both in terms of mission feasibility and viability, show that the concept of space debris recycling warrants further study. However, beyond the potential for a substantial increase in energy efficiency, one principle aspect of a debris recycling mission has not yet been addressed. While it cannot be objectively accounted for, the ”value” of removing debris cannot be understated. Removing high-risk objects such as upper stages in GTO is a key step on the road towards a zero debris environment, as no long-term mitigation strategies for such objects currently exist. Furthermore, the concept of recycling space debris allows for the creation of value which traditional space debris mitigation measures have critically lacked. Only by exploring innovative ideas such as this can a paradigm shift be created in which space debris is seen as more than just a liability. By taking responsibility and laying the foundation now, we can pave the way to foster a more sustainable, safe way of dealing with our precious orbital environment, ensuring the potential for vast space exploration efforts for generations to come.

8.2. Answering Research Questions

At the start of this study, a principle research question was formulated to guide the thesis work. In support of this research question, several underlying sub-questions were defined to break down the broader research question and provide additional depth. In this section, the knowledge acquired throughout the presented study will be compiled and recalled in order to give concise yet concrete answers. The sub-questions will be addressed first before answering the main research question.

1. What is the most suitable space debris target for a recycling mission?

Following the trade-off process detailed in Chapter 3 as well as the extensive orbital transfer analysis in Chapter 6, it can be concluded that the Ariane 5 ESC-A upper stage is the most suitable space debris target for a space debris recycling mission. A total of 63 ESC-A upper stages of 5000 kg individual mass each are currently drifting in GTO, where they present significant risk to operational space assets as they cross both the LEO-and GEO-protected regions defined by the IADC [10]. Simultaneously, their presence in GTO results in a predictable cycle of orbital orientations and for an efficient transfer to the Moon. The inherently high metal fraction of launch vehicle upper stages combined with a large individual object mass further substantiate the ESC-A as an ideal target with a high raw material mass yield upon recycling compared to lighter upper stages. The act of capturing debris in orbit allows for the capture of such heavy targets like the ESC-A without any critical performance penalties while simultaneously maintaining a low launch mass and therefore an overall increase in energy efficiency. While rocket stages in GTO tumble at relatively high rates, it was found that this tumbling motion is slowing down over time due to the numerous perturbing forces these vehicles are subject to. As a result, the inherently long lifetimes of these upper stages means that over time more targets could be captured safely as the potential target pool expands naturally. Finally, the strong working relationships of ESA with CNES and ArianeGroup presents a favorable opportunity for passing many of legal grey areas surrounding the capture of space debris and supports the establishment of a space debris recycling partnership within the context of European autonomy. This is substantiated by the fact that the ESC-A is an outdated vehicle and thus has less ”value” as intellectual property as the Ariane 5 has been decommissioned in favor of the upcoming Ariane 6.

2. What is the the complete process chain for a space debris recycling mission?

Generally, the process chain of a space debris recycling mission can be divided into three main phases: the Earth phase, the space phase and the Lunar phase. This approach is applicable primarily to the single-target debris recycling missions. The notion of a process chain is indicative of the fact that space debris recycling is a linear process. In this way it can be compared to a traditional manufacturing process, as the principle architecture of a space debris recycling mission is to transform space debris into new, usable material for Lunar exploration activities. Since space debris is captured in orbit, the Earth phase is dictated by the launch. The choice of a specific space debris object to target is of key importance as it dictates many of the important input variables for the subsequent processes. The space phase of a debris recy-

cling mission is defined by the relocation of the debris object from its initial orbit, in this case GTO, to the Lunar surface. This transfer is facilitated by a Space Debris Servicing Vehicle (SDSV). At this point, the process chain splits into two potential paths that can be taken defined by the propulsion strategy for the main Lunar transfer. Traditional chemical propulsion presents a simple, well-understood option with a fast transfer though at the cost of potentially spending long phasing times in the Earth's lower Van Allen belt. Alternatively, low-thrust solar-electric propulsion offers a higher potential energy efficiency though at the cost of long transfer times and a greater system complexity. Both of these paths show great potential to be both feasible and viable, and join into a single process chain once again for a Lunar capture manoeuvre that puts the SDSV and the captured debris object into a Lunar orbit. Following a descent to the surface, a final termination burn is required to slow down the stack to an acceptable Lunar impact velocity, after which it will crash into the Lunar surface into space debris fragments. While attractive at face value, the use of a soft landing presents infeasible consequences primarily due to excessive propellant mass requirements. Throughout the Lunar phase, the metal debris fragments are collected using rovers and transported to a nearby recycling facility. The Moon presents the ideal location for the establishment and operation of a recycling infrastructure due to the presence of gravity and the wealth of space available, both of which allow for the translation and implementation of well-understood technologies from the recycling industry on Earth. Induction furnaces present an ideal solution for re-melting such debris fragments under the harsh conditions of the Lunar surface. Finally, the debris is cast either in existing molds or in the Lunar regolith itself to form feedstock material which can readily be stored on the Lunar surface and can be utilized for a large variety of subsequent manufacturing processes whenever required.

3. What are the major challenges to overcome for a space debris recycling mission?

While a space debris recycling mission shows great potential to be both feasible and viable, a number of key challenges and roadblocks exist which must be overcome. These challenges are primarily centered around overall feasibility. From the work performed throughout this thesis study and the preceding literature review, it is concluded that no immediate roadblocks exist that downright prevent a potential space debris recycling mission. Many of the required technologies are already available or are seeing significant advancement due to the growing precedent of solving the space debris problem. Nevertheless, many challenges still remain, from which the three key ones are listed below.

- **The necessity of an updated legal framework for space debris mitigation:** The very concept of capturing space debris in and of itself is hindered significantly by the existing legal challenges, which primarily center around the question of ownership. The 1967 Treaty on Principles Governing the Activities of States in the Exploration and Use of Outer Space, including the Moon and Other Celestial Bodies [21] dictates that jurisdiction and control over any object launched to space remains with the launching states. Within this rule, even the approach of a space object by any party other than the launching states is prohibited without explicit consent. This challenge was partially solved in this study by specifically targeting European rocket bodies. However, the launching states can be made up of several different parties, including the satellite client which are often commercial entities. Ultimately, the existing legal framework is severely outdated considering the fact that the space debris problem has gotten exponentially worse since the signing of the treaty in 1967.
- **The lack of understanding regarding the state of space debris in orbit:** Capturing debris is an incredibly precise endeavor which carries significant risk to create more debris in the case of a collision. Minimizing this risk is of paramount importance. Yet very little is known about the exact state of space debris in orbit, given that such debris no longer transmits its monitoring housekeeping data down to Earth and the current capabilities of tracking debris is limited. This challenge was introduced during the space debris target class trade-off, which specifically highlighted the potential challenge of tumbling. Indeed, the tumbling rate and orientation are the most important aspects regarding the state of debris and form a challenge for any mission involving space debris capture. However, other important unknowns regarding the state of space debris have also been identified. These include the overall structural rigidity of a space debris object, potential micro-meteoroid impacts and the state of potential interfaces.
- **The establishment and operation of a Lunar recycling infrastructure:** Given the rather unexplored nature of space debris recycling, the study detailed in this report has focused primarily on studying overall mission feasibility and the potential for viability through investigating the energy expenditures throughout the process chain. However, this has not included an in-depth analysis on the how the actual establishment and operation of the Lunar segment would be accomplished. While autonomous operation is the ideal solution, the setup of a recycling infrastructure would likely involve the use of astronauts. The proposed collection of debris scrap using rovers, the creation of

an electrical grid to power the induction furnaces and the transportation of cast feedstock material to a utilization site are all challenges that require more analysis on a fundamental level. The Lunar segment in general ultimately requires more complete insight and a more detailed design definition. Additional options will likely appear with the renewed interest for humanity to return to the Moon and as such, the interfacing of a potential recycling infrastructure with concepts for a human settlement must continuously be updated.

4. In what ways can a space debris recycling mission be optimized for increased energy efficiency?

By far the largest energy sink in the process chain of a space debris recycling mission is the launch. The massive amounts of propellant combusted to combat Earth's gravity and the thick atmosphere result in the launch making up as much as 99% of the global mission energy cost for the debris recycling mission scenarios and 92% for the Argonaut alternative mission scenario. As such, the launch is the principle aspect that should be targeted for optimization. Though while launch trajectories are already well optimized, looking instead at the utilization of a launch is key for energy optimization. Space debris recycling missions, by virtue of capturing their principle payload mass in orbit, are characterized by the potential to reduce the launch mass. In this way, the very concept of recycling space debris is already an energy optimization in and of itself as it reduces the mass to be launched by capturing its principle payload in orbit. The feasible single-target space debris recycling mission concepts presented in this study prove that sufficient launch vehicle payload mass margin exists to make the inclusion of a secondary client in a rideshare configuration a feasible and viable consideration. The popularity of GTO as a target orbit for GEO satellites ensures a large potential client pool. By sharing the launch with another satellite, the total launch energy used for the space debris recycling mission can be reduced proportionally to the launch vehicle payload capacity utilization. This yields reductions in total mission energy cost of 23% and 39% for the direct, chemical transfer scenario and the low-thrust hybrid transfer scenario, respectively. Another way to optimize the energy efficiency of a space debris recycling mission is to perform a continuous mission that returns multiple targets instead of only a single one. Depending on the specific number of targets captured over the entire mission lifetime, the energy cost per kg of raw material delivered can be reduced significantly. When capturing 3 targets in total, the energy cost per kg of raw material delivered can be reduced by up to 77% compared to using a conventional lander mission and 43% compared to the single-target, low-thrust hybrid transfer mission scenario. However, the feasibility of such multi-target missions is significantly lower due the various assumptions and simplifications applied within the analysis.

5. What aspects of a space debris recycling mission can justify an increased energy expense?

Overall, there are several aspects of a space debris recycling mission that, depending on mission priority, can justify an increased energy expense. All of these aspects are captured first and foremost by a single principle: simplicity. Given the novel and complex nature of space debris recycling as a concept, simplifying the process chain whenever possible and practical can be incredibly valuable. A specific energy cost per kg of raw material of 1.53 GJ/kg and 1.20 GJ/kg was determined for the direct, chemical transfer and low-thrust hybrid transfer mission scenarios, respectively. While its specific energy cost is higher, the direct transfer mission scenario is significantly simpler by virtue of its Lunar transfer utilizing conventional chemical propulsion. The ability to use J2 phasing to wait for a favorable orbital alignment allows for the use of a relative standard Lunar transfer orbit. The implementation of electric propulsion, despite resulting in lower global specific energy cost, brings significant additional complexities and constraints. For example, the high power draw for the electric thrusters results in a large required solar array area and a generally more complex transfer vehicle design. Increased complexity generally leads to increased cost, which is especially detrimental for a vehicle that has a relatively short mission lifetime before being crashed into the Lunar surface. Additionally, the low-thrust spiral trajectory is significantly more susceptible to Luni-Solar interactions. Especially when reaching higher altitudes, these perturbing forces can significantly alter the trajectory of the transfer vehicle, which complicates the mission planning, analysis and design. Finally, an aspect of lesser direct importance is flight time. A conventional, chemical Lunar transfer has a flight time of around 5 days [84]. The 385 days limit presented in Table 7.1 for the direct, chemical transfer mission scenario is defined by the worst case J2 phasing time required to facilitate orbital alignment. The longer flight time caused by the low-thrust manoeuvre presents more time in which problems could occur and thus a larger overall complexity. All of these complexities should be considered within the context of the fact that the chemical transfer mission scenario already has a 50% lower energy cost per kg of raw material than the alternative lander scenario. As such, sacrificing the additional 11% energy cost reduction associated with the more complex and more costly low-thrust hybrid transfer mission scenario could be justified.

6. How can a space debris recycling mission evolve to continuously suit a growing human presence on the Moon?

The long-term applicability of a space debris recycling mission as it has been defined in this study is largely benefited by the flexibility of its chosen utilization method. The casting of feedstock material presents an ideal starting point for the establishment as well as the growth of a Lunar settlement as its manufacturing capabilities increase in scale and complexity alike. The utilization of feedstock material created through the recycling of space debris therefore has the capacity to evolve with a growing human presence. This segmented approach has found great success in the metalworking industry on Earth, where foundries create metal feedstock material which in turn is used as input material for across various other industries. Metal feedstock material supplied by a space debris recycling mission could be a way of translating this proven and scalable approach to a Lunar settlement. Especially in the early days of a Lunar settlement, when the utilization of in-situ material resources will inevitably be limited, the raw material recovered from space debris would be of great value. As increasingly more manufacturing processes become available throughout the evolution of a human presence on the Moon, the material supplied by a debris recycling infrastructure can be used for increasingly more purposes. The most important of these manufacturing processes to advance the applicability of utilizing space debris is 3D printing. However, it requires the use of liquid water to atomize the metals in order to create the metal powder requires as the input material for metal 3D printing [107, 18]. As such, when in-situ production of water becomes available, the 3D printing of metals has an effectively limitless number of applications and presents perhaps the ultimate utilization scenario for the raw metals recovered from a space debris recycling infrastructure.

However, it is important to understand that ultimately, continuous evolution with a growing human presence on the Moon may not be possible for the complete space debris recycling mission. This is because the number of target stages in GTO and by extension the number of viable space debris targets in general are inherently limited. Space debris mitigation has as its ultimate goal the establishment of a ”zero” debris environment, or at least a net zero accumulation. Assuming that such a vision will become reality, the pool of space debris targets for a recycling mission will inevitably deplete. In this sense, the very concept of recycling space debris is a means to an end. However, even when there is no more space debris to recycle, the proposed recycling infrastructure on the Lunar surface could still be useful. A permanent Lunar presence will naturally see a significant growth in satellites around the Moon. Given the unstable nature of most Lunar orbits, a consolidated space debris landing site as proposed in this study could leverage an established recycling infrastructure to continuously recycle Lunar satellites and even Lunar rovers after the end of their operational lifetime.

• Main research question:

How can space debris be recycled to create an energetically viable means of supplying raw material resources for the establishment and growth of a permanent human presence on the Moon?

A space debris recycling mission first and foremost on the debris target, which dictates a fundamental set of input variables which influence the recycling mission. As such, the first step to establishing an energetically viable space debris recycling mission is not a physical one, but rather the choosing a specific debris object to capture. The Ariane 5 ESC-A upper stage in GTO presents an ideal space debris target for a European space debris recycling mission, as upper stages in GTO represent high-risk objects with high individual target mass and high metal content. Targeting the Ariane 5 ESC-A upper stage, the widely varying orbital orientations of the 63 ESC-A vehicles in orbit present unique initial conditions for the Lunar transfer. For optimal energy efficiency, an object of which the orbit naturally approaches an argument of periapsis value of either 0° or 180° should be targeted. While not of immediate benefit to the space debris recycling mission itself, this condition enables the inclusion of a secondary client to GEO in a rideshare configuration. By sharing the launch, the associated energy expenditure for the debris recycling mission is reduced proportionally to its launch vehicle payload utilization, which yields a substantial increase in overall energy efficiency. This energy optimization is enabled by the fact that a space debris recycling mission captures its principle payload mass in orbit, thus reducing launch mass. Utilizing a stacked dual payload configuration, the Space Debris Servicing Vehicle (SDSV) and the rideshare client are launched on Ariane 64 directly into a GTO such that it matches the main orbital parameters of the targeted debris object. After deploying the rideshare client such that it can perform its own GEO injection at apogee, the SDSV performs its phasing, rendez-vous and capture manoeuvres to secure the targeted ESC-A upper stage. Two feasible transfer strategies can be applied depending on the use of a conventional, chemical propulsion or low-thrust solar-electric propulsion system architecture for the main Lunar transfer. When considering the use of conventional, chemical

propulsion, a phasing time is initiated in which the J2 effect is used to rotate the GTO orbit over time until the apogee crosses the Earth-Moon plane where a Trans-Lunar Injection (TLI) manoeuvre is performed. The specific phasing time required depends primarily on the standing of the Moon and the orbital parameters of the debris, but is bound in the worst case by approximately 380 days. When considering the use of low-thrust propulsion, a thrust-arcing approach in which thrust is applied only in the first half of the orbit while coasting in the second half allows for flexible steering of the apogee passage point in order to facilitate a Lunar encounter regardless of initial conditions. While it allows for a reduction of propellant mass and therefore total laucnh mass, the low thrust levels of this scenario however lead to substantially longer flight times. The maximum flight time estimations are in the order of 636 to 1178 days, depending on chosen thrust level.

Upon reaching the Lunar vicinity, a chemical propulsion manoeuvre facilitates the high-impulse Lunar capture into a staging orbit. A two-impulse Hohmann transfer brings the combined stack of the SDSV and its captured ESC-A target down to the Lunar surface. Craters such as the Gambart crater, proposed as a space debris graveyard for future Lunar missions, can also be utilized for the space debris recycling mission. A shallow impact angle into such craters allows for the dispersion of impact energy while limiting the dispersion of ejecta. A soft landing however was concluded not to be a feasible option, as the large debris mass creates excessive demands in terms of propellant mass and thrust levels required. Instead, a controlled, retro-propulsive crash manoeuvre right before touchdown onto the surface reduces the impact velocity of the stack to 1200 m/s. Significant margin exists for the reduction of this impact velocity if desired, though at the cost of energy efficiency. Upon impact, the SDSV and the ESC-A target will disintegrate into debris fragments to be collected and characterized by rovers on the Lunar surface. Induction furnaces powered by solar arrays are used to process and re-melt the metallic debris scrap recovered in the vacuum conditions of the Moon, after which the molten material is cast into feedstock material. Depending on the use of conventional, chemical propulsion or alternatively solar-electric low-thrust propulsion, a reduction in global mission energy expenditure per kg of raw material delivered of 50% and 61% respectively can be achieved when compared to a conventional Lunar lander mission.

8.3. Recommendations

To close off this study on the concept of recycling space debris, a number of recommendations have been formulated based on the acquired knowledge and understanding of the problem. First and foremost, given the high potential for feasibility and viability found through this study, it is recommended that ESA carries out further studies regarding the topic of space debris recycling. This can be done through a Concurrent Design Facility (CDF) study with the goal to establish a more comprehensive mission architecture and specifically to create a more in-depth and complete definition of the establishment and operation of the Lunar segment. This includes performing preliminary design analyses on the space debris transfer vehicle, the required induction furnaces, rover concepts and the required electrical grid as well as identifying a pool of potential craters suitable for use as a debris landing site. Utilizing the CDF is recommended as an ideal way to approach the broad range of research fields required for a space debris recycling mission. Additionally, the complete orbital transfer should be evaluated using powerful simulation tools to validate and expand on the estimates presented in this report. Following the more in-depth definition of the mission architecture and its numerous components, a new global energy analysis like the one performed in this study should be performed to re-evaluate the energy efficiency of recycling space debris. The inclusion of the energy costs regarding the establishment of the recycling infrastructure is a key expansion on the analysis performed in this study and will allow for a complete mission Life Cycle Assessment (LCA). Given that energy costs for the establishment of the Lunar segment will likely be high, it is recommended to perform a break-even analysis to investigate the increase of energy efficiency over time as more targets are recycled. In tandem with the CDF study, ESA could also leverage its large pool of industry partners through the establishment of one or several Invitation To Tenders (ITT) regarding the analysis of both a complete, high-level assessment of space debris recycling not dissimilar to what was performed in this study as well as more in-depth studies regarding select parts of a space debris recycling infrastructure such as the adoption of induction furnaces to the Lunar surface or the design of debris fragment fetch rovers. Regardless of the route taken, it is highly recommended to actively involve the European space industry within the process of studying the concept of space debris recycling.

Secondly, a number of recommendations for the actual recycling of space debris have been defined. These primarily serve to address some of the key associated challenges identified throughout the study. First, characterizing the state of debris in orbit is imperative not just for a space debris recycling mission but for any space debris mitigation mission in general. As such, it is recommended that ESA invests in the establishment of a mission to validate the behavior of defunct upper stages in GTO, with specific focus on

the tumbling rates. As mentioned earlier in this report, leveraging the ever increasing capabilities of small satellite platforms like CubeSats equipped with relatively simple optical payloads would likely be suitable for this. It is recommended to target a specific upper stage for which a good baseline of light curve data exists, such as the NORAD 43176 ESC-A shown in Figure 3.4, in order to ensure a proper validation. Secondly, the capture of rocket stages specifically requires more research. Nozzle probes likely present the most suitable and most widely applicable option for use across various rocket stages and thus should be taken as the baseline. This is substantiated by the fact that it has already been proven to be reliable method for the capture of large satellites through the success of MEV missions. However, the significantly larger of rocket stages and the larger size of their engines are expected to require stronger and more advanced nozzle probes. Alternatively, the use of robotic arms specifically to capture the payload mounting interface of rocket stages should be studied. Regarding the capture of rocket stages in general, it was found that a number of H10 upper stages currently in orbit present a substantially higher risk. These stages were launched before 1993 and were not passivated after the deployment of their payloads, which means they still carry residual propellants [30]. While the liquid hydrogen and liquid oxygen propellants used by the H10 are not hypergolic, the threat of explosion remains as proven by H10 of Ariane 1 flight V16, which exploded in 1986. As such, these stages should get the highest priority for active removal. An atmospheric re-entry into the pacific ocean will likely be the best option for these objects.

Finally, a better understanding of hyper-velocity impacts on the Lunar surface is required. For this study, it was found that a controlled, retro-propulsive crash was the only feasible option for the landing of rocket stages with large individual object masses. However, while the velocities used were chosen to prevent the melting and vaporization of the material upon impact, they are still in excess of 1 km/s. The actual behavior and dynamics of such hyper-velocity impacts and how they influence the state of the debris are not readily understood and subject to large uncertainties, especially when considering the skidding motion that will likely occur with shallow impact angles. The only thing that can be said is that the servicing vehicle along with the debris will disintegrate upon impact with the Lunar surface. As such, more research is required in order to predict how a specified impact velocity influences the state of debris upon impact. Such research could be based on numerical simulation and modelling, and potentially even based on experimental analysis. However, due to the unstable nature of most Lunar orbits, satellites orbiting the Moon historically have often been deliberately crashed into the Lunar surface or have alternatively been left to decay naturally before crashing. As such, there already exists a substantial sample pool of hyper-velocity impacts that have occured throughout the years which could readily be studied. These include objects such as several Saturn V third stages (S-IVB) used for the Apollo missions, numerous Russian Luna probes and even ESA's SMART-1 satellite. The location of the vast majority of these impact sites is readily known. It is there recommended to use existing or future Lunar orbiters to perform observations on these impact sites to get a better understanding of the state of debris after a hyper-velocity Lunar impact. This is something that could already be done today, using for example NASA's Lunar Reconnaissance Orbiter (LRO). The LRO's spatial resolution of 100 m would require mosaic images which may not accurately display details of the fragmentation. The Chandrayaan-2 orbiter presents an alternative option using its Orbiter High Resolution Camera (OHRC) which has a much better spatial resolution of 0.32 m and could capture a lot more detail. In the future, Lunar rovers could even be used to get in-situ observations on these crash sites.

References

[1] Lockheed Martin. *Orion for Artemis II Powers Up*. June 2022. URL: https://www.lockheedmartin.com/en-us/news/features/2022/orion-artemis-ii-power-on.html (visited on 08/18/2023).

[2] Sagan, C. E. *Pale Blue Dot: A Vision of the Human Future in Space*. 1st ed. New York, USA: Random House, 1994. ISBN: 0-679-43841-6.

[3] Kessler, D. J. and Cour-Palais, B. G. "Collision Frequency of Artificial Satellites: The Creation of a Debris Belt". In: *Journal of Geophysical Research* 83.8A0210 (A6 June 1978), pp. 2637–2646.

[4] Schefter, J. "The growing peril of space debris". In: *Popular Science* 221 (Iss. 1 July 1982), pp. 48–51.

[5] Biesbroek, R., Aziz, S., Wolahan, A., Cipolla, S., Richard-Noca, M., and Piguet, L. "The ClearSpace-1 mission: ESA and ClearSpace team up to remove debris". In: *8th European Conference on Space Debris*. ESA Space Debris Office, 2021.

[6] ESA Space Debris Office. *ESA's Annual Space Environment Report*. Sept. 2023.

[7] International Space Exploration Coordination Group. *The Global Exploration Roadmap - Supplement October 2022. Lunar Surface Exploration Scenario Update*. Washington, DC, Oct. 2022.

[8] Volkert, K. J. "How Can Humans Thrive and Service Satellites in a Geostationary Orbit?" In: *Amazon re:Mars (Session S02-L)*. Satellite Consulting Inc. Las Vegas, Nevada (US), 2020. URL: https://www.youtube.com/watch?v=n2ofwXAtbos.

[9] Koch, F. *A BUSINESS CASE FOR SPACE DEBRIS: Analysis of space debris recycling potential to supply raw materials for construction on the Moon*. Orbit Recycling, European Space Agency, July 2021.

[10] Inter-Agency Space Debris Coordination Committee. *IADC Space Debris Mitigation Guidelines*. Version 3. June 2021.

[11] NASA. *Astromaterials Research & Exploration Science, NASA Orbital Debris Program Office: Frequently Asked Questions*. URL: https://orbitaldebris.jsc.nasa.gov/faq/ (visited on 07/15/2023).

[12] European Space Agency. *ESA Space Debris Mitigation Policy*. Nov. 2023.

[13] European Space Agency, ESA Space Debris Mitigation Working Group. *ESA Space Debris Mitigation Requirements*. Oct. 2023.

[14] Foust, J. *Target of European debris removal mission hit by other debris*. Aug. 2023. URL: https://spacenews.com/target-of-european-debris-removal-mission-hit-by-other-debris/#:~:text=ClearSpace%2D1%20is%20scheduled%20to,on%20a%20Vega%20C%20rocket. (visited on 04/15/2024).

[15] Drake, N. and Howard, J. *A brief history of moon exploration*. URL: https://www.nationalgeographic.com/science/article/moon-exploration (visited on 07/15/2023).

[16] NASA. *Artemis plan: NASA's Lunar Exploration Program Overview*. Sept. 2020.

[17] Choate, W. T. and Green, J. S. *U.S. Energy Requirements for Aluminum Production Historical Perspective, Theoretical Limits and Current Practices*. Business Consulting and Services (BCS) LLC, for U.S. Department of Energy: Industrial Technologies Program, Feb. 2007.

[18] Heumassej, Y. *Literature Study: Recycling Space Debris as a Stepping Stone Towards a Permanent Lunar Presence*. Delft University of Technology & European Space Agency, Unpublished. 2023.

[19] Mclean, F., Lemmens, S., Funke, Q., and Braun, V. "DISCOS 3: AN IMPROVED DATA MODEL FOR ESA'S DATABASE AND INFORMATION SYSTEM CHARACTERISING OBJECTS IN SPACE". In: *Proc. 7th European Conference on Space Debris*. Darmstadt, Germany: ESA Space Debris Office, June 2017.

[20] Kelso, T. S. *CelesTrak*. 2023. URL: https://celestrak.org/ (visited on 04/26/2023).

[21] United Nations Ofice for Outer Space Affairs. *Treaty on Principles Governing the Activities of States in the Exploration and Use of Outer Space, including the Moon and Other Celestial Bodies*. Dec. 1967.

[22] Vaidya, O. S. and Kumar, S. “Analytic hierarchy process: An overview of applications”. In: *European Journal of Operational Research* 169 (1 Feb. 2006), pp. 1–29. ISSN: 03772217. DOI: 10.1016/j.ejor.2004.04.028.

[23] Goepel, K. D. “Implementation of an Online software tool for the Analytic Hierarchy Process (AHP-OS)”. In: *International Journal of the Analytic Hierarchy Process* 10 (3 2018), pp. 469–487. ISSN: 19366744. DOI: 10.13033/ijahp.v10i3.590.

[24] McKnight, D., Witner, R., Letizia, F., Lemmens, S., Anselmo, L., Pardini, C., Rossi, A., Kunstadter, C., Kawamoto, S., Aslanov, V., Perez, J.-C. D., Ruch, V., Lewis, H., Nicolls, M., Jing, L., Dan, S., Dongfang, W., Baranov, A., and Grishko, D. “Identifying the 50 statistically-most-concerning derelict objects in LEO”. In: *Acta Astronautica* 181 (Apr. 2021), pp. 282–291. ISSN: 00945765. DOI: 10.1016/j.actaastro.2021.01.021.

[25] Wertz, J. R., Everett, D. F., and Puschell, J. J., eds. *Space Mission Engineering: The New SMAD*. Space Technology Library. Hawthorne, CA: Microcosm Press, 2015.

[26] Anderson, P. V., Mcknight, D. S., Pentino, F. D., and Schaub, H. “Operational Considerations of GEO Debris Synchornization Dynamics”. In: *66th International Astronautical Congress*. International Astronautical Federation (IAF), Oct. 2015.

[27] Mueller-Wiesner, D., Sieger, E., and Ernsberger, K. “Characterization of Al 2219 material for the application of the spin-forming-process”. In: *ESA Special Publication*. Ed. by Burke, W. R. Vol. 2. ESA Special Publication. Oct. 1991, pp. 755–760.

[28] European Cooperation for Space Standardization (ECSS). *Space engineering - Structural materials handbook-Part 3: Load transfer and design of joints and design of structures ECSS Secretariat ESA-ESTEC Requirements & Standards Division*. Document identifier: ECSS-E-HB-32-20 Part 3A. ESTEC, Noordwijk, The Netherlands, Mar. 2011.

[29] Air Liquide. *Cryogenic tanks for space applications: Cryogenic tanks for launcher propellants and satellite cryogens*.

[30] P. Luquet, M. S. a. “Operations of the Ariane 4 third stage for space debris prevention”. In: *Proceedings of the First European Conference on Space Debris*. Darmstadt, Germany: European Space Agency, Apr. 1993.

[31] Shan, M., Guo, J., and Gill, E. “Review and comparison of active space debris capturing and removal methods”. In: *Progress in Aerospace Sciences* 80 (Jan. 2016), pp. 18–32. ISSN: 0376-0421. DOI: 10.1016/J.PAEROSCI.2015.11.001.

[32] European Space Agency. *Understanding the Tumbling Motion of Space Debris*. May 2023. URL: https://www.esa.int/Enabling_Support/Space_Engineering_Technology/Shaping_the_Future/Understanding_the_Tumbling_Motion_of_Space_Debris (visited on 01/19/2024).

[33] Vananti, A., Kucharski, D., Steindorfer, M., Kanzler, R., Kärräng, P., and Rosebrock, D. C.-M. J. *Tumbling Motion Assessment for Space Debris Objects*. Astronomical Institute University of Bern (AIUB). Dec. 2022.

[34] Nishida, S. I. and Kawamoto, S. “Strategy for capturing of a tumbling space debris”. In: *Acta Astronautica* 68 (1-2 Jan. 2011), pp. 113–120. ISSN: 00945765. DOI: 10.1016/j.actaastro.2010.06.045.

[35] Biryukov, A., Beskin, G., Karpov, S., Bondar, S., Ivanov, E., Katkova, E., Perkov, A., and Sasyuk, V. “The first light of Mini-MegaTORTORA wide-field monitoring system”. In: *Baltic Astronomy* 24 (Jan. 2015). DOI: 10.1515/astro-2017-0208.

[36] Katkova, E. *Satellites identified in MMT data*. Kazan Federal University. 2024. URL: http://mmt9.ru/satellites/.

[37] Gómez, N. O. and Walker, S. J. “Eddy currents applied to de-tumbling of space debris: Analysis and validation of approximate proposed methods”. In: *Acta Astronautica* 114 (May 2015), pp. 34–53. ISSN: 00945765. DOI: 10.1016/j.actaastro.2015.04.012.

[38] Elbert, B. R. *Introduction to Satellite Communication*. 3rd ed. Norwood, Massachusetts, USA: Artech House, 2008.

[39] ArianeSpace. *Soyuz User’s Manual*. Version 2, Revision 0. Mar. 2012.

[40] Kumar, artik, Gómez, N. O., Jankovic, M., Martin, J. M. R., Topputo, F., Walker, S., Kirchner, F., and Vasile, M. “Agora: Mission to demonstrate technologies to actively remove Ariane rocket bodies”. In: *66th International Astronautical Congress*. International Astronautical Federation (IAF), Oct. 2015.

[41] Spaceflight101. *Ariane 5 rolls to Equatorial Launch Pad for Single-Satellite Launch Wednesday*. Mar. 2016. URL: https://spaceflight101.com/ariane-5-va229/ariane-5-rolls-to-equatorial-launch-pad-for-single-satellite-launch-wednesday/ (visited on 02/08/2024).

[42] ArianeSpace. *ARIANE 5 USER'S MANUAL*. Version 5, Revision 2. Oct. 2016.

[43] Redd, N. T. "Bringing satellites back from the dead: Mission extension vehicles give defunct spacecraft a new lease on life - [News]". In: *IEEE Spectrum* 57.8 (2020), pp. 6–7. DOI: 10.1109/MSPEC.2020.9150540.

[44] European Space Agency. *MEV-1 & 2 (Mission Extension Vehicle-1 and -2)*. eoPortal. Feb. 2020. URL: https://www.eoportal.org/satellite-missions/mev-1 (visited on 08/02/2023).

[45] Guardabasso, P., Lizy-Destrez, S., and Ansart, M. "LUNAR ORBITAL DEBRIS MITIGATION: CHARACTERISATION OF THE ENVIRONMENT AND IDENTIFICATION OF DISPOSAL STRATEGIES". In: *8th European Conference on Space Debris*. Darmstadt, Germany: ESA Space Debris Office, Apr. 2021.

[46] Lunar Resources Registry. *Space Debris Lunar Landing Zone – Space Debris Graveyard*. July 2022. URL: https://lunarresourcesregistry.com/infrastructure/space-debris-graveyard/ (visited on 06/06/2023).

[47] Robinson, M. *LROC WAC mosaic of the lunar nearside*. Dec. 2010. URL: https://www.lroc.asu.edu/images/293 (visited on 03/10/2024).

[48] Lunar and Planetary Institute. *Lunar Orbiter Photo Gallery: Mission 4, frame 4120, image h3*. URL: https://www.lpi.usra.edu/resources/lunarorbiter/frame/?4120 (visited on 03/10/2024).

[49] Farries, K. W., Visintin, P., Smith, S. T., and Eyk, P. van. "Sintered or melted regolith for lunar construction: state-of-the-art review and future research directions". In: *Construction and Building Materials* 296 (Aug. 2021). ISSN: 09500618. DOI: 10.1016/j.conbuildmat.2021.123627.

[50] Capozzi, R. *FCC Application to Launch and Operate: Technical Appendix*. Space Logistics LLC, Dec. 2019.

[51] NASA. *Orion By The Numbers*. Mar. 2023.

[52] Kumar, C. *Chandrayaan-2: All you need to know about India's 2nd Moon mission*. July 2019. URL: https://timesofindia.indiatimes.com/india/chandrayaan-2-all-you-need-to-know-about-indias-2nd-moon-mission/articleshow/70325029.cms (visited on 03/20/2024).

[53] Indian Space Research Organization. *LVM3-M4/Chandrayaan-3 Moon mission*. Aug. 2023.

[54] Berthe, P., Over, A. P., Picardo, M., and Byers, A. W. "Orion European Service Module (ESM) development, integration and qualification status". In: *AIAA Space 2018*. American Institute of Aeronautics and Astronautics, 2017.

[55] European Space Agency. *Argonaut*. 2023. URL: https://www.esa.int/Science_Exploration/Human_and_Robotic_Exploration/Exploration/Argonaut (visited on 07/13/2023).

[56] Liggieri, G., Boiron, A., Hansen, B. E., Josefsen, H., Worsley, E., Haynes, A., and Shaw, M. "RELIANCE-Design, Manufacturing and Testing of the Breadboard Engine". In: *Aerospace Europe Conference 2023 - 10th EUCASS - 9th CEAS*. July 2023. DOI: 10.13009/EUCASS2023-470.

[57] Börkey, P. and McCarthy, A. *Working Party on Resource Productivity and Waste: Mapping support for primary and secondary metal production*. Organisation for Economic Co-operation and Development (OECD): Environment Directorate, Mar. 2017.

[58] Totten, G. and Mackenzi, D. *Handbook of Aluminum, Volume 1, Physical Metallurgy and Processes*. New York: M. Dekker, 2003.

[59] Paraschos, T. *Production of aluminum (emphasis on energy and materials requirements)*. Technical University of Crete, Mining Resources Engineering. 2012.

[60] ArianeSpace. *ARIANE 6 USER'S MANUAL*. Version 2, Revision 0. Feb. 2021.

[61] ArianeGroup. *Technical Features*. Nov. 2020. URL: https://ariane6.cnes.fr/en/technical-features (visited on 11/02/2023).

[62] Germani, T., Bandelier, E., Cloutet, P., Ribéreau, D., Garitta, D., Angelone, M., Ciucci, A., Scoccimarro, D., Prel, Y., Robert, E., and Kolsgaard, A. "P120c Solid Rocket Motor Synthesis Of The Development Of The Common Propulsive SRM For Ariane 6 And Vega-c And P160c Way Forward". In: *Aerospace Europe Conference 2023*. 2023.

[63] ArianeGroup. *Vulcain 2.1 Engine*. Tech. rep. Apr. 2020.

[64] ArianeGroup. *Vinci Engine*. Tech. rep. Apr. 2020.

[65] Zandbergen, B. T. C. *AE4-S01: Thermal Rocket Propulsion*. Version 2.08. Delft University of Technology. Aug. 2020.

[66] Sutton, G. P. and Biblarz, O. *Rocket Propulsion Elements*. 9th ed. Hoboken, New Jersey: John Wiley & Sons, 2001. ISBN: 9781118753880.

[67] Linstrom, P. J. and Mallard, W. G., eds. *NIST Chemistry WebBook, NIST Standard Reference Database Number 69*. National Institute of Standards and Technology. DOI: https://doi.org/10.18434/T4D303. Data retrieved between May 12th and December 19th, 2023.

[68] Zandbergen, B. T. C. *Thermochemical Data for Thermochemical Calculations of Various Important Rocket Propellants (LR Technical Note 10006)*. Tech. rep. Delft University of Technology, Feb. 2003.

[69] Calabro, M., Gizzi, E., Wingborg, N., Batonneau, Y., Beauchet, R., and Kappenstein, C. *Propellant requirements and future demands*. Swedish Defence Research Agency (FOI), The Inner Arch (TIA), AVIO, CNRS. Jan. 2016.

[70] Perry, B. *We've Got (Rocket) Chemistry, Part 2*. NASA. Apr. 2016. URL: https://blogs.nasa.gov/Rocketology/2016/04/21/weve-got-rocket-chemistry-part-2/ (visited on 07/09/2023).

[71] Bay, F., Labbe, V., Favennec, Y., and Chenot, J. L. "A numerical model for induction heating processes coupling electromagnetism and thermomechanics". In: *International Journal for Numerical Methods in Engineering* 58 (6 Oct. 2003), pp. 839–867. ISSN: 00295981. DOI: 10.1002/nme.796.

[72] Segura, G. M. *Doctoral Thesis: Induction heating converter's design, control and modeling applied to continuous wire heating*. Universitat Politecnica De Catalunya. June 2012.

[73] Dejaegherre, L., Pierre, T., Carin, M., Masson, P. L., and Courtois, M. "Design and development of an induction furnace to characterize molten metals at high temperatures". In: *High Temperatures - High Pressures* 47 (2018).

[74] The Aluminum Association. *International Alloy Designations and Chemical Composition Limits for Wrought Aluminum and Wrought Aluminum Alloys*. Aug. 2018.

[75] Barry, C. *Weather on the Moon*. NASA Goddard Space Flight Center. 2024. URL: https://science.nasa.gov/moon/weather-on-the-moon/ (visited on 11/17/2023).

[76] Indian Space Research Organisation. *Chandrayaan-3 Mission:* Aug. 2023. URL: https://twitter.com/isro/status/1695725102166671448? (visited on 11/24/2023).

[77] Lea, R. *Why Chandrayaan-3 landed near the moon's south pole — and why everyone else wants to get there too*. Space.com. Aug. 2023. URL: https://www.space.com/chandrayaan-3-moon-south-pole-why-nasa-wants-to-go-too (visited on 11/24/2023).

[78] The Engineering Toolbox. *Metals - Latent Heat of Melting.* 2008. URL: https://www.engineeringtoolbox.com/fusion-heat-metals-d_1266.html (visited on 11/16/2023).

[79] Roncoli, R. B. *Lunar Constants and Models Document*. Document number: D-32296. NASA, Jet Propulsion laboratory, California Insititute of Technology. Sept. 2005.

[80] Uphoff, C. "Practical Aspects of Transfer from GTO to Lunar Orbit". In: *Flight Mechanics: Estimation Theory Symposium, 1993*. Ball Corporation, Space Systems Division. Feb. 1993.

[81] Wakker, K. F. *Fundamentals of Astrodynamics*. Delft: Institutional Repository, Library Delft University of Technology, Jan. 2015. ISBN: 978-94-6186-419-2.

[82] Williams, D. R. *Earth Fact Sheet*. NASA Goddard Space Flight Center. May 2023.

[83] Williams, D. R. *Moon Fact Sheet*. NASA Goddard Space Flight Center. Dec. 2021.

[84] Parker, J. S. and Anderson, R. L. "Transfers to Low Lunar Orbits". In: *Low-Energy Lunar Trajectory Design*. John Wiley & Sons, Ltd, 2014. Chap. 4, pp. 227–262. ISBN: 9781118855065. DOI: https://doi.org/10.1002/9781118855065.ch4.

[85] Biesbroek, R. and Janin, G. "Ways to the Moon?" In: *ESA Bulletin* 103 (Aug. 2000).

[86] Wilhite, A. W., Wagner, J., Tolson, R., and Moen, M. M. "Lunar Module Descent Mission Design". In: *AIAA/AAS Astrodynamics Specialist Conference and Exhibit*. Georgia Institute of Technology. American Institute of Aeronautics and Astronautics, Aug. 2008.

[87] Agency, E. S. *Margin philosophy for science assessment studies*. Version 1, Revision 3. European Space Research and Technology Centre (ESTEC): SRE-PA & D-TEC staf. June 2012.

[88] Uramachi, H., Shiraiwa, D., Takai, T., and Tanaka, N. *Green Propulsion Systems for Satellites-Development of Thrusters and Propulsion Systems using Low-toxicity Propellants-TAKAO KANEKO *2 KATSUMI FURUKAWA *2*. 2019.

[89] Cervone, A. *AE4S07 – Course reader: Micro-Propulsion*. Delft University of Technology. July 2020.

[90] ECAPS. *Thruster A4 Sheets V4*. Acquired from: https://www.ecaps.se/rocket-engines-1. 2024.

[91] Rocketdyne, A. *In-Space Propulsion Data Sheets*. Apr. 2020.

[92] Zandbergen, B. T. C. *Thermo-chemistry: Chemical propellants and (reaction) energy*. Delft University of Technology. Sept. 2021.

[93] Zandbergen, B. *Thermochemistry: Chemical propellants and (reaction) energy*. Delft University of Technology. Mar. 2010.

[94] ArianeGroup. *10N, 200N, 400N: Chemical Bi-Propellant Thruster Family*. 2019.

[95] Zhang, Z., Yan, H., Cai, K., Yang, S., Wang, F., Mao, X., and Yu, Y. "Analysis and Prediction Research for Bipropellant Thruster Mixture Ratio Based on BP-RNN Chain Method". In: *Applied Sciences (Switzerland)* 12 (16 Aug. 2022). ISSN: 20763417. DOI: 10.3390/app12167956.

[96] Muhammad, N., Muhalim, F. B., and Krishnan, S. *Design of Nitrogen-Tetroxide / Monomethyl-Hydrazine Thruster for Upper Stage Application*. Universiti Teknologi Malaysia.

[97] Peet, M. M. *Spacecraft Dynamics and Control - Lecture 13: The Effect of a Non-Spherical Earth*. Arizona State University. Feb. 2023.

[98] European Space Agency. *Earth's plastmasphere and the Van Allen belts*. Sept. 2019. URL: https://sci.esa.int/web/cluster/-/52831-earth-plasmasphere-and-the-van-allen-belts (visited on 02/03/2024).

[99] European Space Agency. *Ion engine gets SMART-1 to the Moon*. Aug. 2006. URL: https://www.esa.int/Science_Exploration/Space_Science/SMART-1/Ion_engine_gets_SMART-1_to_the_Moon (visited on 05/18/2024).

[100] Racca, G. D., Whitcomb, G. P., and Foing, B. H. "The SMART-1 Mission". In: *ESA Bulletin* 109 (Aug. 1998).

[101] A.I. Solutions. *FreeFlyer University*. 2023. URL: https://ai-solutions.com/freeflyer-astrodynamic-software/freeflyer-university/ (visited on 11/10/2023).

[102] Herman, D. A., Gray, T., Johnson, I., Kerl, T., Lee, T., and Silva, T. *The Application of Advanced Electric Propulsion on the NASA Power and Propulsion Element (PPE)*. Presented at the 36th International Electric Propulsion Conference, Vienna, Austria. University of Vienna, Sept. 2019.

[103] Busek Space Propulsion and Systems. *BHT-6000 Hall Effect Thruster*. 2021.

[104] Kramer, H. J. *Artemis-I (Exploration Mission-1)*. eoPortal. Nov. 20149. URL: https://www.eoportal.org/satellite-missions/artemis-i (visited on 03/06/2024).

[105] Williams, D. R. *NASA Space Science Data Coordinated Archive: Apollo 11 Lunar Module / EASEP*. NASA. Oct. 2022. URL: https://nssdc.gsfc.nasa.gov/nmc/spacecraft/display.action?id=1969-059C (visited on 03/06/2024).

[106] Grimwood, T. *UCS Satellite Database*. Union of Concerned Scientists (UCS). May 2023. URL: http://www.ucsusa.org/satellite_database.

[107] Mariappan, A., Kumar, V. R., Weddell, S. J., Muruganandan, V. A., and Jeung, I. S. "Theoretical studies on space debris recycling and energy conversion system in the International Space Station". In: *Engineering Reports* 3 (5 May 2021). ISSN: 25778196. DOI: 10.1002/eng2.12317.

A

AHP Responses

Appendix A shows the global trade-off criteria priorities for each of the AHP participants resulting from their individual pairwise comparisons responses, along with their individual Consistency Ratio (CR). The names of the participants are removed for privacy reasons. It can be observed that the risk posed by debris is considered by 6 out of 10 participants to be the most important. Some outliers can also be seen in the energy cost, mission complexity and debris availability, which are the predominant cause of the relatively low 59.3% group consensus. These outliers also cause the priority of the respective criteria to increase to an extent which may not reflect the consensus shown by the other group members. This is highlighted by taking the median value of each criteria over all participants, which is more robust against outliers. This yields values of 14.0%, 17.6% and 17.4% for energy cost, raw material return and mission complexity, respectively.

Table A.1: Trade-off criteria priorities for each of the AHP participants, anonymized.

Weights	**Risk posed by debris**	**Energy cost**	**Raw material return**	**Mission complexity**	**Debris availability**	**CR**
Group result	31.0%	21.3%	18.0%	20.1%	9.6%	0.9%
By participants:						
1	35.7%	13.7%	15.7%	19.2%	15.7%	4.9%
2	53.3%	17.2%	19.6%	4.8%	5.1%	4.6%
3	31.0%	14.2%	29.8%	18.9%	6.1%	1.7%
4	35.0%	6.0%	29.9%	12.9%	16.2%	6.8%
5	52.3%	13.3%	7.8%	23.2%	3.5%	13.7%
6	6.4%	64.1%	8.9%	11.8%	8.8%	2.6%
7	14.1%	23.0%	4.1%	55.8%	3.0%	10.4%
8	9.7%	26.3%	6.2%	16.0%	41.9%	1.5%
9	55.9%	12.4%	24.2%	4.4%	3.0%	9.0%
10	14.0%	13.5%	25.3%	41.4%	5.8%	9.1%